# POLITECNICO DI TORINO

Collegio di Ingegneria Chimica e dei Materiali

**Corso di Laurea Magistrale**
**in Ingegneria Biomedica**

Tesi di Laurea Magistrale

# Urinary stents made of biodegradable and drug-eluting inorganic composite


**Relatori**

Prof. Valentina Cauda
Dr. Marco Laurenti

**Candidato**

Elena Dragoni


Anno accademico 2018 – 2019

***Sommario***

*Lo scopo principale di questo lavoro di tesi Magistrale è stato quello di sviluppare un metodo ottimale per sintetizzare un innovativo materiale che presentasse le caratteristiche di antibattericità e drug-eluting, sfruttando nanomateriali come l'ossido di zinco poroso (ZnO) e polimeri lineari.*
*Le proprietà antibatteriche dello ZnO e la sua struttura porosa, lo rendono adatta per essere usato come sistema a trasporto di farmaco per il rilascio.*

*Il primo scopo di questo lavoro è stato proprio quello di sviluppare il metodo migliore per sintetizzare questi materiali compositi.*
*Dopo la sintesi dei polimeri e copolimeri, sia puri che combinati con l'ossido di zinco, il secondo obiettivo è stato quello di caricarli singolarmente scegliendo tra due farmaci diversi (Ibuprofene e Diclofenac), in modo da avere a disposizione per ogni campione di ogni materiale, il caricamento sia con uno che con l'altro.*
*Al termine, si è effettuato lo studio del rilascio di farmaco in urina artificiale, confrontando il comportamento del campione fatto con lo stesso materiale, ma con diverse percentuali di polvere di ZnO all'interno.*
*Per misurare la quantità di farmaco assorbita e rilasciata, si sono utilizzati come strumenti la bilancia per il primo caso e la spettroscopia UV nel secondo.*

*Il rilascio è stato fatto in diverse condizioni di pH dell'urina artificiale: fisiologico (7.3), basico (9.3) e acido (5.2).*

*Prima dell'assorbimento di farmaco e dopo lo studio di rilascio, sui campioni si sono effettuate alcune prove di caratterizzazione come FESEM ed EDX, Spettroscopia IR e analisi XRD.*

*I risultati sono esposti all'interno del lavoro di tesi esposto di seguito in lingua inglese.*

# Indice

# 1. Introduction

Nanotechnology represents an innovative approach of study in the field of materials science.
One of the main reasons of interest is the possibility to synthesize functional materials with dimensions lower than 100 nm. This order of magnitude is comparable with the dimension of biomolecules inside cells (J. W. Rasmussen, 2010).

Therefore, there are a lot of applications of nanomaterials in the medical and biological fields, such as separation and purification of biological molecules and therapeutic applications against cancer cells. In the last case, different approaches both involving the use of nanomaterials have been developed. The first one deals with the delivery of drug molecules by porous nanocarriers or by stimuli-responsive nanomaterials, like the temperature increase (hyperthermia). The second one is a diagnostic approach through the detection of specific proteins and antigens related to pathogens.
The first therapeutic approach mentioned before is generally referred to as *drug delivery*. It is an alternative and innovative method by which a drug can be delivered locally and by maintaining efficacious drug levels over the course of device effects. In general, the ability of systems to effectively work for drug delivery applications are assessed with regard to their functional characteristics, effectiveness as a monotherapy, as compared to scaling and root planning, and ability to enhance conventional therapy (Greenstein G1, 1998 May).

Conventional drugs, for example, involve the formulation into a suitable form, such as a compressed tablet for oral administration or a solution for intravenous administration. These formulations have been found to have strict limitations in terms of higher dosage required, lower effectiveness, toxicity and adverse side effects.
New drug delivery systems have been developed or are under investigation to overcome the limitation of the conventional drugs. The therapeutic benefits of new drug delivery systems include (Vaidhya, 2017):

- Increased efficacy of the drug;
- Site specific delivery;
- Decreased toxicity/side effects;
- Viable treatments for previously incurable diseases;
- Potential for prophylactic applications;
- Better patient compliance.

The method by which a drug is delivered can have a significant effect on its efficacy. Some drugs have an optimum concentration range within which maximum benefit is derived, and concentrations above or below this range can be toxic or produce no therapeutic benefit at all. On the other hand, the very slow progress in the efficacy of standard treatments against severe diseases has suggested a growing need for a multidisciplinary approach to the delivery of therapeutics to targets in tissues.
New strategies, called drug release systems are born starting from these needs. These systems are based on interdisciplinary approaches that combine together polymer science, pharmaceutics, bioconjugate chemistry, and molecular biology. Current investigations in the field of drug release systems are focused on minimizing drug degradation and loss, preventing harmful side-effects and increasing drug bioavailability and the fraction of the drug accumulated in the required zone.

According to the type of targeting and of carriers, different kind of systems can be defined, as outlined in Figure 1.

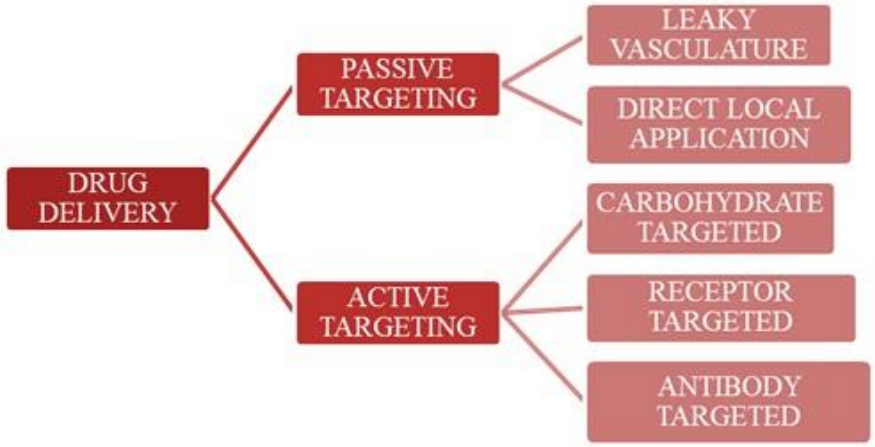


**Figure 1** Types of drug delivery.

Targeting is the ability of driving the drug-loaded system to the site of interest, and it can be distinguished in two mechanism: active and passive.

The *active* targeting involves the surface functionalization of drug carriers with ligands that are selectively recognized by receptors on the surface of the cells of interest. Since ligand–receptor interactions can be highly selective, this could allow a more precise targeting of the site to be reached. Among drug carriers, the most diffused ones include soluble polymers, microparticles made of insoluble or biodegradable macromolecules or inorganic materials, natural and synthetic polymers, microcapsules, cells, cell ghosts, lipoproteins, liposomes, and micelles. The carriers can be made slowly degradable, stimuli-reactive, (such as temperature- or pH-sensitive), and even targeted (e.g., by conjugating them with specific antibodies against certain characteristic components of the area of interest).

*Passive* targeting facilitates the localization of nanovectors within the site to be treat, i.e. tumor microenvironment, owing to distinctive characteristics inherent to the tumor and not normally present in healthy tissues, i.e. the Enhanced Permeation and Retention (EPR) effect.
The successful delivery of nanoparticles to the site of interest is determined by factors associated with the tumor microvasculature, in addition to factors inherent to the nanoparticle itself, such as size, shape and surface charge (Bazak R, 2014).

Furthermore, controversies associated with local delivery are addressed, such as the induction of bacterial resistant strains, the efficacy of systemic versus local drug delivery, and whether local drug delivery should function as an alternative or as an adjunct to conventional treatment (Greenstein G1, 1998 May).
Ureteral stents represent a minimally invasive alternative to restore urinary drainage whenever ureteral patency is deteriorated or is under a significant risk to be occluded due to extrinsic or intrinsic etiologies (Abdulrahman Al-Aown, 2010).

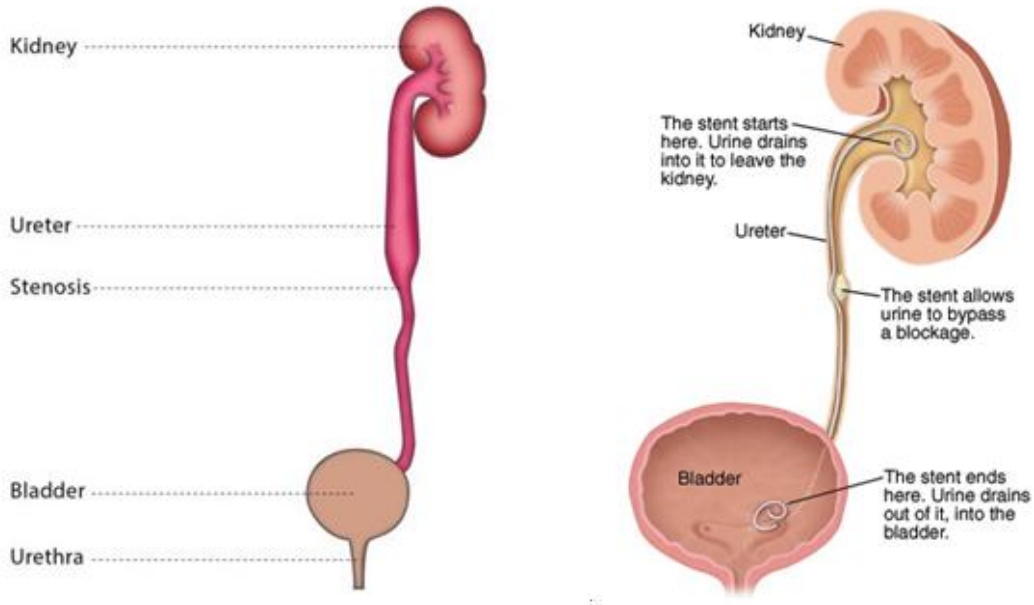


**Figure 2** Ureteric stenting.

Nowadays, the use of ureteral stents is a conventional and routinely practice. However, it shows a huge number of drawbacks due to the absence of material optimization and lack of advanced performances, in particular with respect also to the advancement conducted in the other field of cardiovascular stents.

Ureteral stents show several limitations, such as encrustations of the system by precipitation of inorganic salts from urine and formation of bacteria biofilm, with consequent antibiotic resistance, persistence of the infections, morbidity, urinary retention, ureteral damage, and in the worst cases pyelonephritis and sepsis. As a consequence, all these drawbacks lead to significant patient discomfort (pain, urgency, frequency) and it is necessary a second surgery to remove or replace the stent, supported by an alongside antibiotic, analgesic or others drugs treatments (Luo Yang, 2015 Oct). As a result of frequent re-hospitalization, an increase in public health costs are also evidenced.
The whole of all these drop-down drawbacks is the cause of the difficulty to have a long-term efficacy. For these reasons, the research community is interested to study how to optimize the materials commonly used for ureteral stents, in order to reach the best medical treatment in the shortest time and with the most comfort for the patient.
Several approaches have been investigated over the past decades to modify the stent itself. These strategies include changes to the device design, optimization of the polymeric composition, the use of surface coatings to prevent bacteria and inorganic encrustation, and other advanced applications like drug-elution or complete stent biodegradation to avoid further re-hospitalization (Luo Yang, 2015 Oct).
In particular, both the drug delivery and biodegradability of new generation stents have been successfully demonstrated over time in various pre-clinical studies. For the former, the literature studies showed that antibiotics-coated stent allowed a local release of the drug in the ureter, reducing stent colonization both in vitro and in vivo. Concerning the latter, bioabsorbable materials have also been designed to reduce infections, symptoms and prevent the forgotten stent syndrome (Hilary Brotherhood, 2014 Sep).

The focus of this Master Thesis work is to optimize a composite nanomaterial to obtain efficient antinflammatory drug release, intrinsic antibacterial properties and final biodegradability of the biomedical device in view of fabricating smart and innovative drug-eluting ureteral stents.

To achieve such a challenging goal, the composite is made by the polymer Poly(2-hydroxyethyl methacrylate) (also called polyHEMA) or the crosslinked co-polymer poly(2-hydroxyethyl methacrylate)-co-poly(acrylic acid) (or poly(HEMA-co-AAc)), both showing biodegradability and even swelling properties in different water solutions.
The filler of the composite is a Zinc Oxide (ZnO) powder, characterized by a desert rose-like morphology, i.e. with a high surface area ideal for drug uptake and retention. Furthermore, the use of ZnO give antibacterial property to the whole nanocomposite, in order to prevent the bacterial adhesion and the consequence infection of the urinary tract (Nadia Garino P. S.-B.-R., 11th April 2019).
ZnO is also biodegradable, easily dissolving in water solution at pH below 5.5 or in water solution rich of salts like phosphates (B. Dumontel, 2017).

It is therefore clear that the use of ZnO powders in the composite material, with such particular morphology, can give many advantages. The high surface area available allows to load an adequate amount of antinflammatory drug. The inclusion of the ZnO powder into a polymeric matrix also allows to obtain a sustained release of the drug over time and to limit the burst-release effect typically observed for ZnO-based systems (Laurenti, 2018).

It is also known that high concentrations of zinc cations, released from ZnO during dissolution, produce important antibacterial effects (Nadia Garino P. S.-B.-R., 11th April 2019), as it is explained in the following paragraphs.

It can however happen that ZnO could produce a cytotoxic effect also on healthy cells over a certain concentration (Nadia Garino T. L., 2019), (B. Dumontel, 2017). For that reason, including the ZnO powder into the biocompatible polyHEMA matrix makes sure that the nanomaterial itself is not directly in contact with the ureteral epithelium. As a result, it can be possible to appropriately tune and even increase the amount of ZnO in the composite, in order to increase its antibacterial effect without being harmful for cells.
For this reason, three different percentages of ZnO powders were added in the two polymeric compositions, polyHEMA and the crosslinked poly(HEMA-co-AAc), for the final composite samples preparation.

Afterward, two different antiflammatory drugs were loaded: Ibuprofen and Diclofenac. Both were used in sodium salt form, which allowed to dissolve the drugs simply in water, without using particular organic solvents which can result toxic, both for the operator and for the final composite formulation.

Finally, different experiments in simulated urine solution were performed in order to study the release profile of both drugs, and the degradation behavior of the whole composite material, even at different pH, to simulate various pathological conditions.

The final results show that there is not a real relation between the amount of ZnO in the material formulation and the amount of drug absorbed and/or released. Despite this, it has been studied a new material suitable in the field of ureteral stent, which is innovative, smart and with multifunctional properties such as antibacterial, drug elution and biodegradability.

### *1. 1 Drug Eluting Stent (DES)*

As discussed earlier, the patient discomfort caused by the stent placement is a significant factor in quality of life taken into account by urologists. A commonly used management strategy for stent discomfort is through oral agents, even if this treatment method could be not efficient, due to the systemic action, or could be associated with the possible side effects because of the high concentrations needed.
For these reasons, the use of local drug delivery has been explored as an alternative, by assessing both drug-coated and drug-eluting devices (Luo Yang, 2015 Oct).

The use of DESs in the ureter or urethra is based on the same concept as the use of DESs in coronary vessels, by releasing cytostatic drugs in a controlled fashion.
On the other side, both ureter and urethra are physiologically and histologically different in comparison to the artery, which means that the ideal combination of design, material and drug must be object of studies.
The urothelium comprises a special barrier, which minimizes crossing of substances and the efficiency of the drug coming from DESs may be compromised.
Drug-eluting polymeric and biodegradable stents have been tested with the aim to minimize long-term problems related to the Stents positioning and permanence in the urinary tract.
Even if the tests have been conducted in experimental animal studies and clinical trials only, they have shown favorable results. (Panagiotis S. Kallidonis, 2014).

### *1. 1.1 Stent's Materials*

A biomaterial is defined as a natural or synthetic substance that interfaces with tissues.
By increasing biocompatibility, there is a decreased reaction of the human body on the stent biomaterial and consequently a better integration.
Ureteral stents can be used as a temporary measure in order to prevent damage to a blocked kidney, until a procedure to remove the stone is performed. Indwelling times for these cases are typically from 15 up to 60 days and in this case polymeric-based stents are more common.

The most common biomaterial currently used in this field are synthetic polymers or copolymers such as silicone, polyethylene, polyurethane.

*Silicone* is the "Gold standard" in terms of biocompatibility, that allows to decrease onset of infections and encrustations, and is one of the most lubricious materials currently available.
Nevertheless, it is hardly used because of its softness and high friction coefficient, that can cause a difficult implantation in presence of obstructed or tortuous ureters or extrinsic compression.

On the other side, *polyethylene* results to be stiffer and consequently easier to insert, but it has biocompatibility and stability issues that may lead to stent's fragmentation in long-term applications. For these reasons it was no longer used for stent manufacturing.

Lastly, *polyurethane* (PU) combines the elastic properties of silicone with the rigidity of polyethylene. Thanks to these features, it is one of the materials that are nowadays used in stents, together with *polyvinyl chloride (PVC)* and *ethylene vinyl acetate (EVA)*. It is obtained from the reaction of polyol, isocyanate and a chain extender. By choosing properly these reagents, it is possible to control the mechanical properties of the device, which are different for each application.
It is particularly suited to biomedical industry due to its versatility and low cost.
Compared to silicon and polyethylene, it is less biocompatible than the first, but it has the same stiffness of the latter.
These features have reported some common drawbacks, such as epithelial ulceration and erosion in animal studies or discomfort in patients (Matthias Beysens, 1 February 2018;).

*Metal*-based stents have been developed in last years with the objective to overcome the disadvantages of polymeric-based ureteral stents, including the low load resistance and problems regarding the implantation.
Metal-based stents, as polymeric ones, have problems like biofilm formation, infections and migration; in addition, the characteristic problem of this class of materials is that it induces local tissue hyperplasia, with an uncontrolled growth of endothelial tissue.
Hence, the causes of failure of metal-based stents are mainly due to patient's pain, renal insufficiency, stent migration fungal infections, hyperplastic reaction and encrustation with an average indwelling time of 8 months.

To overcome all these complications, associated to both polymeric and metal ureteral stents, it is usual to chemically functionalize the stent surface with organic and biologically active molecules, in order to obtain a more biocompatible integration and control oveer some biochemical reaction and transduction pathway at the same time.

While the optimization of the superficial functionalization of these material is going on, the next generation of ureteral stent is under development.

The main aim is to overcome the present ureteral stent complications, such as the second procedure of removal and even the "forgotten stent" phenomenon, which is when the ureteral stent remains more time than it is necessary for the treatment, leading to bacterial infections and more serious cases of encrustation.
Concerning ehancements in quality life, they should be designed in order to have a more confortable device for patients.
This third generation that is still under development, consists in biodegradable ureteral stent, with an avarage degradation profile of 2-4 weeks; the main materials used are biodegradable copolymers similar to those used in absorbable sutures.
The degradation should be engineered to occur directional from the distal to the proximal end, in order to avoid ureteral obstruction by fragmants.
Also in this new technology it is possible to incorporate drugs, which are released by a different mechanism than classical DES; the kinetic of release is therfore subject to the intrinsic degradation rate of the material (Matthias Beysens, 1 February 2018;).
In order to be used in biodegradable ureteral stent, the biomaterial should be biocompatible and maintain intact the properties after sterilization. The degree of swelling and degradation rate should take into account the treatment time, always ensuring the flow of the urine from the kidney to the bladder.

Advantages of the degradation have mainly affected problems concerning biofilm and encrustations formation. Beside the fact that the biodegradable ureteral stent can be "forgotten" without becoming a site of colonizzation, another important benefit is the constant changing of physical properties of the surface due to the stent erosion that aims to ostaculate the bacterial and salts adhesion.

Additionally, biodegradable materials are softer than permanent polymers or metals, and thus they might be favorable for patient comfort.
Materials used in the design of biodegradable ureteral stents can be divided in synthetic materials, natural origin materials and also metal biodegradable materials, which are more recent.

The most common *biodegradable materials* used in ureteral stents' field are Polylactic Acid (PLA) and Poly(Lactic-co-Glycolic Acid) (PLGA).
Results obtained from studies on the first polymer have shown good drainage characteristics with antireflux properties, complete degradation after 12 weeks and a good biocompatibility of breakdown products.
On the other side, PLGA's studies in animals have reported good flow characteristics, with correct drainage and antireflux properties, as seen in PLA's analysis, but an unsatisfactory biocompatibility that it was not possible to dispel.
Compared to stable ureteral stent, the third generation of stents seem to support an excellent drainage combined with a lower rate of irritation.
The main problem lies on the mechanism of degradation that characterizes the largest used materials in biodegradable ureteral stents, which is hydrolysis. This way of degradation tends to create blocks that can compromise the urine flow and can become the starting point for bacterial adhesion and biofilm formation.

Regarding *natural origin materials*, the most studied formulations are alginate-polymer-based and polysaccharides-based ones. These materials present a very high biocompatibility, but they are unable to maintain the proper mechanical properties for all the time of the treatment.
Moreover, the degradation rate has proved to be insufficient and has resulted in the need of a second intervention to remove the fragments from the patients' body (Alexandre Barros, December 2017).

### *1. 1.2 Drugs*

In addition to find the most appropriate material, ureteral stent design has evolved to include drugs inside.
Drug-eluting technology is an easy method to obtain a multifunctional device and it has been already used extensively in cardiovascular applications.
Different strategies have been studied with different active compounds, and they have shown to be the most promising in the inhibition of bacterial adhesion, biofilm formation and encrustation, and for avoiding inflammation of the urothelial tissues.

Four categories of pharmaceutical agents could be used on ureteral DESs: anti-inflammatory, anti-bacterial, anti-proliferative and immunosuppressive drugs.
To name a few, some strategies have been tested recently in vitro, on animals and also on human, which are:

- Zotarolimus eluting stent (ZES);
- Triclosan eluting stent;
- Chlorhexidine (CHX) eluting stent;
- Rifampin and tigecyline immersed ureteral stents;
- Ketoprofen-eluting biodegradable stent.

The effect of *Zotarolimus eluting stent* has been evaluated in the porcine and rabbit ureters in order to minimize the hyperplastic reactions, which are the negative effects mostly related to bare-metal stent (BMS) application.
Results of several studies have shown that hyperplastic reaction occurred in both stent types, but in ZES did not result in obstruction, as in case of BMS.
The action of Zotarolimus, which is a semisynthetic derivative of the immunosuppressive rapamycin, is based on the inhibition of smooth muscle cell and T-cell proliferation, by binding on FK-506 binding protein-12 (Panagiotis S. Kallidonis, 2014).
Comparing the inflammation rate, it was present in all ureters without any significant difference among stent. This means that the main aim of Zotarolimus elution is to prevent hyperplastic reactions, which lead to the failure of the implant (Karnabatidis, October 2011).

Concerning the pharmacokinetics, the chemical properties of this agent allow to obtain a slow release rate, in order to favor efficient drug distribution.
In studies made on Zotarolimus-coated balloons to treat peripheral vascular disease, the pharmacokinetic of this agent has been calculated accurately.
Its kinetics exhibited a first order release profile, described by the following exponential equation:

$$J_b(t) = A_1(1 - e^{-k_1 t})$$

with constants $A_1$ and $k_1$ have been estimated as 24 μg/cm$^2$ and 0.009221 s$^{-1}$, respectively ($R^2$ = 0.9999) (Vijaya B. Kolachalama, 2013).

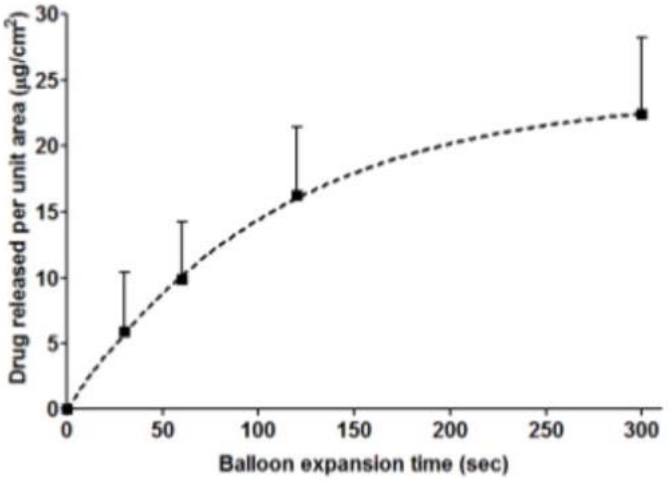


**Figure 1.1.2** Zotarolimus release per unit area of each balloon during the latter's expansion at different times **(Vijaya B. Kolachalama, 2013)**.

Regarding the adverse effects reported by patients undergoing ureteral stenting, the most frequent have been pain and urinary tract difficulties, also caused by infections and encrustations. By the way, no current ureteral stent or exogenously applied therapy adequately deals with these problems.

*Triclosan* is a broad-spectrum antibacterial agent widely used in numerous healthcare products and has been previously shown to reduce inflammation on the skin and in the oral cavity.
Several studies have been conducted in order to test the ability of triclosan-impregnated ureteral stent to reduce infection and encrustations and consequently to reduce patience's pain.
Nevertheless, it has been observed that the addition of this agent in eluting stents was ineffective to reduce infection rates. However, it was able to reduce several common ureteral stent-related symptoms, including pain during indwelling.
Hence, these studies aimed to discover that this eluting system may have a role in treating patients, better if used in combination with standard antibiotic therapy.
Despite this, this stent is no longer clinically used because it may induce bacterial resistance (Mendez-Probst CE1, 2012 Sep).

The inefficiency and drawbacks related to the use of antibiotic treatments is the reason why the quest to reduce stent infection continued to this day.
Alternative methods may require the direct incorporation of antibiotics or antiseptics to the stent, in order to use a lower amount of drug and to become an effective tool.
An example of this type of drug, used as coating stent, is *chlorhexidine*, which has demonstrated promising results against different type of common urinary pathogens.
In particular, an in vitro model study was prepared in ethyl cellulose, polyethylene glycol, and KlucelTM EF, in order to estimate the chlorhexidine release and its effect against the following bacteria: Enterococcus, Escherichia, and Pseudomonas.
It has been observed that the antimicrobial effect could be prolonged by increasing the concentration from 1% to 2% SRV (SRV= sustained release varnish).
Moreover, by using a varnish to incorporate the active agent, a more stable and controlled system was obtained, characterized by a slow release and essentially prevented colonization for all the bacteria tested.

The observed inhibitory effects against bacteria also suggested that this technique might play a significant role in reducing ureteral stent-associated urinary tract infection (UTIs) (Zelichenko G1, 2013 Mar), (Hilary Brotherhood, 2014 Sep).

In particular, to fight infections due to Enterococcus faecalis, the efficacy of combining *tigecycline* and *rifampin* together has been investigated.
These two different antibiotics are directly included together in the coating of the stent, and their effects have been tested even in a concentration-dependent manner.
Tigecycline has exerted stronger bactericidal effects than rifampin, but it has been observed that tigecycline had a Minimal inhibitory concentration (MIC) and Minimal bactericidal concentration (MBC) lower than when it was used in absence of rifampin.
These results highlighted the potential usefulness of tigecycline in preventing enterococcal ureteral stent infections and the role of rifampin as an interesting antibiotic enhancer (Minardi D1, 2012 Jul).

Another drug recently used to cover metallic stents and also polyurethane covered stents, is *paclitaxel*, which has been tested in urethra of dogs and in ureter of porcine model, using the commercially available paclitaxel-eluting stent.
In the first experimental animal study, the analyses were performed after 2 different times of follow-up, 4 and 8 weeks, performing histologic evaluation of the stented urethras.
Paclitaxel is known for its action in stabilizing the microtubules, which are necessary for the transition of the cell cycle from phase G2 to M-phase, by the polymerization of the subunits of tubulin. Moreover, it inhibits the proliferation and migration of smooth muscle cells, decreasing hyperplastic reactions.
Actually, after 4 weeks of the experiment, a significantly lower hyperplasia in urethra could be observed (Panagiotis S. Kallidonis, 2014).

Although incredible progress has been made, none of the technological developments have led to the "ideal stent", especially in term of material biodegradation combined with the most appropriate drug-eluting technologies.

## *1. 1.3 Biofilm formation and antibiotic resistance*

Medical devices provide a surface for bacterial biofilm formation. The biofilm lifestyle may turn normally harmless, commensal bacteria into pathogens and is associated with increased antimicrobial resistance.

Bacteria biofilm refers to the complex combination of microbes found either attached to a surface or buried firmly in an extracellular matrix as aggregates. The biofilm matrix surrounding bacteria makes them resistant to hostile environmental conditions like starvation, desiccation and makes them capable to cause a broad range of chronic diseases.

The dense environment of the biofilm allows bacteria living inside to have significantly different properties from free-floating bacteria, both in behavior and in phenotypic. For example, they are surrounded and protected by the film, and it allows them to cooperate and interact in various ways. This condition makes them less susceptible to prophylactic antibiotics and increases their resistance to detergents (F. Cauda, 2009).
To date, this increasing resistance has become an emergency because it has really become difficult to treat bacteria with efficacy. Antibiotic resistance has been accelerated by the misuse and overuse of antibiotics, as well as poor infection prevention and control.
Furthermore, the antibiotics available till date have higher values of minimum inhibitory concentration (MIC) and minimum bactericidal concentration (MBC). That means they are ineffective for treating bacteria biofilm related infections (Ranita Roy, 2018).
Hence, it is critically important for implants to be designed and superficially functionalized in order to be intrinsically antibacterial or bactericidal. In this way, the bacterial adhesion (antibacterial effect) or the biofilm formation (bactericidal effect) is prevented.

In order to design areas with the properties mentioned above, it is necessary to understand the mechanism of biofilm formation, which includes nature and structure of biofilm, nutrient and oxygen availability to the bacterial cells and intrinsic and acquired bacterial resistance. Furthermore, considerations should be given to different models and various methods used for biofilm detection.

Biofilm formation on any surface involves mainly 3 stages.

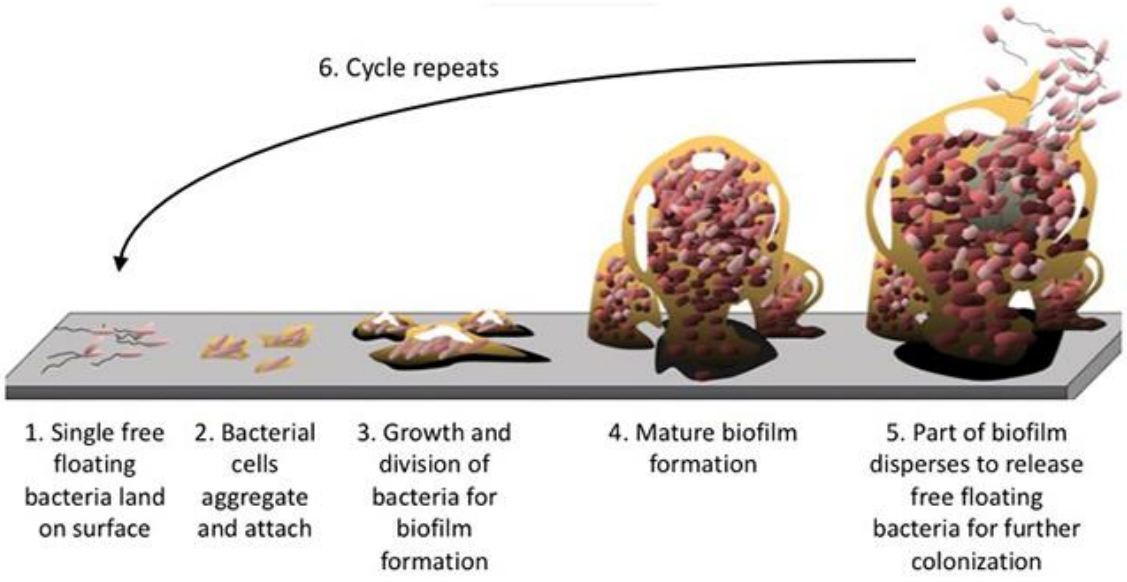


**Figure 1. 1.3** The life cycle of biofilm.

As shown in the Figure 1.1.3, the first stage (1) involves the floating of bacteria on the surface, followed by (2 - 3) the adhesion and the aggregation of the cells to form microcolonies. Finally (4) the differentiation leads to the formation of biofilm into a mature structure. After the complete development of biofilm, (5) its disassembly or dispersion takes place through both mechanical and active processes. Deposition of bacteria is especially mediated by sedimentation, Brownian motion and hydrodynamic forces, whereas adhesion to the substratum is governed by Van der Waals, acid–base, hydrophobic, electrostatic interaction forces.

In biofilms, the bacterial cells are enclosed in an extracellular matrix, which is a complex and highly polar mixture of biomolecules including proteins, polysaccharides, nucleic acids and lipids. The matrix provides protection from various stress conditions such as antimicrobial exposure or immune cells attack. However, the matrix of the biofilm does not act as a mechanical barrier for the antimicrobial agent.
Once the bacteria start secreting extracellular polysaccharide substance (EPS) continuously, starts the irreversible process of development of the biofilm, till reaching the safe attachment of bacteria to the surface. The mature biofilm includes small channels, which transport nutrients, water and waste for the bacteria, which in general become more resistant to hard conditions while they are inside the biofilm.
At the end of the cycle, large parts of the biolfim are sloughed off and get detached, emptying the cavities floating bacteria and allowing the release of fresh bacteria into the environment (Ranita Roy, 2018).

Despite the drug resistance emergency, antibiotics are still orally administered whenever stent is replaced or inserted for preventing infections, because these approaches have been proved to be mostly ineffective.
For these reasons, stent surface modifications have been proposed to prevent bacterial and inorganic molecule adhesion (Cauda, 2012).

In this work, the intrinsically antibacterial effect is given by the inclusion of ZnO powders inside the polymer in order to solve the root of the bacterial adhesion problem.

### *1. 1.4 Encrustation of ureteral stent*

As previously mentioned, ureteral stenting is a common surgical procedure to preserve urinary drainage and to treat ureteral obstruction, which is often caused by urinary stones or malignancy.
However, several complications are associated with stent use. Beside the risk of infection in the short-term application, which can lead to damage of the parenchymal, also the long-term stent use is associated with infection and precipitation of salts from the urine, which can lead to a build-up of crystalline deposits on the stent surface, making stent removal difficult and painful.
Urease producing bacteria in the biofilm seem to be the most likely cause influencing encrustation of the stent surface.

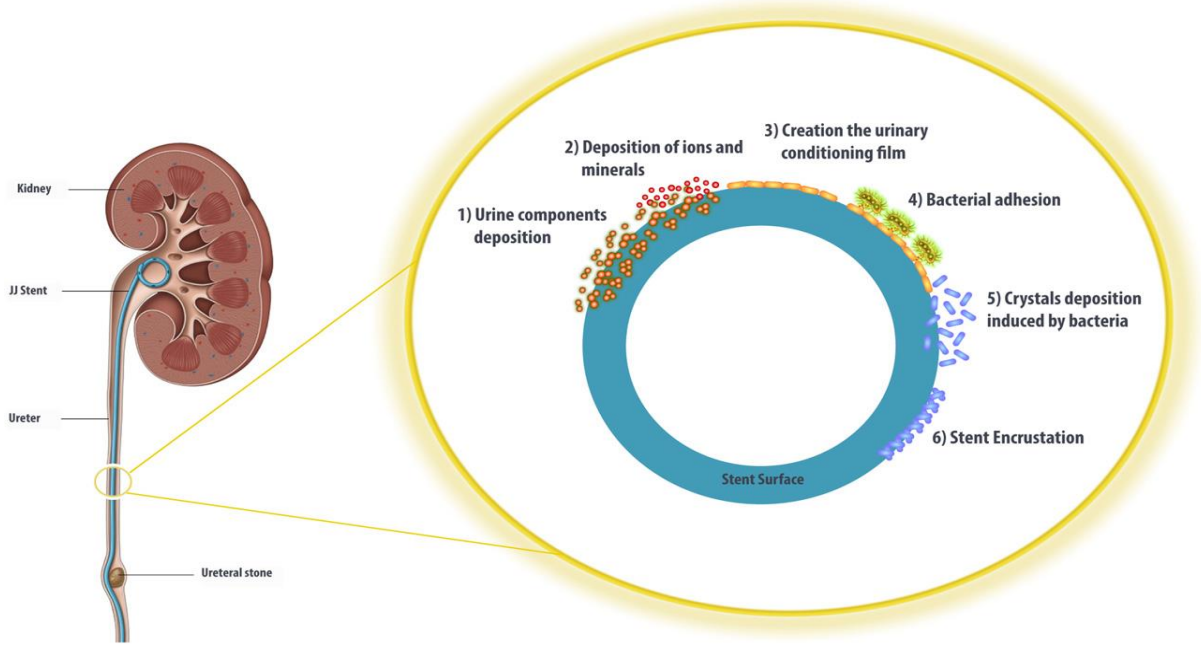


**Figure 1. 1.4 (1)** Mechanism of bacterial adhesion, after ureteral stent insertion: (1) Interaction between urine components deposits and stent surface, (2) deposition of minerals, (3) formation of the suitable environment for the film formation, (4) bacterial adhesion and consequently infection. (5) Interaction of ions and minerals with biofilm components and bacterial induced crystallization and the precipitation of encrustation in the stent surface **(Alexandre Barros, December 2017)**.

Stent encrustation is the major problem and an extremely difficult one to prevent, and it may block urinary drainage, resulting in patient symptoms or significantly complicate stent removal (Matthias Beysens, 1 February 2018;).
In the Figure 1. 1.4 (2) below, is shown how a stent covered by salt encrustations appears.

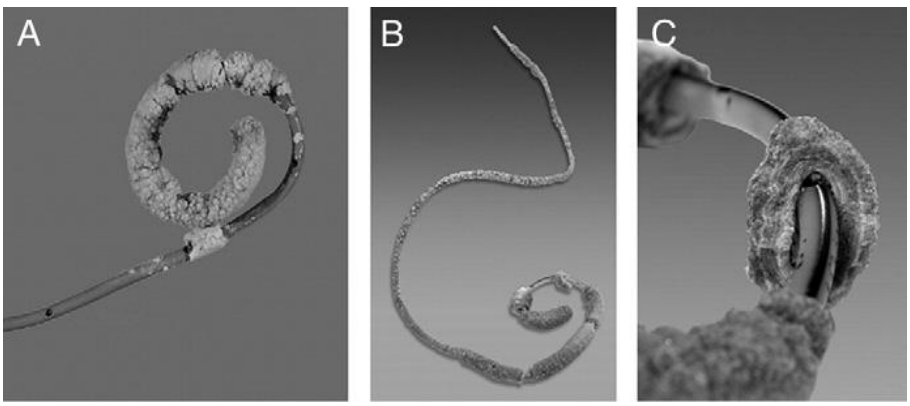


**Figure 1. 1.4 (2)** Problem of phosphate salt mineralization after only few weeks of indwelling. Massive struvite/carbonate hydroxyapatite mineralization after A) 8 weeks and encrustation after. B) - C) 7.5 months of indwelling (Norbert Laube, 1 May 2007).

When in contact with urine, ureteral stents become frequently covered by calcium phosphate and calcium oxalate crystal-containing encrustations which can contribute to damage the uroepithelium produce patient's pain and have been proposed to promote infections.
Moreover, the application of ureteral stent is necessary to patients which have already problems to the urinary tract. That means they present a pathologic urine which is richer of salts and pathogens, such as *Proteus mirabilis* and *Pseudomonas aeruginosa*, that are known to promote crystal growth.

In addition to these mentioned bacteria, other common urinary tract pathogens such as *Escherichia coli* or *Enterococcus* have been identified in ureteral stent encrustations (Matthias T. Buhmann, 2019 Apr 13).

Bacteria seem to be involved in salts deposition because after the biofilm formation, ammonia is produced by urease-producing bacteria, infecting the urinary tract and stent. The consequent pH increase of the urine causes the precipitation of inorganic compounds, such as the crystallization of calcium oxalate, magnesium ammonium phosphate (struvite) and calcium phosphates (hydroxyapatite and brushite) (V. Cauda, 2016), (F. Cauda, 2009).
Figure 1.1.4(3), taken by the study made in the article 'Encrustations on ureteral stents from patients without urinary tract infection', shows the SEM image of dominant crystalline phases in ureteral stent encrustations (Matthias T. Buhmann, 2019 Apr 13).

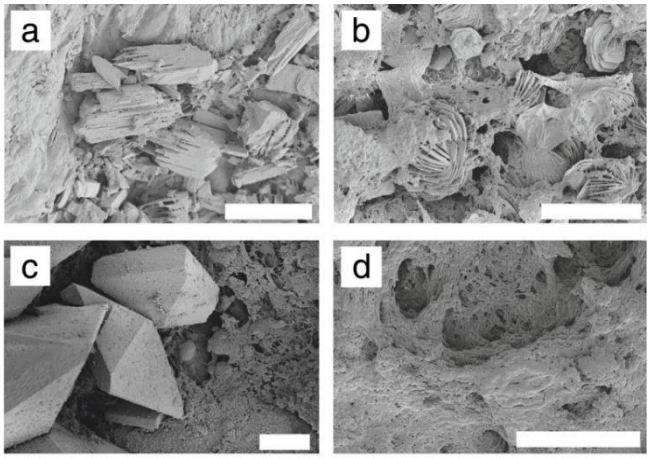


**Figure 1. 1.4(3)** Representative scanning electron micrographs of dominant crystalline phases in ureteral stent encrustations. Scale bars = 10 μm. A) Dicalcium phosphate dihydrate. B) Whewellite. C) Weddellite. D) Absence of crystals, organic deposits. E) Distribution of encrustation biomass.

The bulk of the encrustations consists of crystals or fibrous organic deposits.
SEM imaging indicated thick crystal-containing layers in more than 50% of the samples, frequently in tetragonal dipyramidal shape indicative for weddellite (calcium oxalate dihydrate, $CaC_2O_4 \cdot 2H_2O$), or in prismatic shape indicative for whewellite (calcium oxalate monohydrate, $CaC_2O_4 \cdot H_2O$) (panels b, c of Figure 1. 1.4(3)).
In a low number of samples, however, crystalline material seemed to be absent according to SEM and XRD analyses, despite of high biomass, as determined by weighing the abraded encrustations (panel d of Figure 1. 1.4(3)).

### 1. *1.5 Solution to overcome biofilm and encrustation problems*

The first step to prevent the biofilm formation and salt deposition by ensuring the proper integration of the construct in the body at the same time, is to choose the correct biomaterial for stent.
As mentioned above, the most common material used for ureteral stents is the polyurethane (PU), manufactured with the correct shape (double-J stents).

To date, temporary preventions from encrustation have included stent replacement at regular intervals, washing with acidic and antiseptic or saline solutions.
However, all these approaches are mostly ineffective and for this reason new strategies, some showed in Figure 1.1.5 (1), have been proposed.

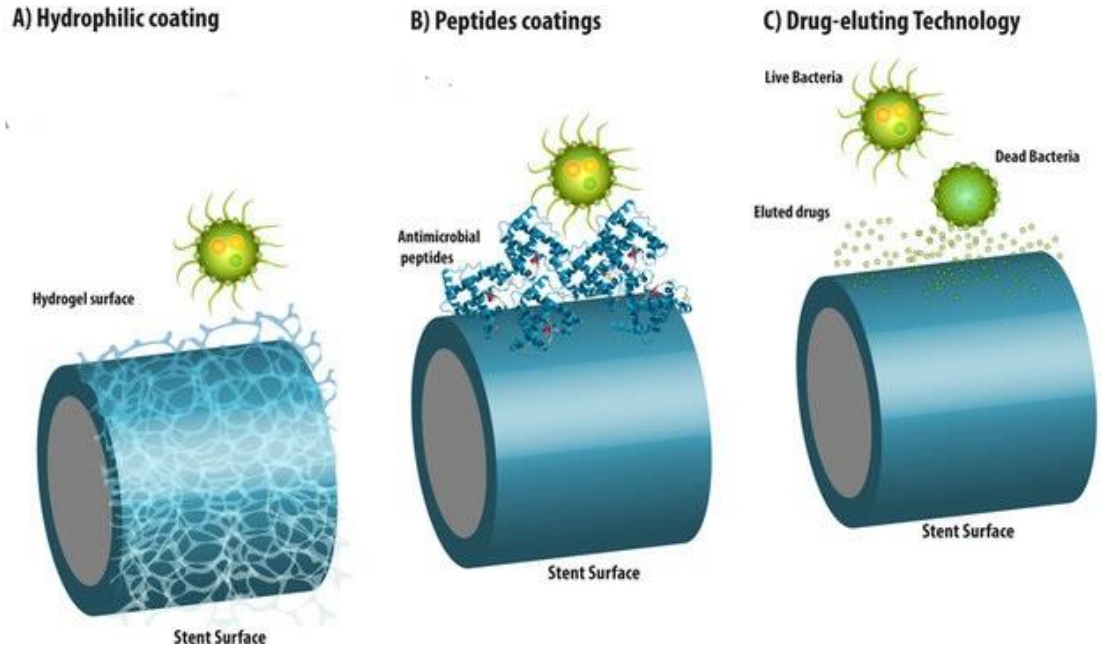


**Figure 1.1.5 (1)** Strategies to avoid the ureteral stent-associated problems, (A) Hydrophilic coatings form an external film of water and decrease the bacterial fixation. (B) Coatings with antimicrobial peptides, avoid the bacterial reach the stent surface and break up the bacterial membrane. (C) Drug-eluting technology, stent release specific drugs (antibiotics) in the ureter, allowing it to interact with the bacteria (Alexandre Barros, December 2017).

To increase biocompatibility in order to reduce device-associated biofilm formation or encrustations, or even to decrease the surface friction coefficient facilitating stent manipulation, several different coatings have been applied on stent surfaces (Matthias Beysens, 1 February 2018;).

The study made in the chapter “Polyurethane in Urological Practice” (Cauda, 2012), compares the uncoated PU and PU with two different strategy of surface modification: Heparin and Diamond- Like Carbon (DLC, also known as amorphous carbon).
The first is a highly sulfated, anionic polysaccharide with a strong negative electrical charge which makes it able to prevent cells adhesion, since bacterial' cell membrane surface is also
negatively charged. On the other side, Plasma deposited Diamond-Like amorphous Carbon (DLC) coating, is a thermodynamically meta-stable state of carbon, which showed excellent properties of corrosion resistance biocompatibility.
Recent studies have been focused on its ability to decrease the formation of crystalline bacterial biofilm by testing the DLC-coated ureteral Double-J-stents in vivo.

Also previous different works have showed the superiority of both coating, in order to prevent biofilm adhesion and encrustation.
In the heparinized stents, the significant reduction of encrustations was observed, in term of consistency and compactness, with no changes in the layer itself ( (Furio Cauda, 20 Mar 2008).

By different analyses made on the uncoated PU and the PU with the 2 different coatings, bacterial biofilm was not detected at all on the surfaces of the coated PU stents. By contrast, in the former surface a higher level of inorganic encrustation with respect to both surface-modified stents has been observed.
These two types of coating have also shown an excellent and facile placement and removal handling, a less painful replacement procedure and high tolerance of application, reported by physicians and patients and mainly due to the low friction (Norbert Laube, 1 May 2007).

Even if the inhibition in biofilm deposition and encrustation was due to the surface modification, it has been observed that in highly pathological cases, such as in patient with recidivist calculosis, the continuous deposition of biofilm and salts at the stent surface inhibited the reducing effect of the coating (Heparin and DLC both) in preventing encrustation.
Nevertheless, it has been concluded that both the covalent heparin bonding and the coverage of DLC decrease the adhesion of both biofilm and encrustations to the polyurethane surface and ensure their stability for long time.

Other types of coating have been studied for ureteral stent applications, like the hydrophobic Teflon, i.e. the conventional name which refers to polytetrafluoroethylene (PTFE), or even hydrophilic coatings, silver and biomolecules as chitosan.

With reference to the polymer usually called Teflon, it is a hydrophobic compound which displayed superlubricious properties and its main advantage lies on its lowest coefficient of friction (0.05-0.1), even lower than DCL's one.
It could be able to prevent the biofilm formation due to its resistance to van der Waals forces, which are, as said before, the main forces involved during the initial surface attachment.
Despite these features may hold promise against film formation and encrustations in ureteral stent, additional works are needed to evaluate the urinary pathogens' ability to colonize and cause infection on these coatings (Luo Yang, 2015 Oct).

*Hydrophilic coatings*, in particular Polyethylene glycol (PEG), have been deeply studied in stent applications, due to their hydrophilic properties which are at odds with hydrophobic bacterial surfaces and most important allow the formation of a superficial thin film of water which reduces its coefficient of friction and isolates the substrate from surroundings.
Their ability to adsorb a high number of water's molecules prevents the deposition of particular proteins and components, such as fibrinogen or platelets, that may lead bacterial adhesion (Joey Lo, 2014).
Because of PEG's instability during the anchoring process, it has been developed a new approach for attaching PEG to surfaces that includes the use of DOPA, a peptide mimic based on the adhesive proteins used by mussels for attachment in marine environments (Messersmith, 2005).
Tests in vivo of DOPA conjugated PEG have shown effective inhibition in biofilm formation and in particular, the reduction of Escherichia coli adherence (Luo Yang, 2015 Oct).

*Silver* has been widely used, already in the past, for its antimicrobial property characterized by an efficiency that increases with the amount of the compound.

The mechanism by which silver prevent the film formation is well known and is based on the destabilization of bacterial membrane and the deactivation of a lot of bacterial enzymes by strictly binding with these last.
The silver coatings demonstrated good distribution of silver particles to the substrate, with a low amount of silver ion released, and proved an effective antibacterial capability in simulated biological conditions (Ian Richard Cooper, 1 December 2016).
Its combination with other antifouling or antimicrobial strategies could be indicated as a good defense against urinary tract infection.

## *1. 2 Zinc Oxide*

### *1. 2.1 General properties and applications*

Among metal oxides, Zinc Oxide (ZnO) is one of the most studied thanks to his versatility and multifunctionality.ZnO is a white, odorless inorganic solid compound.
This material can arrange itself in 3 different crystal forms, which are wurtzite, zinc-blend and rock salt, as showed in Figure 1.2.1(1).

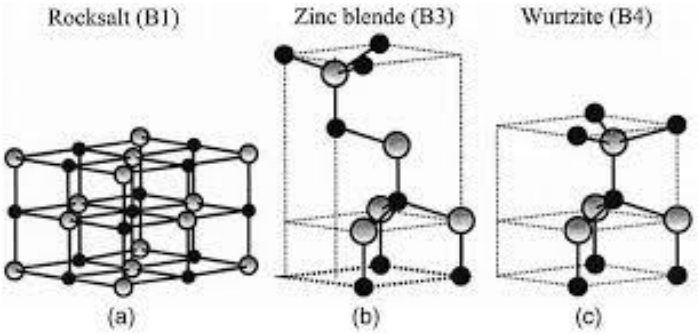


**Figure1. 1.1(1)** Crystal forms of ZnO (a) Rocksalt, (b) Zinc-blend, (c) Wurtzite.

The form that is thermodynamically more stable at room temperature is the wurtzite one, in which each zinc atom is surrounded by 4 oxygen atoms which are arranged to form a tetrahedron. This organization forms an alternating combination of plans that include zinc and oxygen atoms.
The tetrahedra of oxygens are geared in one direction only, resulting into a hexagonal symmetry of the crystal lattice (Ahmed M. Nawar, Jul-Aug. 2014).
ZnO is considered a multifunctional material due to its very interesting physical and chemical properties, which are listed below.

| | |
|---|---|
| Physical appearance | White, colorless, odorless solid |
| Crystalline structure | Wurtzite |
| Molecular Weight | 81.38 g/mol |
| Electron effective mass | 60 |
| Melting Point | 1,975°C |
| Density | 5.47 g/cm$^2$ |
| Isoelectric point | 9.5–10 |
| Space group | $C_{6v}{}^4$-$P6_3mc$ |
| Standard molar entropy | 43.9 J·K$^{-1}$mol$^{-1}$ |
| Standard enthalpy of formation | −348.0 kJ/mol |

**Table 1.2.1** Main properties of ZnO.

It is a material that can be used for a huge number of applications. Its multi-functionality and versatility are also due to the presence of several morphologies characterized by a high surface area, that can be obtained from a variety of synthesis methods.
Some of the most common ZnO nanostructures are shown in Figure 1. 2.1 and can be organized in different classes, which include for instance (Marco Laurenti, 2017 Nov)

- Nantubes and nanowires (a);
- Nanobelts and nanoring (b);
- Flower-like morphology (c);
- Nanosprings (d);
- Multipods (e);
- Nanoparticles (f).

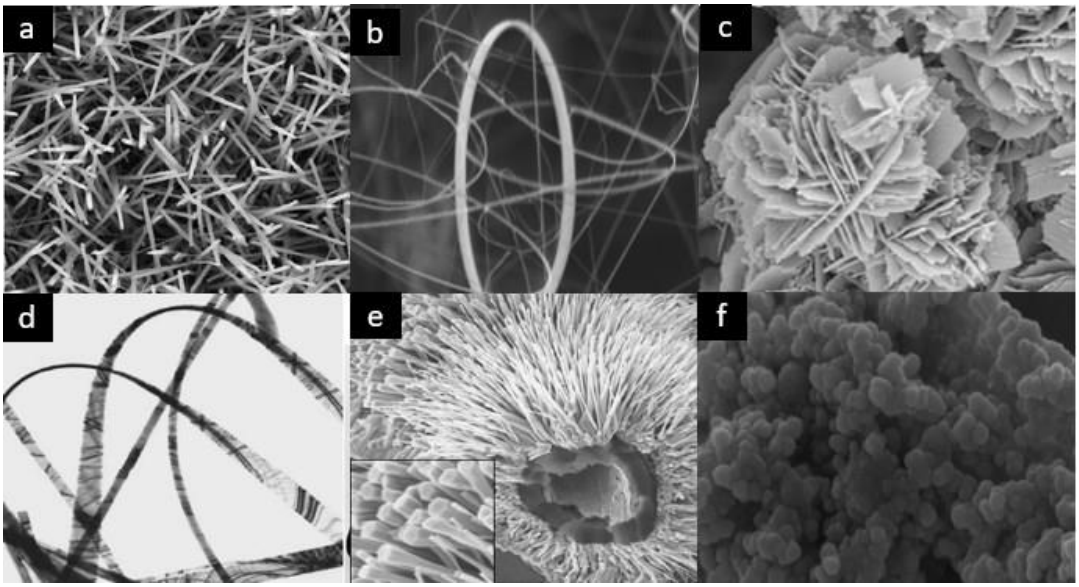


**Figure 1. 2.1 (2)** Different morphologies of ZnO: (a) Nanorods, (b) Nanorings, (c) Flower-like, (d) Nanobelts, e) Nanowires, (f) Nanoparticles.

The possibility to induce the nucleation and growth of different ZnO morphologies mainly depends on the following important parameters: material's composition used as source of $Zn^{2+}$ ions, the growing temperature and the diffusion rate (Valentina Cauda, January 2014).

## 1. *2.2 Antibacterial effect of ZnO*

Nowadays, infections due to both Gram positive and negative pathogens are developing an evolved resistance to conventional antibiotics, impairing the effects of these drugs and posing serious problems to public health in the long term.

A more innovative approach is the use of intrinsically-antimicrobial nanomaterials, where the antimicrobial activity is not as a result of the pharmaceutical effect of an antibiotic, but instead comes directly from the intrinsic properties of the nanosized material.
Among them, zinc oxide (ZnO) is one of the most promising inorganic antimicrobial materials and can overcome bacterial resistance to a certain extent.

It is a material "*generally recognized as safe*" (GRAS) approved by the US Food and Drug Administration (FDA), even if some doubts concerning its potential toxicity to eukaryotic cells at high concentration have to be solved.
The antibacterial activity of ZnO nanostructures is related to three main probable mechanisms:

1) Reactive oxygen species (ROS) generation.
2) Release of $Zn^{2+}$ cations.
3) Electrostatic interactions between ZnO nanomaterials and the bacterial surface.

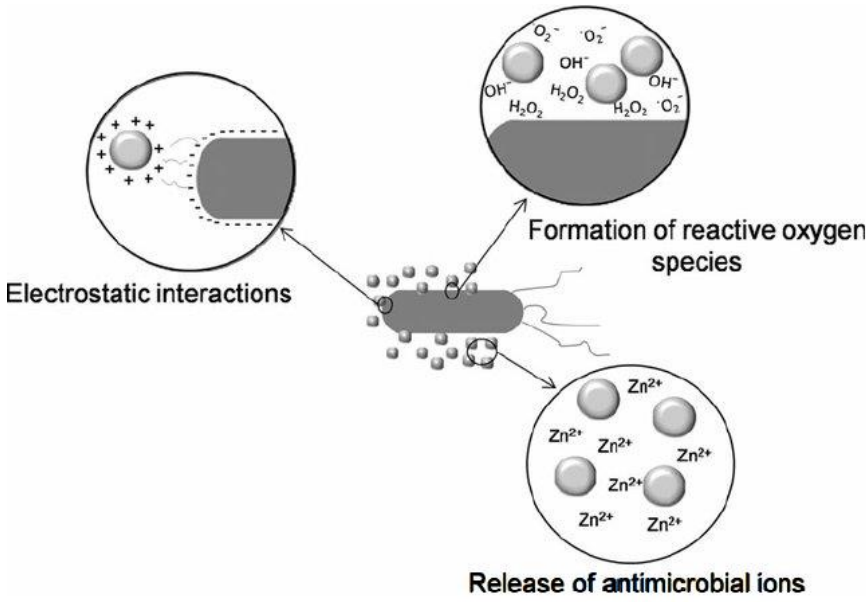


**Figure 1.2.2 (1)** Different mechanisms of antimicrobial activity of ZnO nanoparticles **(Paula Judith Perez Espitia, July 2012)**.

ROS generation is the most important mechanism and is promoted by the presence of crystalline defects in nano-sized ZnO structures. ROS toxicity is due to their high reactivity and oxidizing properties. They can thus destroy the cell wall of different microorganisms, like lipids, as well as other cell components like DNA and proteins.

The formation of ROS starting from ZnO follows the photochemical reactions reported below:

$$ZnO + h\nu \rightarrow e^- + h^+,$$
$$h^+ + H_2O \rightarrow {}^\bullet OH + H^+,$$
$$e^- + O_2 \rightarrow {}^\bullet O_2^-,$$
$${}^\bullet O_2 + H^+ \rightarrow HO_2^\bullet,$$
$$HO_2^\bullet + H^+ + e^- \rightarrow H_2O_2.$$

Due to the semiconductor band structure of ZnO, the electrons ($e^-$) are promoted in the conduction band, whereas unpaired holes ($h^+$) remain in the valence bands. The migration of both $e^-$ and $h^+$ at the surface of the nanomaterials promotes their combination with water-adsorbed molecules, generating ROS, such as hydroxyl radicals, singlet oxygen and superoxide radicals.
Hydroxyl radicals are the most reactive species and they can quickly interact with every type of biological molecules.

The release of $Zn^{2+}$ ions from ZnO nanostructures is another important mechanism in the antibacterial activity of ZnO.
$Zn^{2+}$ ions can adsorb to the negatively charged bacteria surface through electrostatic forces. This interaction leads to the loss of the charge balance and deformations of the cell occur with consequent bacteriolysis.
At the same time, $Zn^{2+}$ can penetrate the cell membrane and interact with functional groups as sulphate and phosphate groups, provoking the destruction of bacteria by unbalanced metabolism and causing the bacterial death.
The anti-bactericide action of zinc oxide is effective for both Gram-Positive and Gram-Negative bacteria. The main difference among them lies on the thickness of the bacterial wall.

This phenomenon is specifically due to the high specific area and surface energy of ZnO nanomaterials, which are able to adsorb and accumulate at the membrane and in the cytoplasm.
Despite these most probable mechanisms against bacteria, the influence of ZnO morphology, chemical reactivity and surface, also the bacteria cell type also has to be considered.
Therefore, the real antimicrobial mechanisms are still under investigation.
It is thus crucial to control the ZnO particles' size, morphology and surface chemistry to efficiently tune the antibacterial properties and the biocompatibility towards healthy cells in case of biomedical implants or drug delivery devices (Nadia Garino T. L., 2019).

In several studies, ZnO nanoparticles has been tested against some Gram-positive bacteria such as *Bacillus subtilis* and *Staphylococcus aureus*, and also against Gram-negative bacteria like Pseudomonas aeruginosa and Escherichia coli.
The latter has shown higher susceptibility to ZnO nanoparticles compared to S. aureus.

The higher resistance of S. aureus to ZnO nanoparticles can be related to its intracellular antioxidant content, which promotes a great oxidant resistance as well as the presence of potent detoxification agents such as antioxidant enzymes.
However, the increased sensitivity of S. aureus to ZnO nanoparticles has also been reported.
There are two conditions for synergy between ZnO and S. Aureus that have been shown: the affinity of ZnO to the membrane of S. Aureus and this microorganism's sensitivity to stress caused by the ZnO production of $H_2O_2$.

On the other hand, Gram-negative bacteria have shown less sensitivity to reactive oxygen species (ROS) when compared with Gram-positive bacteria. One of the main reasons for this higher resistance is the structural differences in the bacterial membrane, which are shown in the Figure 1.2.2 (2) below.

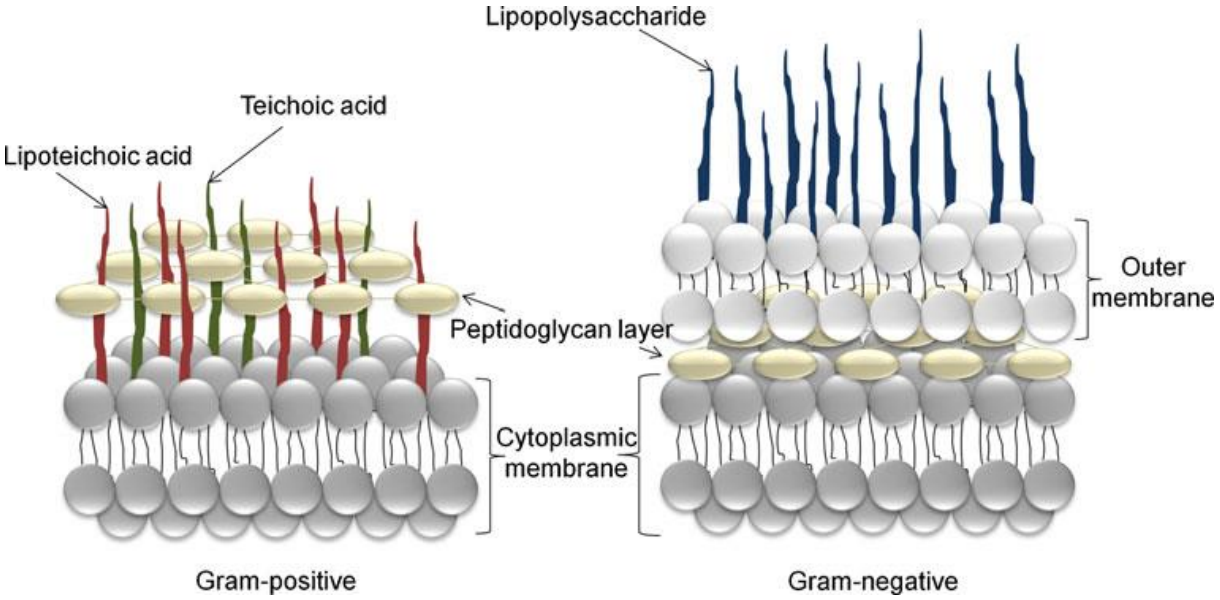


**Figure 1.2.2 (2)** Structural characteristics of the membranes of Gram-positive and Gram-negative bacteria.

Gram-positive bacteria have a membrane and a cell wall primarily made up of peptidoglycan layer as well as teichoic and lipoteichoic acids.
The cell wall of Gram-negative bacteria, instead, is more complex due to the presence of an outer membrane, which is composed mainly of lipopolysaccharide (LPS), in addition to a thin peptidoglycan layer.
Thus, the outer membrane of Gram-negative bacteria acts as a permeability barrier, so that the absorption of ROS into the cell is reduced.
Another explanation for the increased resistance to ZnO activity observed in E. coli compared with S. aureus is due to differences in the polarity of the cell membrane, since the membrane of S. aureus has less negative charge than E. coli.
This would allow a greater penetration level of negatively charged free radicals, causing damage and cell death in S. aureus at concentrations below that required to cause the same effect in E. coli.

Although several mechanisms have been proposed to explain the differences in the antimicrobial activity of ZnO against Gram-positive and Gram-negative bacteria, there are still some uncertainties; therefore, more studies should be done in order to clarify the sensitivity of these microorganisms to ZnO nanoparticles (Paula Judith Perez Espitia, July 2012).

## 1. 2.3 ZnO-polymer composites

Polymer nanocomposites are defined as a multicomponent system containing a filler with dimensions < ~100 nm in at least one dimension. Nanofillers can act as smart dopants to confer the polymeric matrix unprecedented properties or to improve the already existing ones. Moreover, their large surface area resulting from the very high aspect ratio can be also exploited, for example to include into the final nanocomposite several biomolecules of interest like drugs. The incorporation of ZnO nanomaterials into polymers has been already tested in cardiovascular grafts and stents, showing enhancement in hemocompatibility, antithrombogenicity, mechanical and surface properties (Muthu Vignesh Vellayappan, 2015).
Other improvements regard the biological aspects, such as improved moisture resistance, antibacterial and fungal properties.
It has been also well established that the ZnO addition to the polymer matrix can achieve a lower friction coefficient with respect to the pristine polymer, useful to overcome the problem of discomfort of traditional ureteral stents; for these reasons it was decided to test the nanocomposites behavior also in this field.
There are already many examples in literature of inorganic nanomaterials introduced into polymer matrices, resulting in polymer nanostructured materials exhibiting multi-functional, high performance polymer characteristics.

Zinc oxide powders are usually prepared via coprecipitation and used as inorganic materials.
Like other nanoparticles, they possess high surface energy, that allows to be dispersed in organic matrix, such as Polyvinyl alcohol (PVA), Poly(methyl methacrylate) (PMMA), polypropylene (PP), polystyrene (PS), with different methods of insertion.

Polyvinyl alcohol (PVA) is a hydrophilic polymer that was tested for its tensile
strength and Young's modulus when ZnO particles were added to it.
To obtain ZnO- PVA nanocomposites, the polymer was firstly dissolved in deionized water and stirred with a magnetic stirrer to be mixed thoroughly. Then, an amount of undoped ZnO powder was dispersed in aqueous polymer solution separately and continuously stirred until transparent ZnO - polymer multi-component dispersions was obtained.
It is known that to improve the dispersibility of the powders in polymer matrix avoiding the formation of agglomerated nanoparticles, the surface modification of the final composite results to be very useful.
The final results of this coprecipitation process were characterized in morphology and properties by different methods.
From this fabrication, the powders have a size of 20-150 nm, and the morphology can be controlled by selecting the process parameters as precursor, temperature and the starting composition, without modifying the crystalline structure of ZnO.
Concerning the properties, nanopowders were proven to have antibacterial capability, keeping the properties and original size of the starting particles, even after dispersion into polymer matrix.
The polymers can effectively inhibit the aggregation of the ZnO nanoparticles by organic surface modification and keep the ZnO nanoparticles well dispersed inside (A. Matei, April 2008).

In the case of ZnO composites with polypropylene (PP), the mechanical properties varied depending on the nature of ZnO and its amount. For example, the tensile strength, modulus and elongation at break values depending on the interfacial interaction on ZnO nanoparticles to polymers stress transfer and its dispersion inside the matrix. In particular, these parameters reached the optimum value at concentration of 1.5 wt.% for ZnO.

At this amount of filler, the loss modulus of PP increased substantially due to the reinforcing effect of ZnO through the formation of a rigid percolating network within PP.

Concerning the polystyrene (PS), nanocomposites with ZnO are formed by a simple solution casting process. In this case, at 5 wt.% of ZnO the modulus increased significantly, while in presence of the filler, tensile strength decreased very slightly because of the less interfacial adhesion of the composite (Deepalekshmi Ponnamma, May 2019).

# 2. Materials and Methods

## *2.1 Zinc oxide synthesis*

It was used a low-cost hydrothermal process in order to obtain a flower-like crystalline structure with a relatively high surface area (16 $m^2g^{-1}$) (Carmine Lops, 2019).
For the preparation, the amount of 5.58 g of potassium hydroxide (KOH) and 14.8 g of zinc nitrate hexahydrate ($Zn(NO_3)_2$) were both dissolved separately in 100 mL of bidistilled water each. Magnetic stirring was applied to dissolve the reagents in water as well as few seconds in ultrasound bath for the zinc nitrate solution.
Then, the zinc nitrate solution was dropped slowly into KOH, put under vigorous stirring, allowing the reaction. During the process of dropping, a sol is formed followed by gelation.

**Figure 2.1 (1)** Dropping of zinc nitrate into KOH solution.

The gel was placed in a closed Teflon bottle at 70 °C for 4 h. After this time, a precipitated white powder formed at the bottom of the vessel. The surnatant solution pH was 14.

In the hydrothermal process, the hydroxyl groups are able to bind to metal cations through coordination or electrostatic interactions. The absorbed $Zn^{2+}$ ions react with $OH^-$ groups to form the growth unit of $Zn(OH)_4^{2-}$, (eqn 1).
Then, $Zn(OH)_4^{2-}$ forms ZnO by dehydrating (eqn (3)). Therefore, the $Zn(OH)_4^{2-}$ precursor plays an important role in determining the morphology of ZnO crystallites due to the concentration of $OH^-$ in the reaction solution, which should be a key factor for controlling the growth rate of different crystal faces and thus lead to the formation of an anisotropic particle such as rod-like or flower-like morphology.
Thus, the basicity is a key factor for a controllable synthesis, especially for the morphologies of typical flower-like ZnO.

Eqn 1: $Zn^{2+} + 2OH^- \rightarrow Zn(OH)_2$
Eqn 2: $Zn(OH)_2 + 2OH^- \rightarrow Zn(OH)_4^{2-}$
Eqn 3: $Zn(OH)_4^{2-} \rightarrow 2ZnO + 2H_2O + 4OH^-$

As mentioned above, $Zn^{2+}$ reacts with KOH to produce a growth unit of $Zn(OH)_4^{2-}$. Then, very tiny ZnO particles are formed under the hydrothermal conditions.

A lot of ZnO nuclei are formed due to fast nucleation rates. At the initial stage, large amounts of ZnO nuclei and growth unit $Zn(OH)_4^{2-}$ are formed rapidly at the same time (Ruixia Shi, 2012).

ZnO particles were carefully separated from the solution by filtration, washed repetitively with deionized water until the pH neutralization, and dried at 60 °C overnight in air.

**Figure 2.1 (2)** Filtration process for washing the produced ZnO powders.

**Figure 2.1 (3)** Single batch of powders.

*2.2 PolyHEMA synthesis*

Poly(2-hydroxyethyl methacrylate) or pHEMA is a polymer that forms an hydrogel in water. To synthesize this polymer was used the radical polymerization method.

The reagents that have been used for the synthesis of the linear polymer are:

- 5g of 2-Hydroxyethyl Methacrylate (HEMA), liquid reagent.

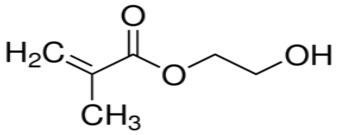

- 2% (0,1g) of initiator 2,2-Methylpropionitrile (AIBN) 98%, solid reagent.

These two reagents were mixed together and then it was used 50 mL of toluene as solvent to create the solution.

Before to start the polymerization, the solution has been put under a flow of nitrogen, in order to remove the oxygen. This is important because oxygen is an inhibitor of the polymerization.

To start the radical polymerization, the initiator must be activated; the latter is a temperature sensitive reagent, and its bounds gets destroyed at a temperature over 65°C.

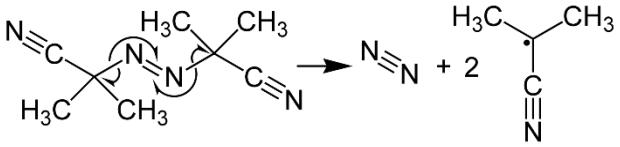

Increasing the temperature, the double bind gets broken in an homolytic way and are created 2 activate radicals.

In order to induce this homolytic breakup, the solution has been put under magnetic stirring at the stable temperature of 70°C for about 6 hours.

The polymerization is visible through the color of the solution that becomes opaquer over time.

As a consequence of this polymerization, a linear polymer has been obtained due to the reaction from a monofunctional monomer, which has only one double bind. The chemical structure of this linear polymer obtained from the radical reaction is:

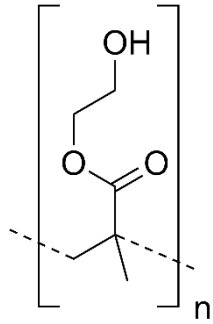

At the end of the reaction, after 6 hours, the polyHEMA is formed and the toluene must evaporate to be removed from the solution. A drawback of the solvent is its high boil point, around 110°C. In order to remove the toluene from the solution without using high temperature, which could damage the polymer, it is used the distillation under reduced pressure. Reducing the pressure, it is possible to decrease the boil point of the solvent, in order to have its faster evaporation.

Initially, for this procedure the working conditions have been set as following:

- Pressure 111 mbar.
- Temperature 70 °C.

After a while, the pressure was decreased until 44 mbar and then until 15 mbar; the reduction of pressure was made gradually in order to not damage the pump.

At the end, it has been collected an amount of 3 g from the synthesis.

### *2.3 Synthesis of composites based on polyHEMA/ZnO and poly(HEMA-co-AAc)/ZnO*

After obtaining and analyzing the polyHEMA polymer, its copolymer and the Zinc Oxide powder, the composites have been prepared through two different methods.

The mold used for the polymerization was made of silicon rubber (PDMS, polydimethylsiloxane) and had a rectangular form with 3 cm x 2 cm x 0.3 cm in dimensions.

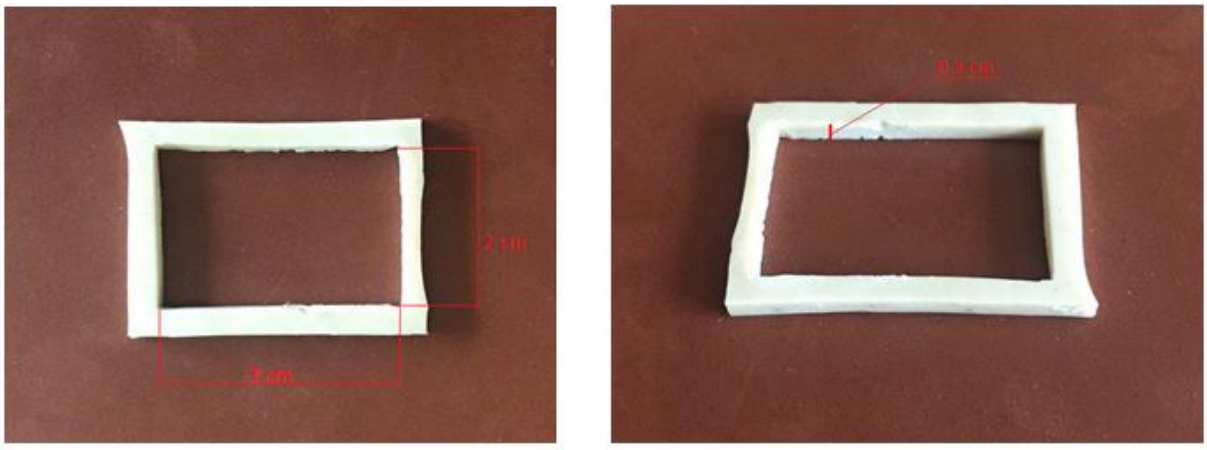

**Figure 2.3 (1)** Shape and dimensions of the mold.

The monomer solution consisting of HEMA or HEMA-co-AA were then mixed with the ZnO powder (in an amount which will be better defined below) and loaded in a syringe with a stainless steel needle. After the filling with the monomer+ZnO composite solution, each mold has been sealed between two plates of Teflon which were immobilized by two clamps.

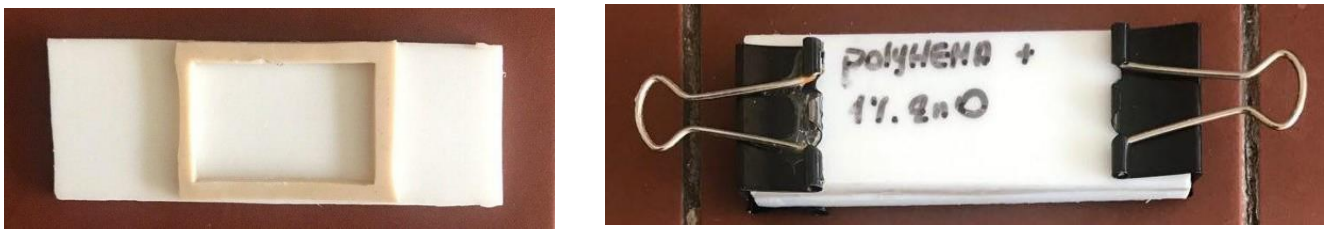


**Figure 2.3 (2)** Image of the sample which includes the silicon rubber mold and plates of Teflon.

The material chosen for the plates has proved to be suitable to avoid the adhesion of the polymeric solution in the mold during the polymerization.

The first method of synthesis provided for the preparation of the monomeric solution filled with ZnO powders was filling the mold by a needle. Once the mold was ready, it was put in an oven for 5 hours at the stable temperature of 70 °C, in order to obtain the complete polymerization of the monomer. The composite which was obtained from this process, showed however a bilayered structure: the lower part showed the accumulation of the powders trapped inside the polyHEMA, while the higher layer was made by polyHEMA only. This was due to the precipitation of ZnO powders that happened at the beginning of the polymerization, when the monomeric solution is still liquid and show a low viscosity.

In order to improve the ZnO dispersion in the polymer, it has been thought to fill the mold with a pre-polymerized solution. The solution with monomer and powders in a glass becker has been first put on a hot plate at 90°C, until it became viscous, approximately after 30 minutes. In that moment, the reaction must be immediately interrupted, putting the becker in ice. Thereafter the pre-polymerized composite was filled inside the mold and then left in oven for 4 hours at 70 °C, which resulted enough to complete the polymerization.
The composites obtained from this method were easier to remove from the plates and did not show any bilayer structure, whereas the powders resulted homogeneously dispersed throughout the whole polymeric matrix, thanks to the pre-polymerization step and the high viscosity of the solution achieved.

After choosing the methods to be used, then it has been decided to create 3 types of materials, each based on the use of the same amount of HEMA monomer.
The 3 types of materials are polyHEMA, the copolymer poly(HEMA-co-AAc) and the copolymer Poly(HEMA-co-AAc)-ZnO crosslinked by Ethylene Glycol Dimethacrylate.
The second material is a copolymer because of the presence of the second monomer, Acrylic Acid (AAc), which should lead the final material to have a faster degradation.
In the last class instead, the crosslinker is used in order to increase the stability of the material. Without its support, the copolymer shows to go under degradation after one day of application only; this time is insufficient thinking about its use as stent.

For each type, 3 different samples have been prepared with the same reagents involved in the polymerization, but with different concentrations of Zinc Oxide (0,1%, 1% and 2%, in relation to total volume of monomers which are in the solution).
In order to obtain the polymerization, 1% of Benzoyl Peroxide was used as initiator (percentage relates to the total amount of monomers) for the synthesis of both composites and copolymers.

Originally, it was thought to use both methods to synthesize each class of materials, in order to evaluate if the different distribution of ZnO could affect the release of drug.
However, during the first trials of synthesis, the first method has proved to be improper due to the difficult placement and keeping of the liquid solution between the plates, and the tight attachment of the sample to the mold.
For these reasons, only the method based on the pre-polymerization was used to create the different classes of materials.

As already explained previously, Zinc Oxide possesses an antibacterial behavior, but in too high concentrations it can be toxic also for healthy human cells. The selection of 3 different weight percentages, to be dispersed inside the polymers and copolymers, relied on the literature, in particular on the paper by K. M. Reddy published by the NIH (National Institutes of Health, United States) in 2007. This work shows the effects of ZnO nanoparticles in different concentrations against two different types of bacteria, *Escherichia coli* and *Staphylococcus aureus*, and towards human T-cells. The aim was to find the best concentration in order to have the correct balance between the antibacterial behavior and safety of healthy cells. It was found that ZnO nanoparticles with 13 nm of diameter are able to kill *E.coli* at a concentration of 3.4 mM, whereas *S.aureus* are killed at a lower concentration of 1 mM (K. M. Reddy, April 2007 ).
To evaluate the correct concentration of zinc oxide for ureteral stent applications, the toxicity against *E.coli* could be an interesting benchmark because they can be normally found inside the urine. From these considerations, the higher molarity of ZnO found in the study of the article (3.4 mM) has been chosen as reference to calculate the first and lower concentration to put inside the materials.

To show how the lowest percentage has been obtained, the calculations referred to the composite polyHEMA-ZnO are reported below.
The volume of the solution is the volume of the HEMA monomer 4 mL (HEMA has the same density of water, thus the volume corresponds to 4 g).

$$Molarity = \frac{moles}{1\ L_{solution}}$$

$$N_{moles} = 3.4\ mM * V_{solution} = 3.4 * 10^{-3}\frac{moles}{L} * 4 * 10^{-3}\ L = 13.6 * 10^{-6} moles$$

$$MM_{ZnO} = MM_{Zn} + MM_{O} = 65.39 + 16 = 81.39\frac{g}{moles}$$

$$Weight_{ZnO}[g] = N_{moles} * MM_{ZnO} = 13.6 * 10^{-6} * 81.39 = 1.1mg$$

$$[ZnO]_{\%} = \frac{1.1mg * 100}{4g} = 0.0275\%$$

This value would have been the lowest amount of powder to put inside the monomer solution before the pre-polymerization. However, the sensitivity of the precision scale was not enough to weight such a small amount without doing significant errors.
The concentration 0.1% of ZnO has been thought as the best compromise in order to be both as similar as possible to the minimum value taken as reference and enough high to be correctly weighted.
Concentrations 1% and 2% have been also chosen to analyze the differences in drug uptake and delivery, and in the future the antibacterial behavior and toxicity of the materials depending on the amount of ZnO.

In Table 2.3 is shown the list of the 3 different classes of samples which were prepared.

| Class of materials | Preparation |
|---|---|
| Composites polyHEMA-ZnO | This composite was made preparing 4 mL of HEMA monomer mixed with 1% vol of initiator (refers to the volume of HEMA) and the proper amount of ZnO (0.1%, 1% and 2% wt, referred to the weight of polymer). |
| Copolymer Poly(HEMA-co-AAc)-ZnO | The preparation started by weighting again 4 mL of HEMA and 5%vol of AAc (0.2 mL). Then 1% vol of initiator and the proper amount of ZnO are mixed. The percentages of both these last two reagents, the initiator and ZnO, refer to the total volume of monomers (4.2 mL). |
| Copolymer Poly(HEMA-co-AAc)-ZnO crosslinked by Ethylene Glycol Dimethacrylate | The preparation of the copolymer is the same as above, but with the addition of crosslinker Ethylene Glycol Dimethacrylate in amount of 5 %vol, referred to 4mL of HEMA.<br>The percentages of initiator (1%vol) and ZnO are both related to the total volume of monomers and 5% of crosslinker (4.4 mL). |

**Table 2.3** List of classes of materials prepared.

*2.4 Ibuprofen and Diclofenac uptake*

In order to prepare the samples for the drug uptake, it was decided to use the second method of synthesis only, due to the many problems associated with the first one which makes the implementation of a statistically relevant number of samples difficult. Furthermore, it was decided to consider the composite made by polyHEMA and the one made by crosslinked-copolymer, both with the addition of ZnO powders.

For the amount of powder, the concentrations of 0.1% and 1% were chosen, in order to have a ratio of 1:10 between the samples within the same class. Another reason why the concentration of 2% was not considered is that this amount of ZnO could be cytotoxic for the cells of the ureter's epithelium.

Once the method of synthesis and the concentration of ZnO have been decided, we moved to the choice of drugs to be used for the ureteral application. Ibuprofen and Diclofenac were chosen, being nonsteroidal anti-inflammatory drugs. The type of both drugs used was in the Sodium Salt form, showing high solubility in water, and thus preventing the use of toxic organic solvent to be employed for their dissolution and uptake into the polymeric matrices.

Three samples of the two concentration of ZnO within the same material's class and for each drug were prepared in order to get the statistical validity.

In Table 2.4 are shown the prepared samples:

| | | | |
|---|---|---|---|
| Class 1 | PolyHEMA | 3 x Ibuprofen | 3 x Diclofenac |
| | PolyHEMA + 0.1 % ZnO | 3 x Ibuprofen | 3 x Diclofenac |
| | PolyHEMA + 1 % ZnO | 6 x Ibuprofen | 6 x Diclofenac |
| Class 2 | Crosslinked Poly(HEMA-co-AAc) | 3 x Ibuprofen | 3 x Diclofenac |
| | Crosslinked Poly(HEMA-co-AAc) + 0.1 % ZnO | 3 x Ibuprofen | 3 x Diclofenac |
| | Crosslinked Poly(HEMA-co-AAc) + 1 % ZnO | 6 x Ibuprofen | 6 x Diclofenac |

**Table 2.4** Samples prepared to make the release analysis.

The extra samples with 1% of ZnO for each class and in absence of drugs were also prepared in order to study the degradation behavior of the composite in artificial simulated urine.

# 3. Characterization techniques

## *3.1 Field-emission Scanning Electron Microscope and Energy-dispersive X-ray spectroscopy (EDX)*

Field-emission Scanning Electron Microscope (FESEM) is a particular microscope used in chemistry and physics to observe structures as small as 1 nanometer. Its particularity lies in the use of an electron beam instead of light, which are delivered by a field emission source and accelerated in a high electrical field gradient.

The extraction of the primary electrons from the source and their acceleration take place within a high vacuum column ($10^{-8}$ Torr). Inside the column there is an accurate system of electronic lenses which aims to focus and deflect the primary electrons' beam to the sample.

In an ordinary Scanning Electron Microscope (SEM), electrons are generated by heating a tungsten filament by means of a current to a temperature of about 2800 °C. The thin filament act as a cathode in front of a primary and secondary anode. Between anode and cathode is originated a voltage of magnitude of 0.5 to 30 KV, that is needed to accelerate electrons and transmit to the sample enough energy in order to generate a signal to be detected.

FESEM use the same mechanism of electrons' generation of SEM, but the electron beam produced by its source is 1000 times smaller; this allows to obtain a better quality of the image.

In order to obtain an image through the use of FESEM, the preparation of the sample is also needed. In particular, it has to be conductive for the current. For that reason, the morphology of the ZnO powders prepared in this work was analyzed by placing a very low amount of powder on a conductive carbon tape. Then, the excess of powder was removed in order to avoid the dispersion of some grain of powder inside the high vacuum column. The FESEM imaging of the composites was instead performed by coating the samples with a 5 nm-thick Pt film deposited by sputtering, prior to load the samples inside the FESEM chamber.

After the formation of the primary beam of electrons, it bombards the sample with a proper speed and from that collision secondary electrons are emitted from each spot on the object. The emission of this secondary beam is related to the surface structure of the sample and is detected and transformed in an electronic signal, in order to obtain the final image (Geert-Jan Janssen).

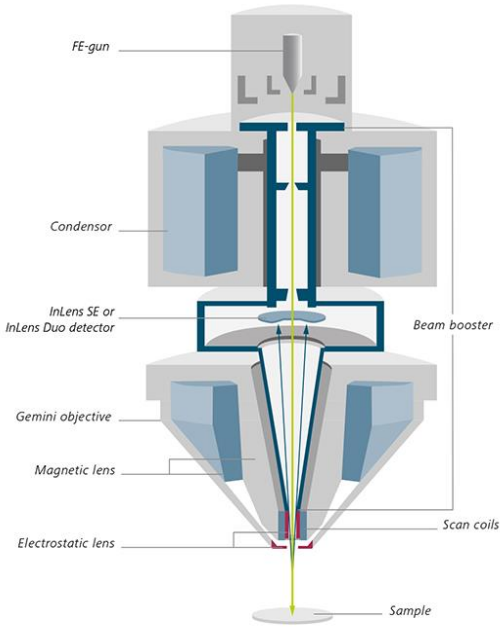


**Figure 3.1 (1)** Scheme of FESEM.

Another techniques closely related to FESEM analysis is the energy-dispersive X-ray spectroscopy (EDX).
Scanning electron microscopes (SEMs) employ electron beams in order to get information about composition from a sample at the nanoscale. This analysis can be both qualitative, recognizing the type of elements, and quantitative, giving the percentage of the concentration of each element
The incident electron beam interacts with the sample and generates a variety of signals that carry different information about it.

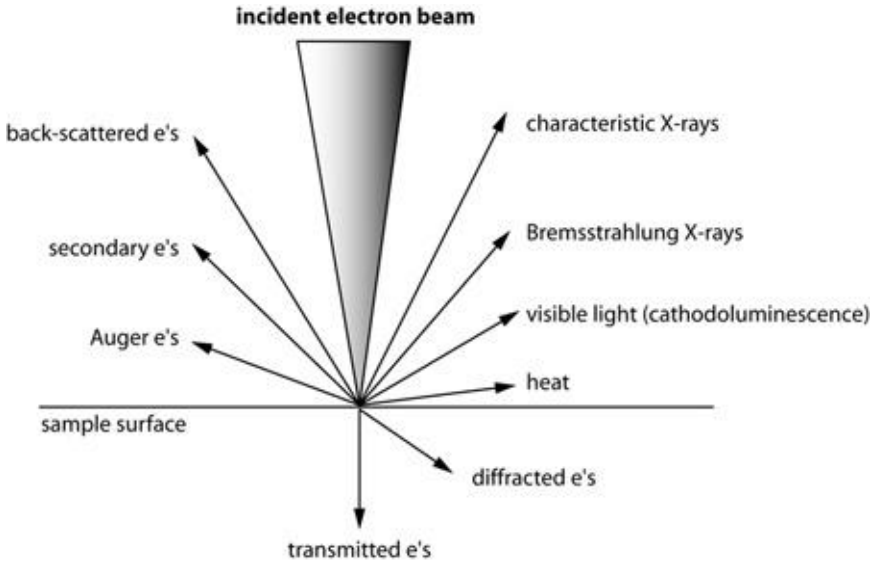


**Figure 3.1 (2)** Illustration of the electron-matter interaction depicting its different products.

From that analysis, the main type of signals that are detected and used to getting information are the backscattered (BSE) and secondary electrons (SE).
These types of signals generate a grayscale image of the sample at very high magnifications; in particular, BSE electrons produce images that allows to get information on the differences in atomic number, while SE electrons give topographic information.

Another type of signal that is widely used in SEMs is X-rays, which are generated in two-step process. In the first step, the electron beam hits the sample and transfers part of its energy to its atoms.
If the energy is enough, electrons can use it to "jump" to a higher energy shell or be knocked-off from the atom. If one of these two events occur, the electron leaves behind a hole which has a positive charge.
After that, the second step of the process starts, in which the positive charge of the holes attracts the negatively-charged electrons from higher-energy shells. When this shell-to-shell transition occurs, the corresponding energy difference is released in the form of an X-ray, which is the signal has to be detected. In turn, this energy difference depends on the atomic number, which is a unique property of every element. That means that the X-ray signal becomes the discriminant factor to recognize each element present in the analyzed sample.

The final data that is generated by EDX analysis consists of spectra with peaks corresponding to all the different elements that are present in the sample (Figure 3.1 (3)).

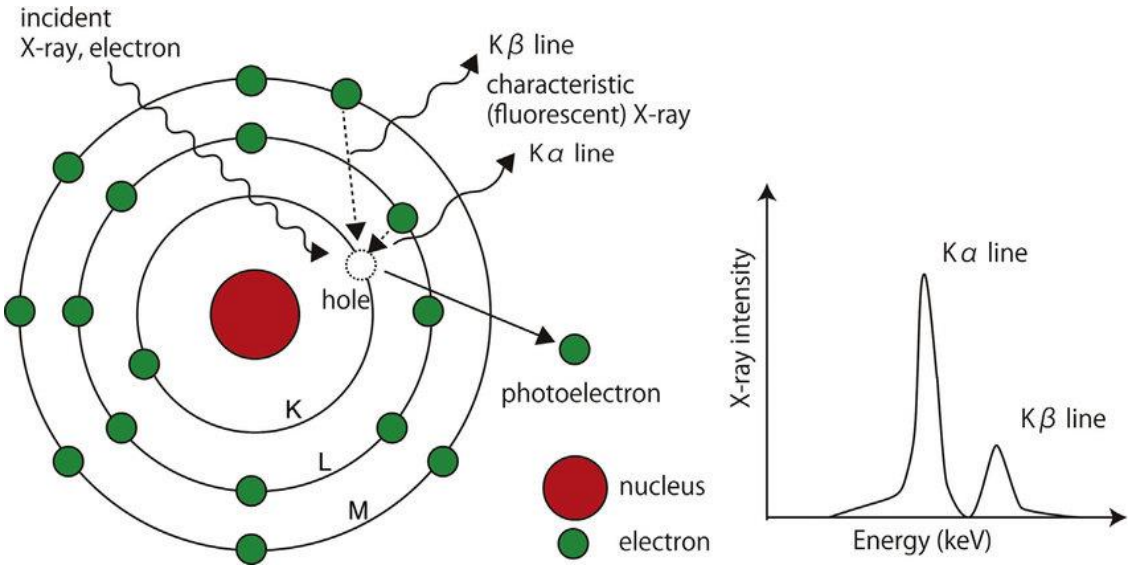


**Figure 3.1 (3)** Two step X-ray generation process: 1) The energy transferred to the atomic electron knocks it off leaving behind a hole. 2) Hole is filled by another electron from a higher energy shell and the characteristic X-ray is released.

The software usually available inside SEMs enables auto-identification of the peaks and calculation of the atomic percentage of each detected element.
One more advantage of the EDX technique is that it is a non-destructive characterization approach, which requires little or no sample preparation (Nanakoudis, 2018 ).

## *3.2 X-Ray Diffraction*

X-Ray Diffraction is used to detect information about the crystal structure of materials, in this case of Zinc Oxide powders. In addition, this analysis can also determine strain, preferred orientation, crystallographic structure and grain size of crystalline materials (Material Interface inc., 2019).

The patterns that are generated by diffraction of a X-rays' beam is directly related to the crystal structure of the material that is targeted. The main effect that occurs from this interaction between the beam and the target material is scattering of X-rays from atoms within the target material.

The outgoing beam is collected by a detector which uses the Bragg's equation in order to calculate the distance between each plane of the crystal reticulum:

$$n\lambda = 2dsin(\theta)$$

This law describes the process of diffraction, by which a beam of waves is spread out through a diffraction grid, typically accompanied by interference between the wave forms produced. This process is typical for material that have a crystalline structure.

The directions of the diffractions depend on the size and shape of the unit cell of the material, while the intensities of the diffractions depend on the arrangement of atoms in the crystal reticulum (XOS, 2019).

Figure 3.2 below explains the diffraction process described by the Bragg's law.

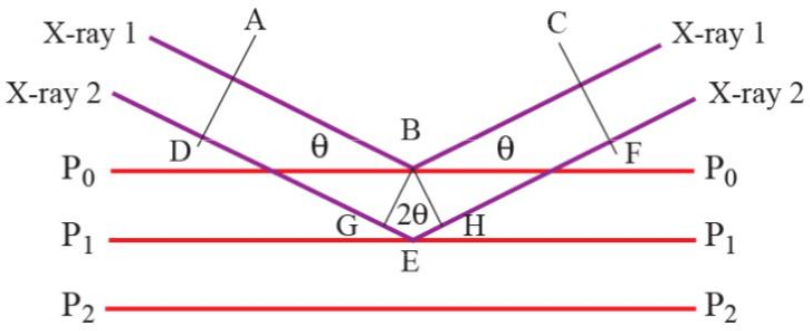


**Figure 3.2** Atomic planes of a crystal reticulum. Explanation of Bragg's law.

It is shown a family of atomic planes with spacing d.
X-ray 1, striking the first atomic plane $P_0P_0$, is diffracted at incident angle θ; the same for each X-ray signal that impacts against a plan of the reticulum.
When a crystal is placed in the X-ray at an orientation that satisfies the Bragg equation (n =1), a beam of diffracted X-rays will strike the detector.

Of each signal collected by the detector, the incident angle θ, the coefficient n and the wavelength of the incident X-ray are known. From these, inverting the Bragg's equation, it is possible derive the distance d between planes of the reticulum.

On rotation of the crystal there will be further "reflections" detected when the Bragg equation is satisfied at certain θ angles (n = 2, 3, 4 etc).

## *3.3 UV-Vis Spectroscopy*

Ultraviolet (UV) and visible radiation comprise only a small part of the whole electromagnetic spectrum, which includes other forms of radiation at different wavelengths, as radio, infrared (IR), cosmic, and X rays.

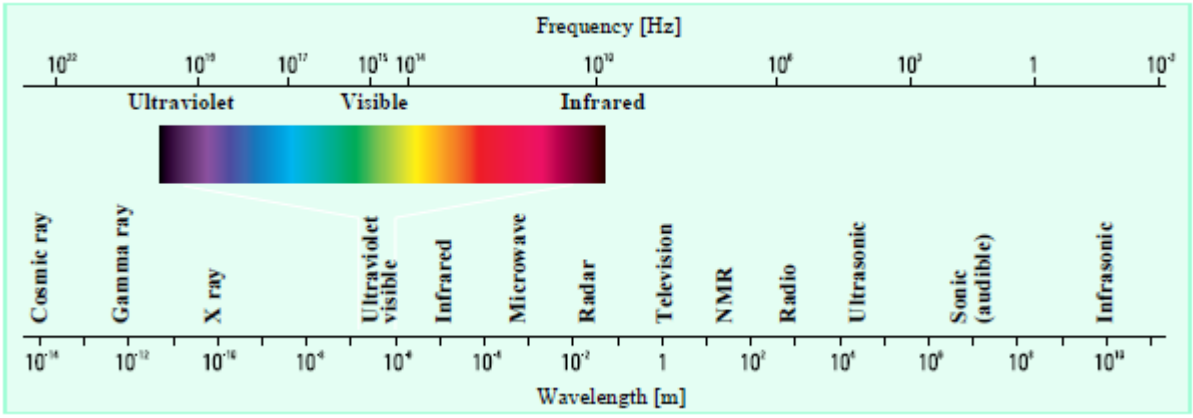


**Figure 3.6.3 (1)** Electromagnetic spectrum.

UV-Vis spectrophotometer uses visible light and ultraviolet to analyze the chemical structure of substance.
UV and visible absorption spectroscopy measures the absorption of a beam of light after it has passed through a sample or after reflection from sample surface.
The spectrophotometer measures the intensity of light, known the wavelength.

When various organic compounds are crossed by ultraviolet, they will absorb the radiation. In this way, it is possible to detect the outgoing signal from the sample and, known the intensity of the incident beam, to measure the absorption of the compound. From this, the molecular structure of the substance is obtained and then also the chemical structure.

Radiations in general act as waves, and that is why they can be identified by either wavelength or frequency, which are related by the following equation:

$$\nu = c / \lambda$$

$\nu$: frequency (s);
c: the speed of light ($3 \times 10^8$ m·s$^{-1}$);
$\lambda$: wavelength (m).

The range of wavelengths covered by this analysis is usually expressed in nanometers (1 nm = $10^{-9}$ m).
It follows from the above equations that radiation with such a short wavelength has on the other side a high energy. Therefore, in UV-visible spectroscopy the low-wavelength UV light has the highest energy.
Despite a number of processes could occur when the radiation interacts with matter, including reflection, scattering, absorbance, and so on, during UV-visible spectroscopy it is intended to occur only absorbance and transmittance.

Considering that light is a form of energy, when it hits the matter it transfers some amount to this, causing the increase of the energy content of molecules or atoms of the substance.

When the energy increase, transitions between the different electronic energy levels inside the material can occur.
In Figure 3.6.3 (1) are shown the electronic transitions and how to build the spectra of atoms, in order to understand the phenomenon just described.

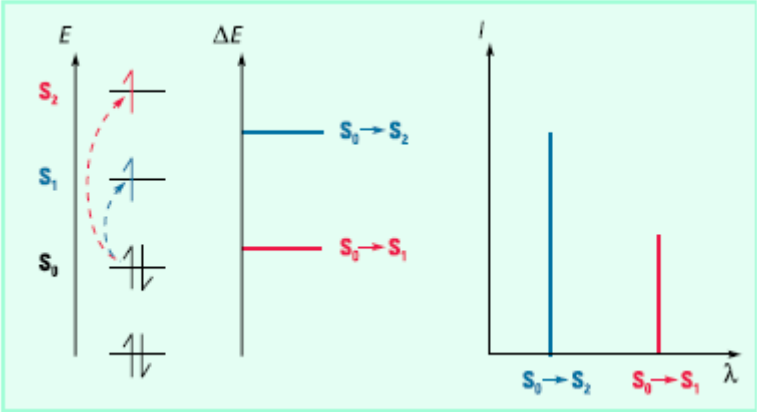


**Figure 3.6.3 (2)** Electronic transitions and spectra of atoms.

When light passes through the sample, it is needed to measure the amount of light (and therefore energy) absorbed.
This can be done simply by doing the difference between the incident radiation ($I_o$) and the transmitted radiation detected by the Spectrophotometer (I).
Hence, if $E_0$ and $E_1$ are the energies of ground state and excited state of a molecule, respectively and ΔE is the difference in energy between two states, then:

$$\Delta E = (E_1 - E_0) = hv = hc/\lambda$$

The amount of light absorbed can be expressed as either transmittance or absorbance.
The former is usually defined in the following way:

$$T = I/Io$$

,while the absorbance is defined as follows (Remondini, December 20, 1996):

$$A = -\log T$$

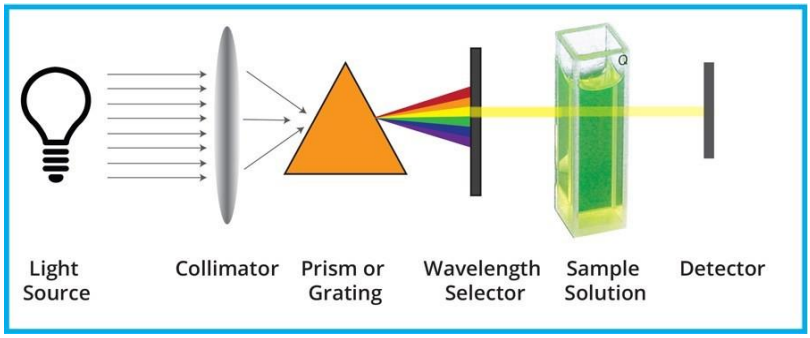


**Figure 3.6.3 (3)** Functioning sketch of UV-Vis Spectroscopy.

The absorption of radiant energy is based on two laws:

1. Beer's Law;
2. Lambert's Law.

Beer's Law states that the amount of energy absorbed is directly proportional to the concentration of absorbing solute or number of absorbing molecules present in a medium.

$$A = \log (I_0/I) = \varepsilon c$$

A: absorbance;
$I_0$: intensity of incident radiation;
I: intensity of light transmitted through sample;
ε: absorption coefficient/absorptivity;
c: concentration of absorbing material in sample.

Lambert's Law states that fraction of light absorbed by a homogenous medium is independent of the intensity of light and light absorption is directly proportional to path length of light.

$$A = \log (I_0/I) = \varepsilon l$$

l: path length.

Combining these two laws, we get Beer-Lambert Law which is expressed as

$$A = \log (I_0/I) = \varepsilon c l$$

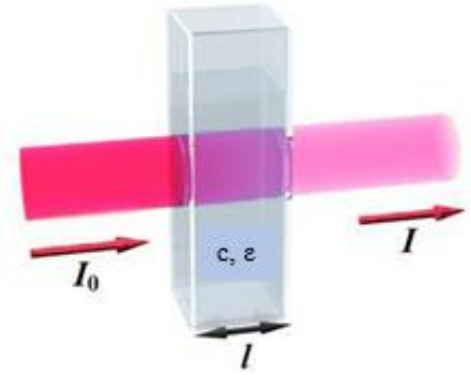


**Figure 3.6.3 (4)** Lambert-Beer Law.

The measuring instrument on which it is based this analysis, the spectrophotometer, works on the principle of this combined Law (TM, 2018).

The Lambert-Beer Law says that " the amount of energy absorbed or transmitted by a solution is proportional to the solution's molar absorptivity and the concentration of solute".
That means that a more concentrated solution absorbs more light than a more diluted solution does.

Once the UV-Vis Analysis has provided the absorptivity of the solution, it is possible to obtain the concentration using the reversal formula.

### *3.4 Fourier-transform infrared spectroscopy (FT-IR)*

Fourier-transform infrared spectroscopy, also called FT-IR, is a method of analysis in "bulk", used to understand the chemical properties of the sample. It is useful for analyzing the chemical composition of smaller particles, as well as larger areas on the surface. These details can be obtained from a trace or a small piece of material in the sample.
Chemical compounds have different chemical properties due to the presence of different functional groups.
It is an analytical technique, that takes advantage of the vibrational transitions of molecule in order to chemically classify substances.

As it can be understood by the name, this technique uses infrared light (about 10000 to 100 $cm^{-1}$) and sends the radiations through the sample to scan it. Radiations which are absorbed are converted in energy which makes the sample molecules vibrate or rotate. Actually in molecules, the covalent bonds are not rigid, but they can be stretched and bent. Moreover, the movement includes not only facile rotation of groups around single bonds, but also a wide variety of vibrational motions, which are characteristic of their component atoms.
A molecule composed of n-atoms has 3n degrees of freedom, six of which are translations and rotations of the molecule itself. This leaves 3n-6 degrees of vibrational freedom (3n-5 if the molecule is linear). The typical names given to vibrational modes are descriptive of the movement, such as stretching, bending, scissoring, rocking and twisting.
Hence, infrared radiations are absorbed by molecules, in order to create the characteristic vibrations of the functional groups that form the compound.

The result is a signal collected by the detector and transformed in a spectrum, representing the molecular fingerprint of the sample.

The production of a unique spectral signal by each molecule or chemical structure of the sample is what makes FT-IR analysis reliable and accurate.

The functioning of infrared spectrometer is similar in principle to the UV-Visible spectrometer. It is the analysis of infrared light interacting with a molecule, and it can be made in three ways by measuring absorption, emission and reflection. From that, it is possible to recognize the functional groups in molecules and so the chemical structure of the analyzed substance.
Generally, stronger bonds and light atoms will vibrate at a high stretching frequency (wavenumber).

The final spectrum obtained by the analysis reports on the abscissa the wavenumber of the incident photon and in the ordinate the related amount of energy absorbed by the sample. The intensity of the peak is correlated to the quantity of functionality present in the sample (RTI Laboratories, 2015).

Therefore, once the polyHEMA has been collected, the FT-IR characterization was made in order to verify the quality of the radical polymerization.

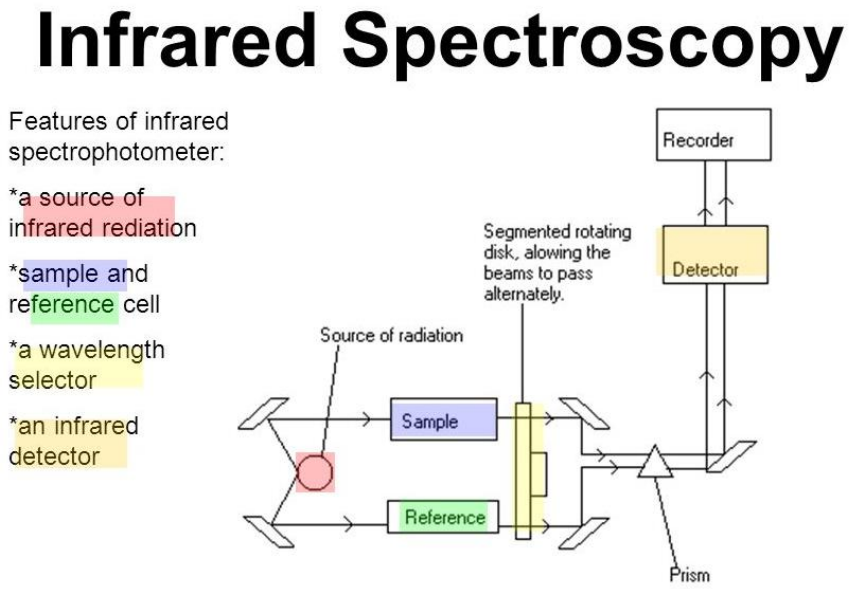


**Figure 3.4** Functioning of FT-IR analysis.

### *3.5 Differential Scanning Calorimetry (DSC) Analysis*

In order to obtain information about the thermal behavior of polyHEMA, it has been used the Differential Scanning Calorimetry Analysis (DSC).

This thermal analysis technique allows the detection of thermal transitions such as melts, phase changes, curing and glass transitions. This last characteristic is more important concerning polymeric materials.

Inside the instrument there is a place for the reference and one for the sample. Depending on the specific setup adopted for the measurement, the reference can be empty or also include water with a heat capacity of 1J/M, which means that it takes 1 joule of energy to heat 1 cc of water 1 degree. The other place near the reference has inside a known amount of material. In general, during a thermal analysis, are made both heat and cool flow.

During the analysis, both the sample and the reference are kept at the same temperature. Given that the two templates have different content, the instrument must give (heat flow) or remove (cool flow) a different amount of heat from those. The final DSC signal is made by the heat's difference which is measured between the sample and the reference for each temperature.

Normally the graph can show endothermic or exothermic peaks. The first happens when the sample absorb more heat than the reference and it results cooler, thus the instrument must supply more heat to the sample to keep it at the same temperature. Exothermic behavior in the opposite event, where energy is released to the sample because its transformation is producing heat (PerkinElmer, Inc., 2013).

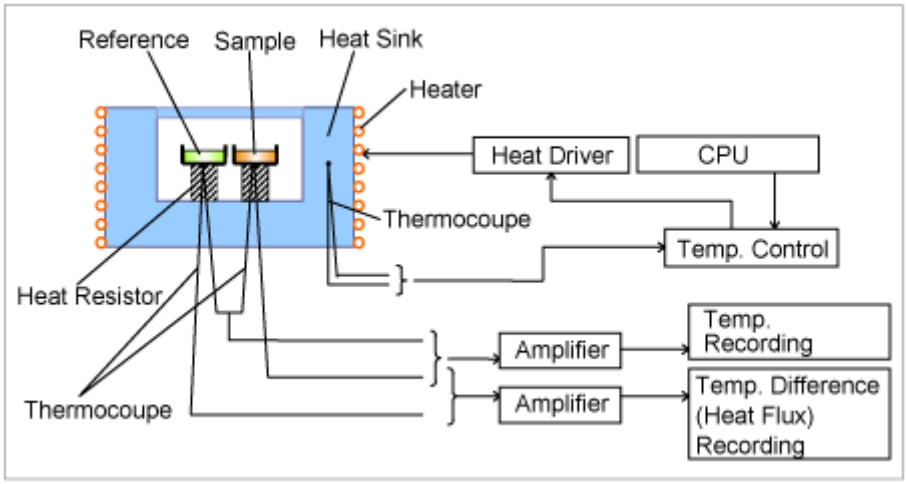


**Figure 3.5** Functioning sketch of DSC.

## *3.6 Thermal Gravimetric Analysis (TGA)*

Thermogravimetric Analysis is a technique widely used to characterize and verify materials. During this destructive analysis the sample specimen is subjected to a controlled heating in a controlled atmosphere, and its weight is measured for each temperature in order to calculate the mass' loss.
A TGA instrument consists of a sample pan, inside the oven, that is supported by a precision balance, while the sample purge gas controls the sample environment which can consist in inert atmosphere or a in reactive gas that flows over the sample and exits through an exhaust.
The main purpose of this instrument is to quantify the loss of mass upon heating, and it gives back a spectrum which has in the abscissa the range of temperature touched during the heating and in ordinate the weight of the sample that is not degraded yet.

Usually, during the experiment, the sample is heated in an inert atmosphere in order to have the unique reaction of the sample with the temperature during the decomposition.
In other experiments it could be useful to have an environment with a reactive gas, for example oxygen, in order to identify the percentage of carbon in the sample.

During the decomposition of the sample in the TGA analysis, gas products can be evolved. Several techniques are used to analyze the gas products from the TGA experiment, for instance the one which combine the TGA analysis with the FT-IR technique. It is the most common type of Evolve Gas Analysis system and it consists in the transfer of the evolved gases produced during the heating to the IR cell, where these components can be identified (PerkinElmer, Inc., 2010).

**Figure 3.6 (1)** Example of TG-IR.

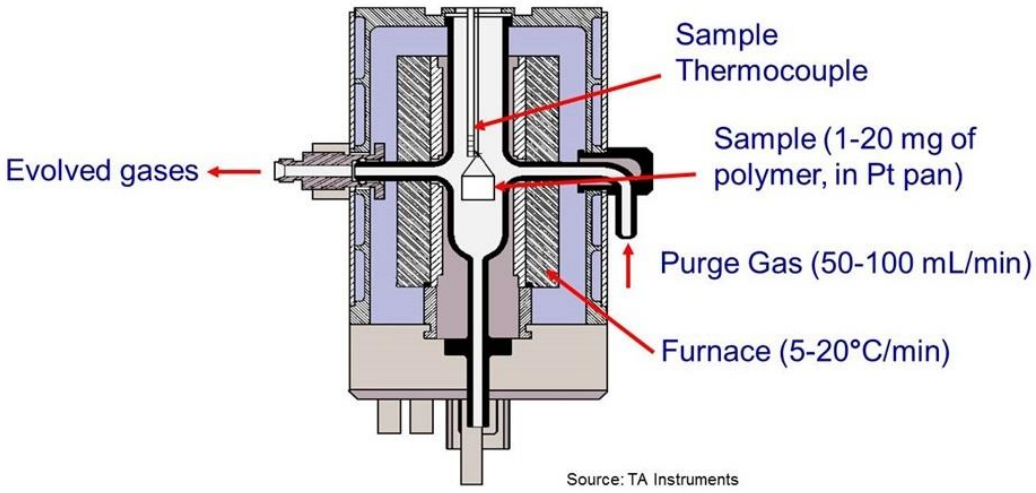


**Figure 3.6 (2)** Functioning sketch of TGA.

## *3.7 Analysis of drugs*

### *3.7.1 Ibuprofen*

Ibuprofen is a propionic acid derivate and nonsteroidal anti-inflammatory drug (NSAID) with anti-inflammatory, analgesic, and antipyretic effects. It is able to inhibits the activity of the enzyme cyclo-oxygenase I and II, decreasing the formation of precursors of prostaglandins and thromboxanes. This leads to decreased prostaglandin synthesis, that is the main physiologic effect of ibuprofen (NIC - Institute, 2019).

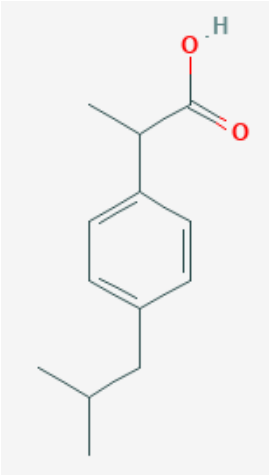


Ibuprofen is commonly used specially to treat fever, weakness and medium-scale aches due to inflammation or post-surgery. This drug is considered to be among the safest NSAIDs and is generally well tolerated but can, nevertheless, rarely cause clinically apparent and serious acute liver injury (LiverTox, 2019).

Until today, this drug has been usually administered orally, but because of the poor solubility in water, that lied to an insufficient absorption, it is needed a high amount of drug, in order to ensure its effectiveness.

**Figure 3.7.1 (1)** Structural formula of Ibuprofen.

In order to exceeds this limit, are being developed parenteral or topical solutions to treat the aim locally, such as foam or gel.
A medicament made by foam loaded with ibuprofen has been shown to be reliable and safe with regard to healthy cells and also easy to use. Moreover, this solution should ensure the same low release of ibuprofen over time, in order to be effective against the temporary pain and even to prolong the drug effect against the persistent ones.

As previously said, in this work of Master thesis, the ibuprofen drug in form of salt was used. In this form, the drug is less hydrophobic, and it was possible to use water as solvent for the uptake of drug inside the samples.

| | |
|---|---|
| Molecular weight | 228.267 g/mol |
| Water solubility | 0.0219 mg/mL |
| pKa | 4.15 |

**Table 3.7.1**Chemical-Physical properties of Ibuprofen sodium salt [Drug Bank].

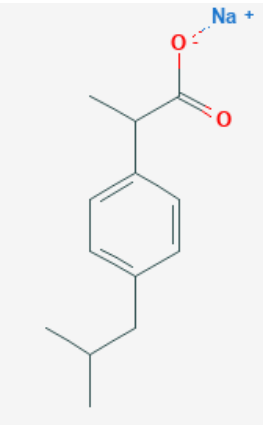


**Figure 3.7.1 (2)** Structural formula of Ibuprofen Sodium Salt

### *3.7.2 Diclofenac*

Diclofenac is a nonsteroidal benzeneacetic acid derivative, with anti-inflammatory activity (NSAID). Its action lies on binding both isoforms of cyclooxygenase (COX-1 and-2) in order to block the conversion of arachidonic acid to pro-inflammatory-prostaglandins. Hence this drug acts as a Cyclooxygenase Inhibitor.
When inhibiting COX-2, diclofenac may be effective in relieving pain and inflammation; when inhibiting COX-1, it may produce unacceptable gastrointestinal side effects.

Diclofenac is used to treat aches and pains, especially as regards problems with joints, muscles and bones. It comes as tablets, capsules and suppositories, but it can also be given as injection or gel (Information., 2019).
Several reviews suggested that the topical solution had a better tolerability property than oral Diclofenac, especially due to side effects of gastrointestinal bleeding with the utilization of the oral format. In addition, the topic solution has revealed to be equally effective, with minimal side effects (Tieppo Francio V, 2017 Jun).

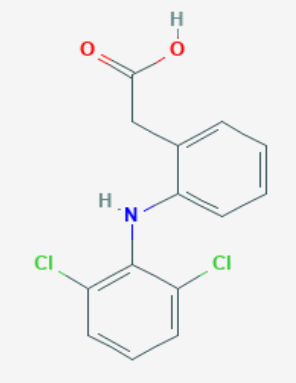


**Figure 3.7.2 (2)** Structural formula of Diclofenac.

For the same reason of Ibuprofen, it has been chosen to use the sodium salt form.

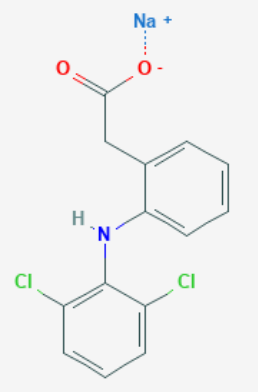


**Figure 3.7.2 (2)** Structural formula of Diclofenac sodium salt.

| | |
|---|---|
| Molecular weight | 318.1 g/mol |
| Water solubility | 0.00482 mg/mL |
| pKa | 4.26 |

**Table 3.7.2** Chemical-Physical properties of Diclofenac sodium salt [Drug Bank]

### *3.8 Synthesis of artificial urine*

Once the drugs have been loaded into the composite samples, it was needed to create a stock of artificial urine, in order to simulate a physiological condition to study the drug release.
For that reason, it was made a literature research to find the recipe that best suited for this application.

The final recipe found from literature research is shown below (Latifa B. Khan, 2017):

| Ingredients | Amount [g/L] |
|---|---|
| Potassium chloride | 0.2 g/L |
| Sodium chloride | 8 g/L |
| Di-sodium hydrogen phosphate | 1.14 g/L |
| Potassium dihydrogen phosphate | 0.2 g/L |
| Milli-Q water | up to 1 L |
| Hydrochloric acid or sodium hydroxide | to adjust pH to between 7.5 and 8.0 |

**Table 3.8** Elements used to create the artificial urine.

The original recipe included also the use of queen yellow food color, 200 µL/L, but for this study, it was preferred to keep the solution transparent. The yellow color indeed, would be required simply for a matter of aesthetics, but it would be irrelevant for the final results.

On the other hand, in several other recipes that have been found in different articles, it was also used the urea (Deepak S. Ipe, 2016), (Dexue Liuab, 2019), (Monika Pietrzyńska, 2017).
This is an organic chemical compound, which represents the principal nitrogen part of urine. Urea is able to decompose by hydrolysis, a process that trigger a series of chain reactions that lied to the production of ammonia and consequently to the increase of the pH of urine.
By adding urea at the recipe of artificial urine, it is not possible to control this degradation process, leading to uncontrolled rise of the pH, reaching high values even in a very short time.

In this study, the aim was to study the release of two different drugs from the various composite samples in different conditions of pH, separately. Firstly, the release was made at physiological pH (around 7) and then, both pathological conditions of acid and basic urines have been studied.
Therefore, it was important to maintain constant the pH value for all the time of each release, and for that reason it has been decided to not include the urea in the recipe, in order to maintain the maximum control of the pH.

To prepare the artificial urine, first of all a 500 mL becker was filled with bidistilled water and put on a heating magnetic stirrer. Once the temperature rose till 37 °C, a magnet was put inside the becker. Then, all the reagents were added inside the volume of solution (amount of reagent considering 1L of water) and in the same time, the magnetic stirring was applied in order to easily dissolve them in water.

When all the elements were dissolved and the solution in becker appeared clear, the final pH value was checked using the pH meter.
The first pH measured had a value of 7.3, thus it was not necessary to add hydrochloric acid or sodium hydroxide to arrange it.

Then, the solution obtained was transferred in 1L-flask and extra bidistilled water was added until reaching 1L of artificial urine.
At the end, the whole volume was transferred inside a 2L-bottle and stored in the fridge at +4 °C.

# 4. Results

*4.1 Results obtained by Zinc oxide synthesis*

The following Table 4.1 reports weights of powders obtained by different synthesis batches of ZnO.

| | Empty tube weight [g] | Tube with powders weight [g] | Powders' weight [g] | |
|---|---|---|---|---|
| DR1 | 6.2424 | 9.6427 | 3.4003 | Batch 1 |
| | 6.2353 | 9.7165 | 3.4812 | Batch 2 |
| DR2 | 5.8585 | 9. 58 | 3.4673 | Batch 1 |
| | 5.6683 | 9.0152 | 3.3469 | Batch 2 |
| DR3 | 5.6599 | 9.1448 | 3.4849 | Batch 1 |
| | 5.6515 | 9.1432 | 3.4917 | Batch 2 |
| DR4 | 5.8438 | 9.3717 | 3.5279 | Batch 1 |
| | 5.6849 | 9.1841 | 3.4992 | Batch 2 |
| DR5 | 5.6494 | 9.2517 | 3.6023 | Batch 1 |
| | 5.8484 | 9.4278 | 3.5794 | Batch 2 |

**Table 4.1** List of powders' weights for each synthesis.

*4.2 FE-SEM Characterization*

For each synthesis batch prepared according to Table 4.1, FESEM analysis has been performed in order to check the morphology of the as-prepared ZnO powders.

In Figure 4.2.1 (2) and (3), FESEM images of the synthesized ZnO powders are presented, clearly showing the presence of a flower-like morphology.

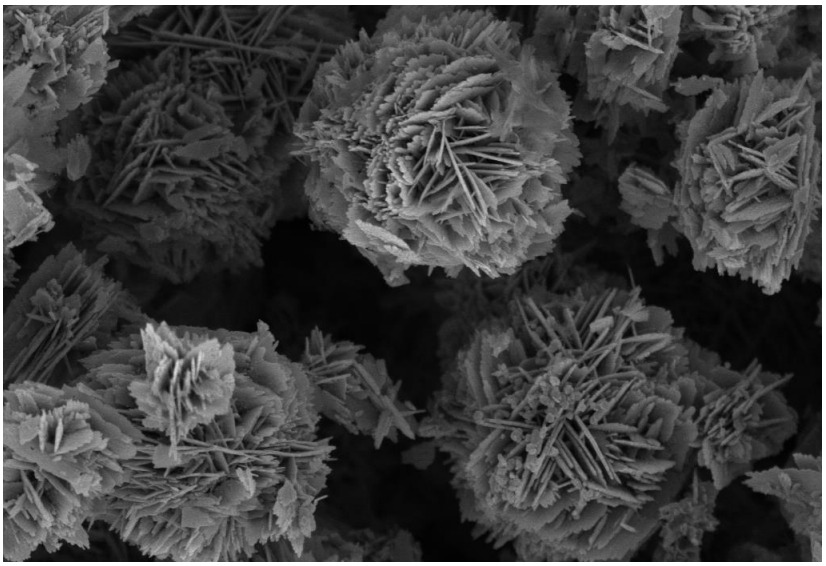

**Figure 4.2 (1)** FESEM image of ZnO flowerlike microparticles prepared at 70 °C. Magnification 50k.

Increasing the magnification, it was possible to measure the diameter and the thickness of rose petal-like planes.

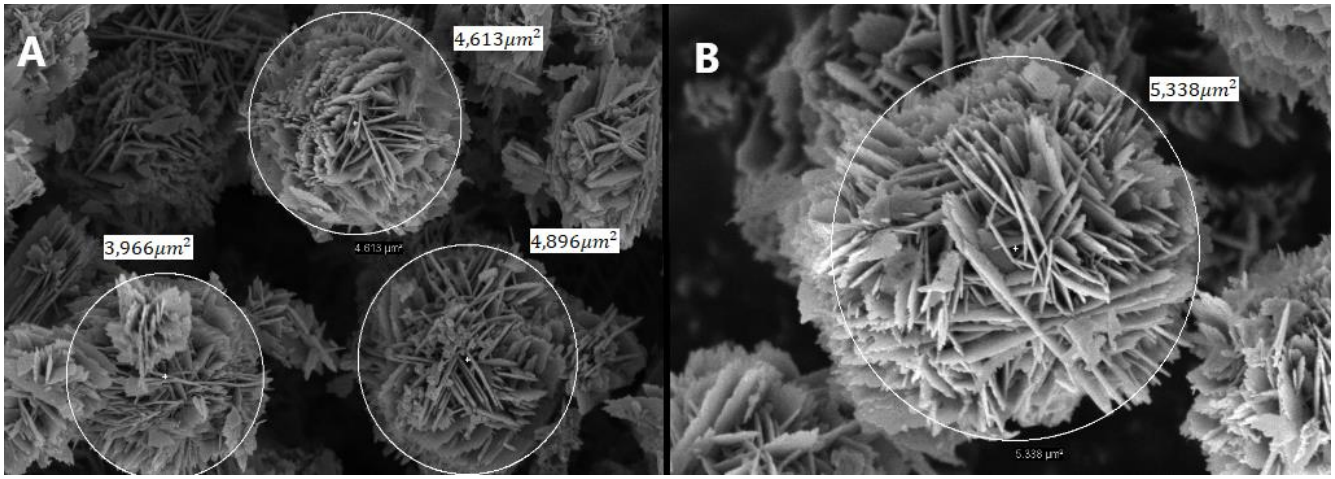


**Figure 4.2 (2)** FESEM image of ZnO flowerlike microparticles prepared at 70 °C. Area of each desert roses-like crystal. [A] Magnification 50k. [B] Magnification 80k.

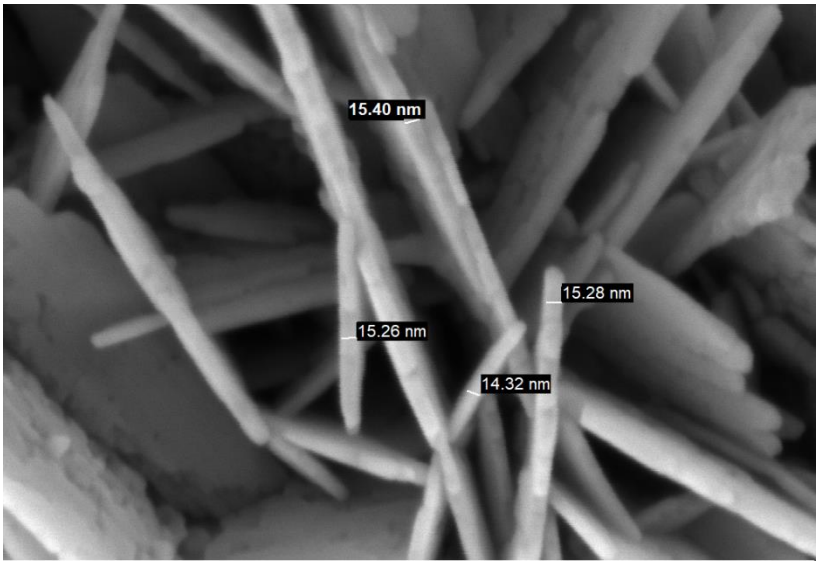


**Figure 4.2 (3)** FESEM image of ZnO flowerlike microparticles prepared at 70 °C. Thickness of planes. Magnification 500k.

From the Figure 4.2 (2) it can be noticed that the average area of grains is around 4,70 $\boldsymbol{\mu m^2}$.
From this value, it is possible to obtain the average diameter using the formula $\frac{\pi}{4}d^2$, which results to be around 2.45μm.

The detected dimensions of microparticles (2.5 μm diameter of grains, 15nm thickness of petals) are acceptable and in line with literature, where it was seen that when the reaction time is extended to 4h, the size does not increase anymore, and it remains stable at about 1,5 -5 μm (Ruixia Shi, 2012).

### *4.2.1 FE-SEM and EDX of samples*

After having made all the samples, it has been used both FESEM and EDX analysis in order check the real presence of ZnO inside the composites.

FESEM was used in order to get the images and to find the impression left from the powder; the following Figure 4.2.1 (1) and (2) show the imprint of ZnO in polyHEMA + 0.1% and polyHEMA + 1%.

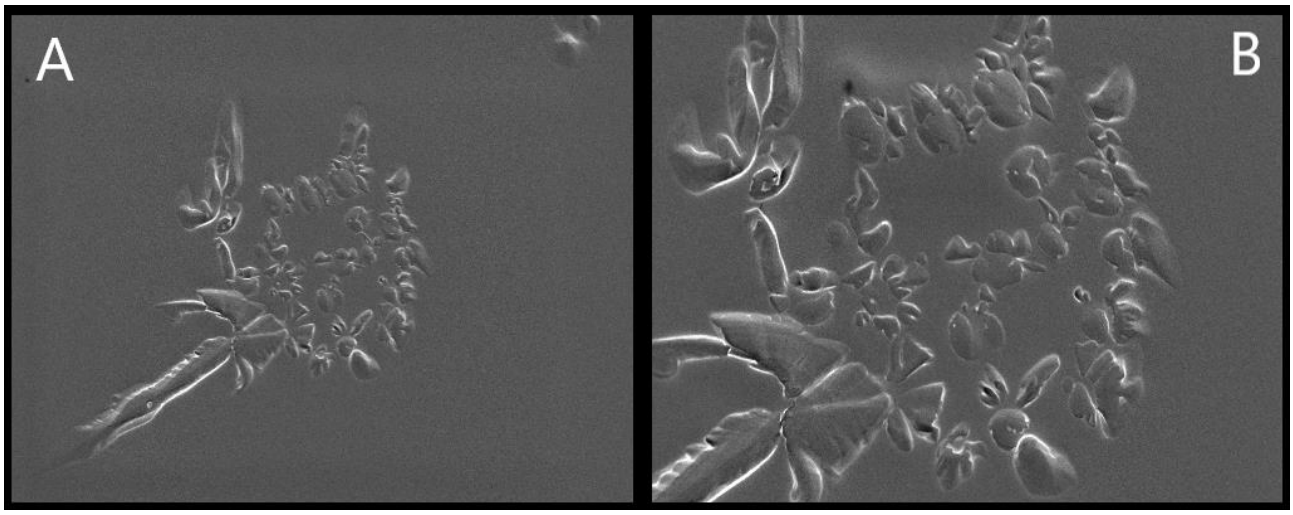


**Figure 4.2.1 (1)** Impression of ZnO powder in PolyHEMA + 0.1% sample. (A) Magnification 25k. (B) Magnification 50k.

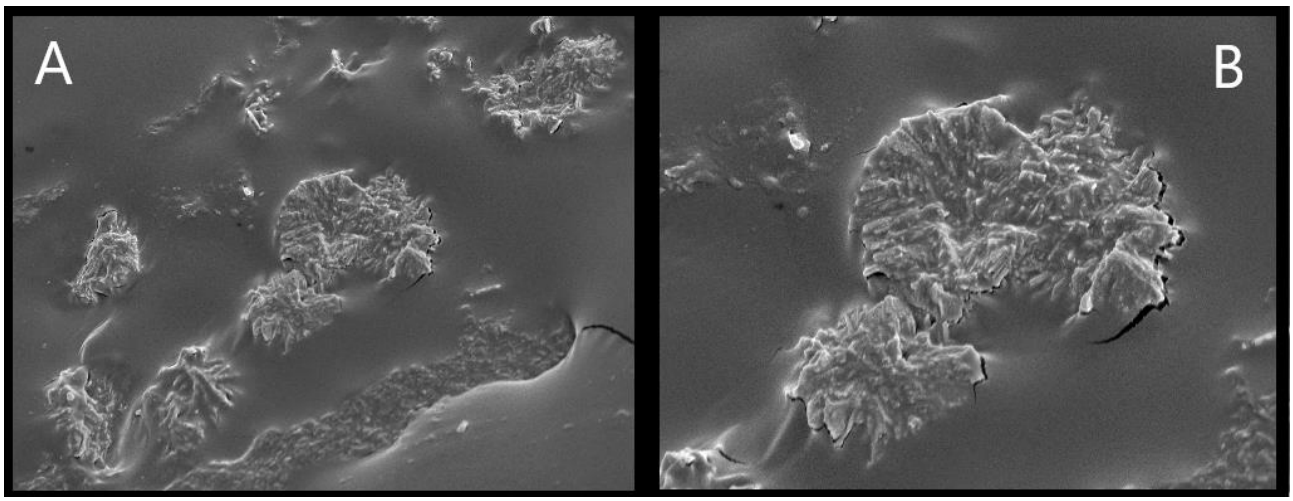


**Figure 4.2.1 (2)** Impression of ZnO powder in PolyHEMA + 1% sample. (A) Magnification 25k. (B) Magnification 50k.

On the other hand, also the EDX analysis has been made, in order to characterize the impressions that have been found, in terms of chemical composition. As a result, it is possible to verify if the print really belongs to the powder.

Concerning the images shown above, results of EDX analysis made on both the samples are reported below.

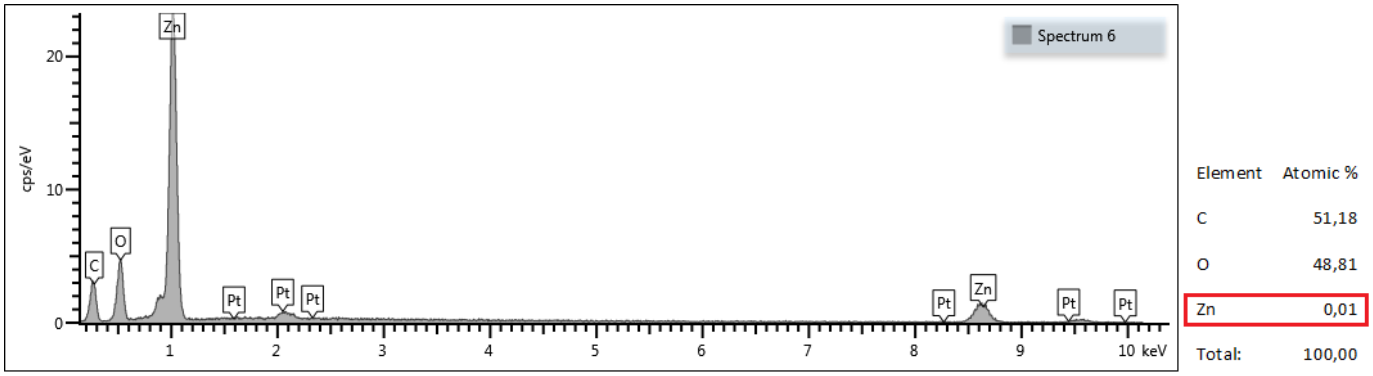


**Figure 4.2.1 (3)** EDX spectrum of PolyHEMA + 0.1% ZnO. Table with % atomic weight of each element.

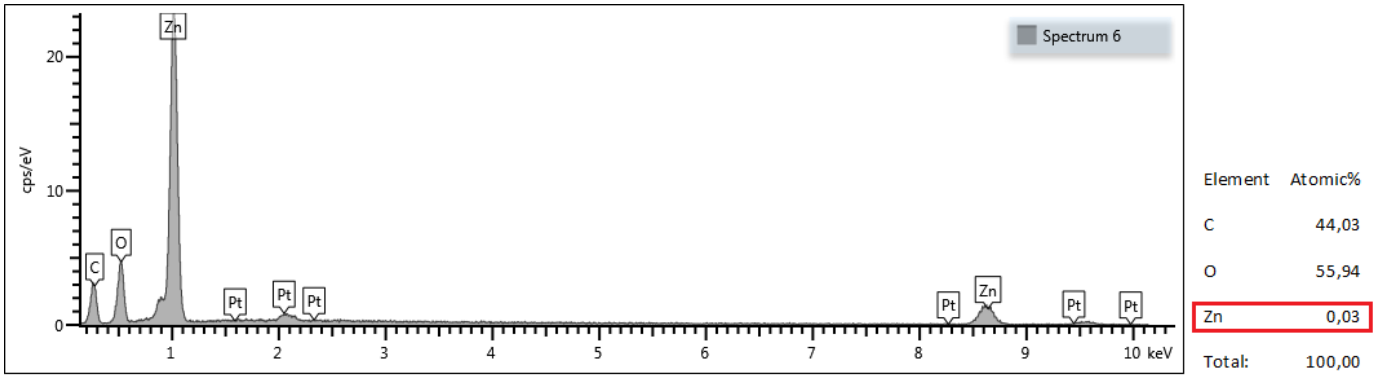


**Figure 4.2.1 (4)** EDX spectrum of PolyHEMA + 1% ZnO. Table with % atomic weight of each element.

Even if the presence of ZnO has been just slightly detected by EDX, it is still possible to notice that the sample added with 1% of ZnO shows a higher atomic percentage of Zn compared to polyHEMA with 0.1% of ZnO. This result is in line with the composition of the composites.

*4.3 X-Ray Diffractometry Characterization*

*4.3.1 X-Ray Diffractometry of Powders*

The most important aspect that can be noticed from the XRD analysis of the ZnO powders, is that the prepared materials have a crystalline structure.
X-Ray Diffraction (XRD) patterns of ZnO flowerlike microparticles prepared at 70 °C are reported in Figure 4.3.1.

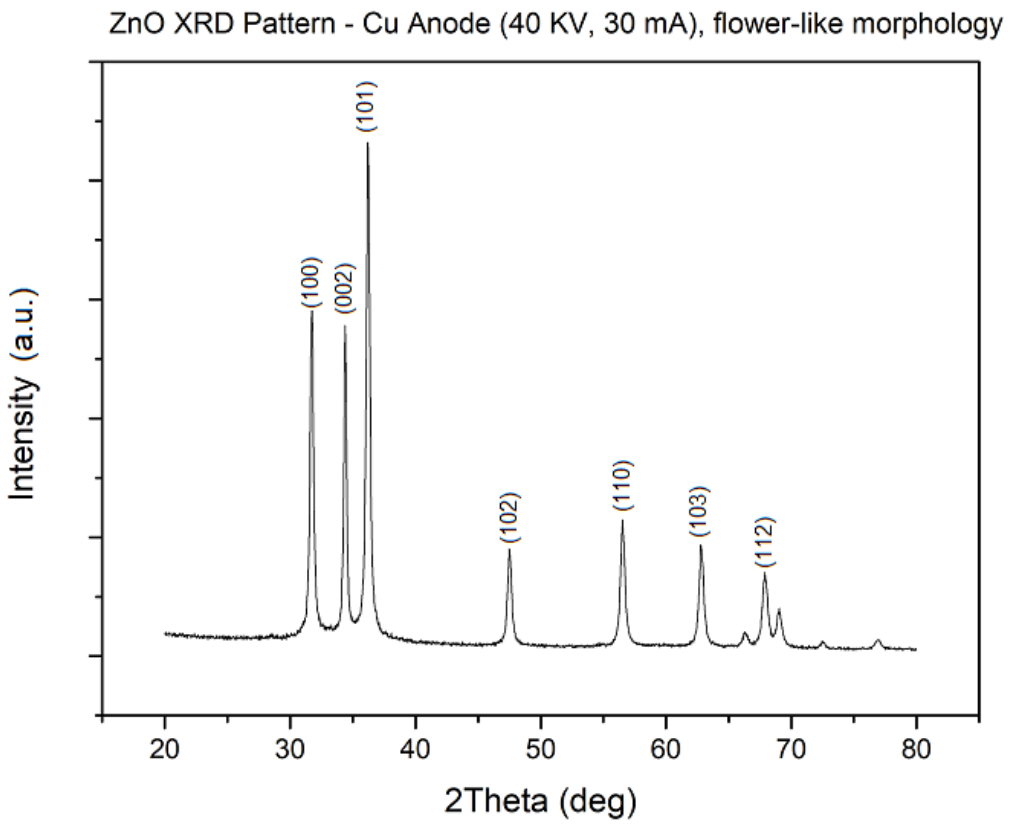


**Figure 4.3.1** XRD patterns of ZnO microparticles with flower-like morphology.

The diffraction peaks show the good crystalline quality of the powder, with the presence of a pure hexagonal wurtzite structure (JCPDS file, No. 80-0074).
Actually, the X-ray diffraction patterns present the typical reflection peaks of that phase, indexed as (100) at 31.82°, (002) at 34.54°, (101) at 36.42°, (102) at 47.46°, (110) at 56.74°, (103) at 62,6° and (112) at 67,8°, according to the JCPDS file (JCPDS File, 1998).

### *4.3.2 X-Ray Diffractometry of composite samples*

After preparing all samples of each class of material, the XRD analysis have been carried out on the samples, in order to compare the different patterns within each class, by varying the amount of powder as filler in the polymer matrix.

In the following are shown the X-Ray Diffraction patterns of the pure polyHEMA and copolymer, and the comparison among the polyHEMA class and copolymer class.

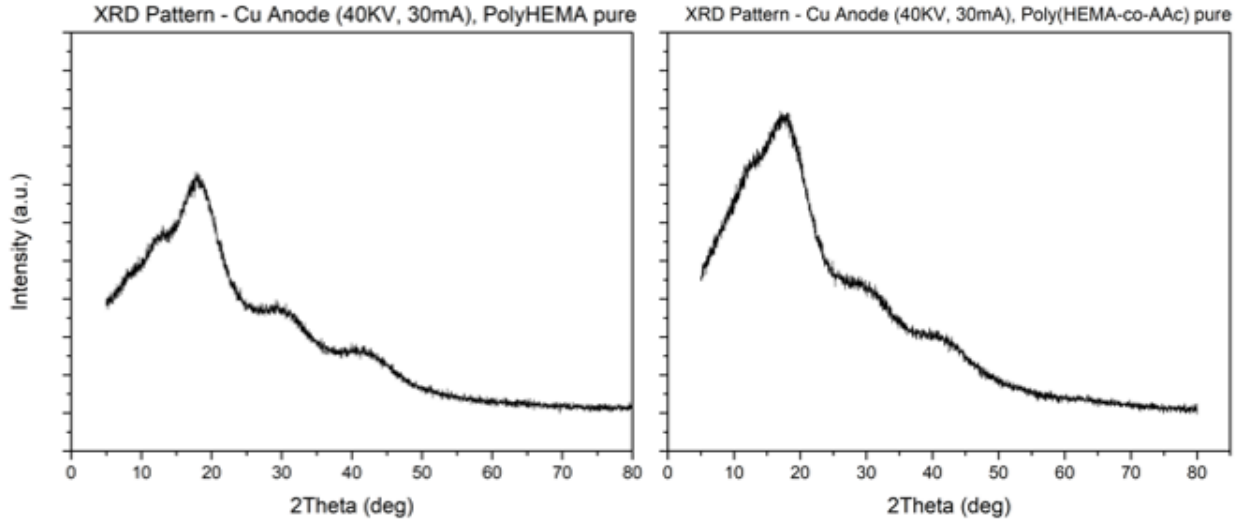


**Figure 4.3.2 (1)** XRD patterns of PolyHEMA and Poly(HEMA-co-AAc) samples, both pure.

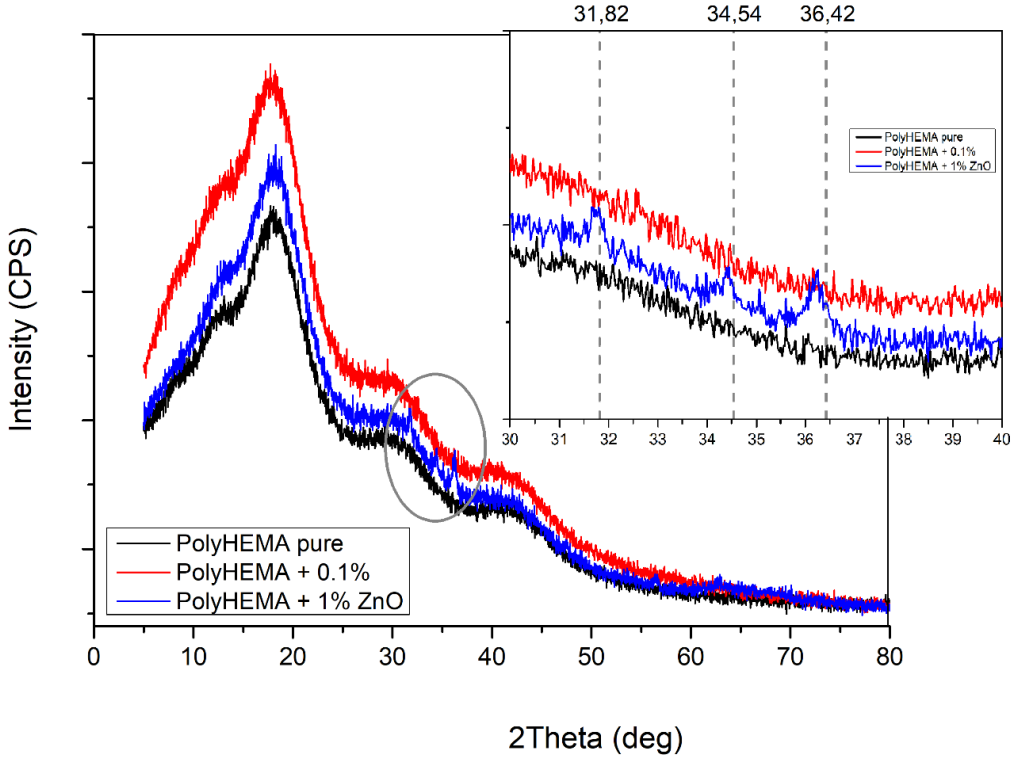


**Figure 4.3.2 (2)** XRD patterns of polyHEMA class of materials. Focus on the intensity associated to the main peaks of ZnO, 31.82°, 34.54°, and 36.42°s in the red spectrum (0.1%wt content of ZnO ) and in the blue one (1%wt ZnO).

In Figure 4.3.2(2) are shown the XRD patterns of the three composites based on polyHEMA, which incorporate different percentages of ZnO.

This analysis has been made on the final prepared samples, in order to verify the effective presence of ZnO in the different composites.

From the different XRD patterns of the polymer, it has been compared the intensity corresponding on the main peaks of ZnO spectrum at 31.82°, 34.54° and 36.42°. It can be seen that with increasing the amount of powder, the intensity on these 2Theta values increases consistently.

In the red spectrum of the sample with 0.1%wt of ZnO, the peaks on these points are very difficult to notice, even in the magnified portion of the graph. That is due to the very small amount of the powder. On the other hand, in the sample with 1% of ZnO (blue spectrum), the peaks in the magnified graph are high and clear to see.

These evidences have confirmed the effective presence of ZnO and also its different amount between the different composite samples.

The same results have been obtained for the class of copolymer poly(HEMA-co-AAc).

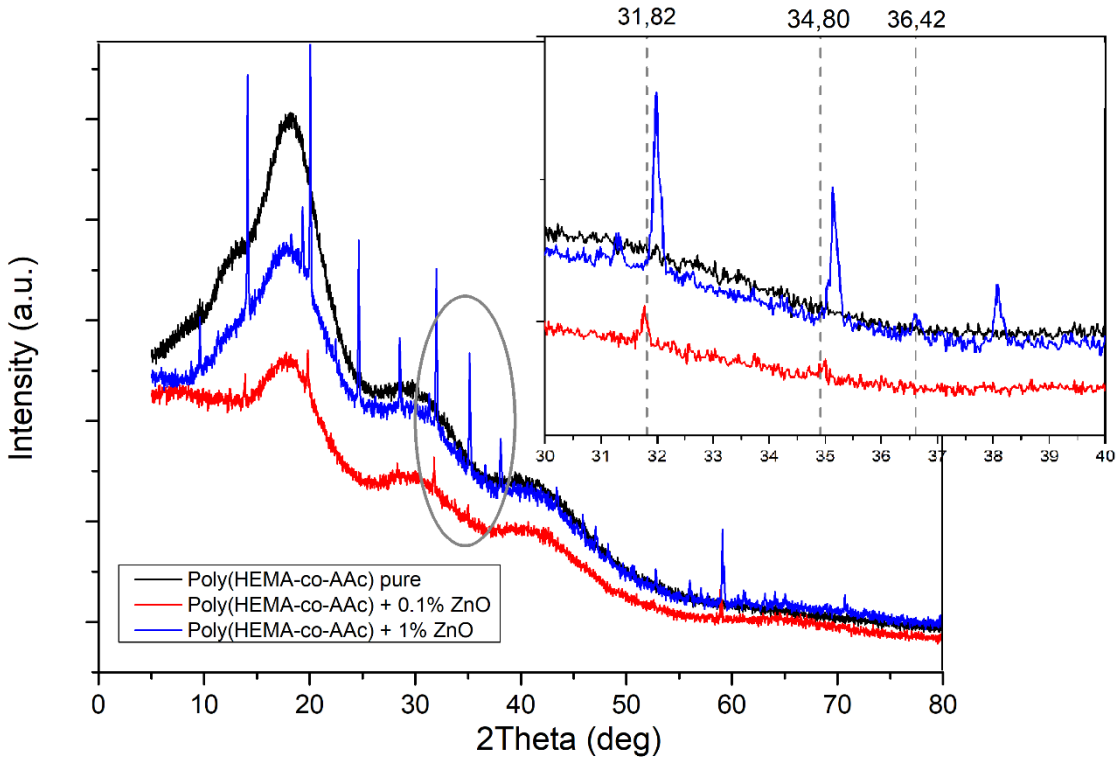


**Figure 4.3.2 (3)** XRD patterns of poly(HEMA-co.AAc) class of materials. Focus on the intensity associated to the main peak of ZnO, 31.82°, is in the red spectrum (0.1%wt content of ZnO ) and in the blue one (1%wt ZnO).

*4.4 FT-IR Analysis of polyHEMA and composites with ZnO*

In the following are shown in the same graph both the FT-IR spectrum of the monomer used for the polymerization, and the polyHEMA's ones, in order to compare them.

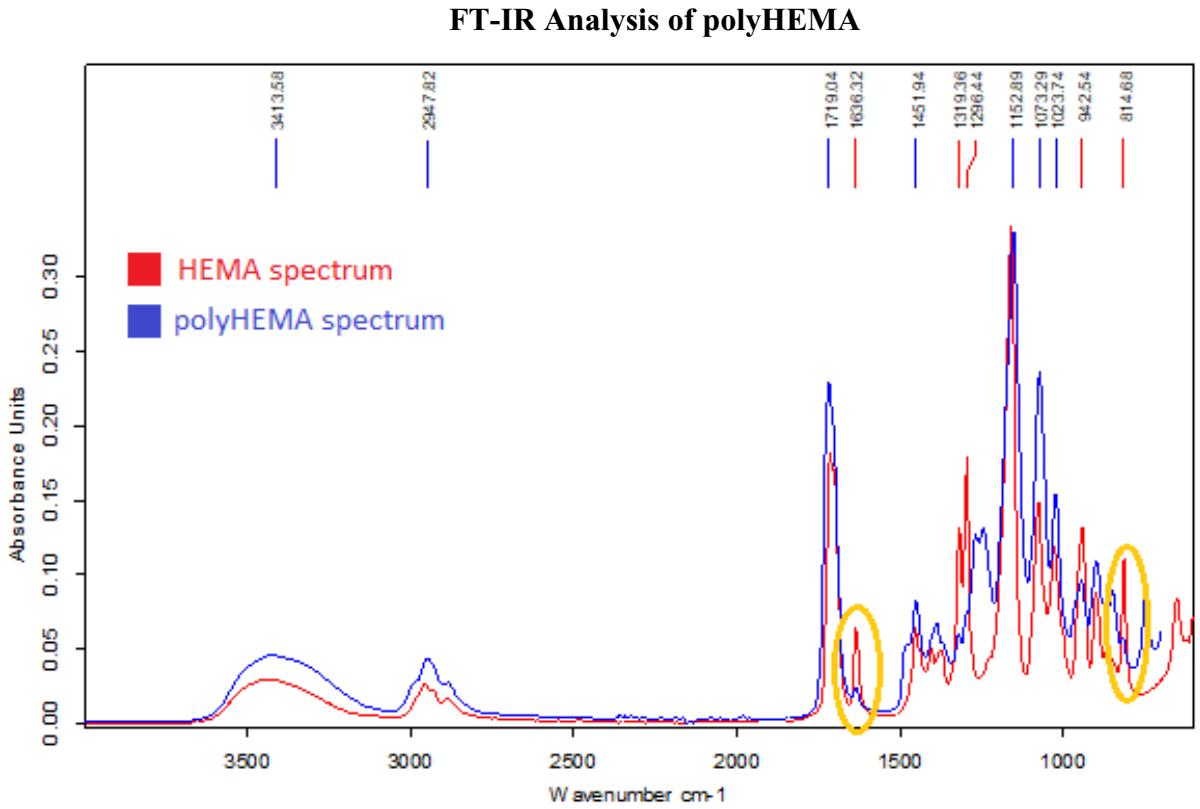


**Figure 4.4 (1)** Indices of peaks corresponding to different functional groups. In red is the spectrum of HEMA monomer. In blue is the spectrum of polyHEMA.

The only difference between the monomer and the final polymer is the presence in the first of double bond of the carbon ($H_2C=C$).

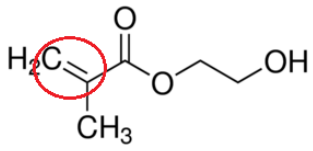


The two typical wavenumbers corresponding to carbon's double bond are one around 1600 $cm^{-1}$ and the other less than 1000 $cm^{-1}$.
In order to valuate if the polymerization has occurred correctly, differences should be observed in the intensity of these peaks in the two spectra at these wavenumbers' values.
In particular, the monomer's spectrum shows a higher intensity than the polymer's one at both wavenumbers, which should not be present at all. The possible presence of a low peak over these wavenumbers in the spectrum of the polymer might reveal the presence of a small amount of monomer that did not react during the polymerization.

To have a complete analysis of the spectrum, other peaks are associated to the other functional groups that are in common both to the monomer and the polymer. The first peak, over 3500 $cm^{-1}$, relates to the OH groups. The peak over 3000 $cm^{-1}$ is associated to $CH_3$ and $CH_2$ groups. At lower values of wavenumber, it can be seen a peak over around 1700 $cm^{-1}$ which is associated to the carbon's double bond with the oxygen, while the peak over around 1250 $cm^{-1}$ corresponds to the carbon's double bond with $CH_2$ group.

Concerning the analysis made to the different composites prepared, the FT-IR characterization was made to compare each other the samples belonging to the same group, having different concentrations of ZnO.

**FT-IR Analysis of polyHEMA with ZnO**

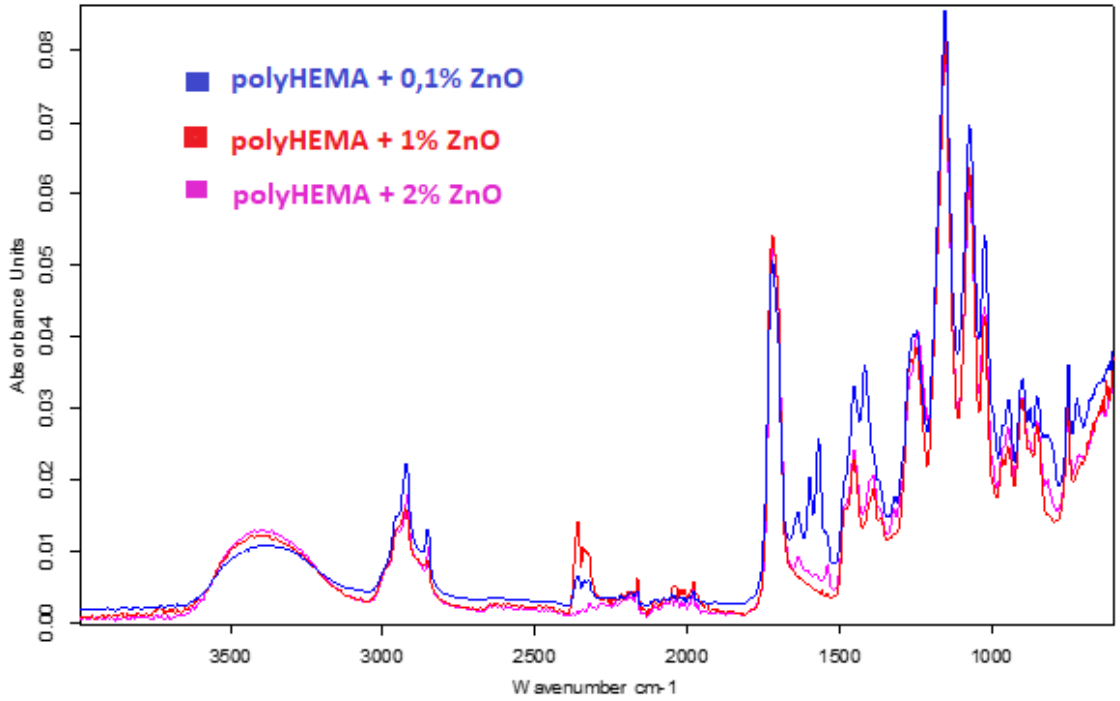


**Figure 4.4 (2)** Comparison of FT-IR spectra of polyHEMA's samples with different percentages of ZnO.

The spectra of the other two groups of materials (copolymer and copolymer with crosslinker) with the same amount of ZnO's powders are reported in appendix.

*4.5 DSC Analysis of polyHEMA*

DSC analysis has been made in order to sensitively detect the small heat capacity change due to the glass transition temperature for pHEMA.
During the preparation of the analysis, a small hole was made to the sample's holder in order to allow the evacuation of gasses which could be formed during the thermal process.

Both the sample's and the reference's holders are made by aluminum.

Working condition are as follows:

- Sample mass: 9,11 mg;
- Reference mass: 38.88 mg;
- Inert Argon atmosphere;
- Temperature range: from 26,1 °C to 150 °C;
- Heat flow 1 (26 °C → 150 °C) + cool flow (150 °C → 20 °C) + heat flow 2 (20 °C → 150 °C).

This first thermal analysis was done in order to obtain the characteristic temperature of glass transition of polyHEMA. For this reason, it is important to properly choose the final temperature of heating in order to avoid the degradation of the sample and then its irreversible damage.

Heating 1: the curve shows an exothermal peak which could represent the process of post-polymerization.

It can be measured a temperature of glass transition (Tg) of 77.7 °C; that means that under this temperature the polyHEMA is solid, while up to that value of temperature the polymer starts to become more plastic.

After this first analysis, using the same sample was made a second heating, from 29.2 to 300 °C, to discover the temperature at which starts the degradation of polyHEMA.

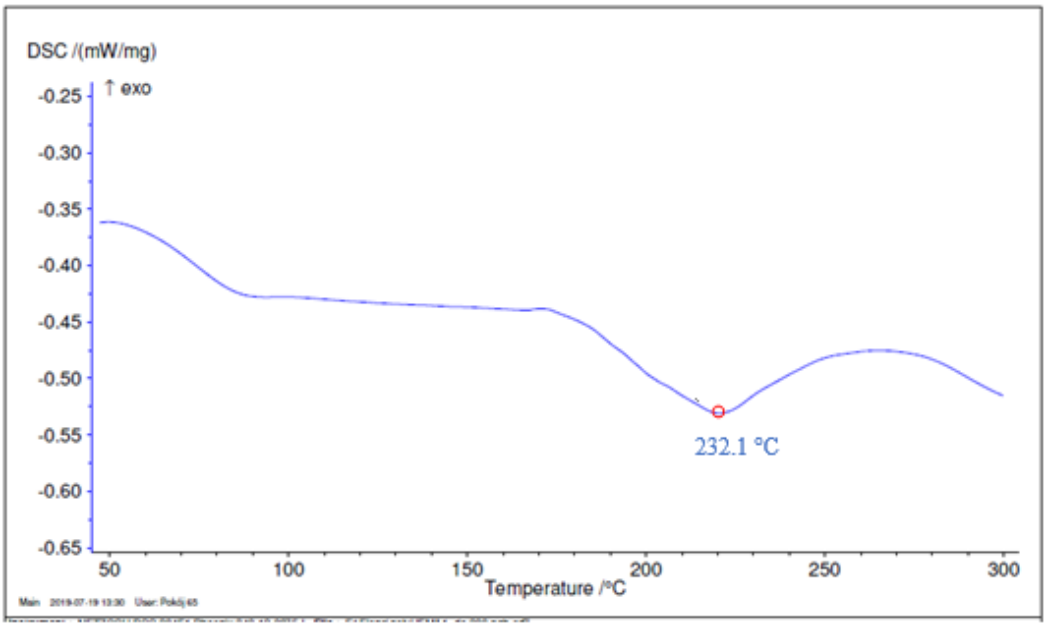


**Figure 4.5 (1)** Thermal Degradation analysis of polyHEMA by DSC.

Heating 2: in Figure 4.5 (1) is not observed any mass loss until 232.1 °C, in which the amount of weight reduction is about 5%.

*4.6 TGA-FT-IR Analysis of PolyHEMA's composites and copolymers*

About the TGA analysis that have been made, the curves of the three types of composites with 0.1%wt of ZnO are shown below, in comparison with the line of ZnO powders.

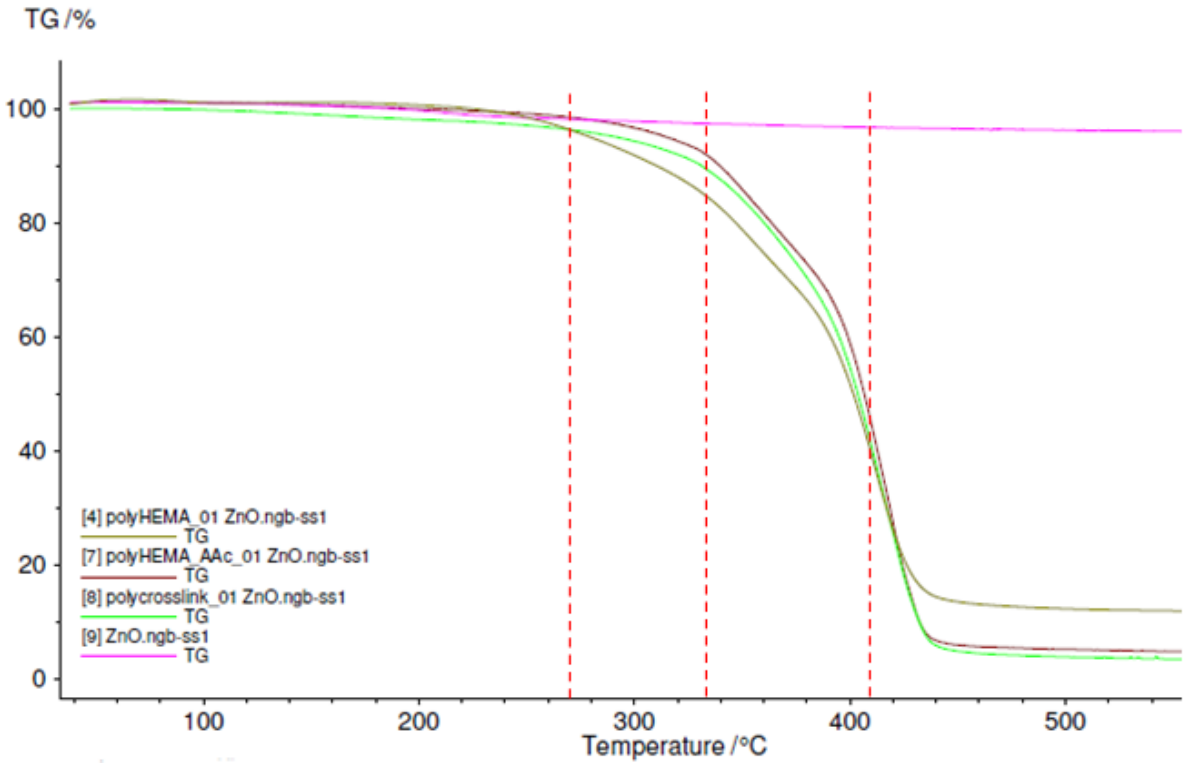


**Figure 4.6 (1)** TGA curves of the composite samples and ZnO powders recorded at a heating rate of 10 °C/min in Helium atmosphere: (4) Poly(HEMA-co-AAc)+0.1% ZnO; (7) PolyHEMA+0.1% ZnO; (8) PolyHEMA crosslinked+0.1% ZnO; (9) ZnO, control sample.

The analysis has been made starting from a temperature of 35 °C up to 700 °C with a heating rate of 10 °C/min, in order to examine the composition effect on thermal degradation of different composites with the same amount of ZnO (0.1%).

From the resultant curves, it can be seen that the sample degradation is a three stages process; this is evidenced by appearance of distinct peaks in TG thermograms.
On the other hand, the mass loss of pHEMA reaches a maximum at 428.71 °C

The poly(HEMA) polymer showed improved thermal stability as observed by a reduction in mass loss rate from the TGA measurements in Helium atmosphere (Figure 4.6 (1)). The results of TGA analyses showed that the weight loss for all composites occurs in three steps. The first step is due to the evaporation of non-bonded water and other volatile compounds from room temperatures to ~273

°C. The second step, that occurs around ~337 °C, is probably due to the emission of residual monomer that was still inside the composites.
To complete, the third step of thermal degradation is due to the emission of carbon mono- and di-oxide, which are obtained because of the high temperature, starting at ~408.6 °C.

It is interesting to notice that, even if the analysis was made in inert atmosphere without oxygen, however oxides were formed. That happened because the hydrolysis of HEMA, which is an ester, produces COOH groups. By them, at high temperature the reaction of decarboxylation takes place and emits carbon mono- and di- oxide.

HEMA ⟶ COOH
Hidrolysis

COOH ⟶ Carbon Oxide
High Temp

The emissions from TGA has been evaluated and identified by FT-IR Analysis, which gives a 3D spectrum of gases produced during the thermal degradation.

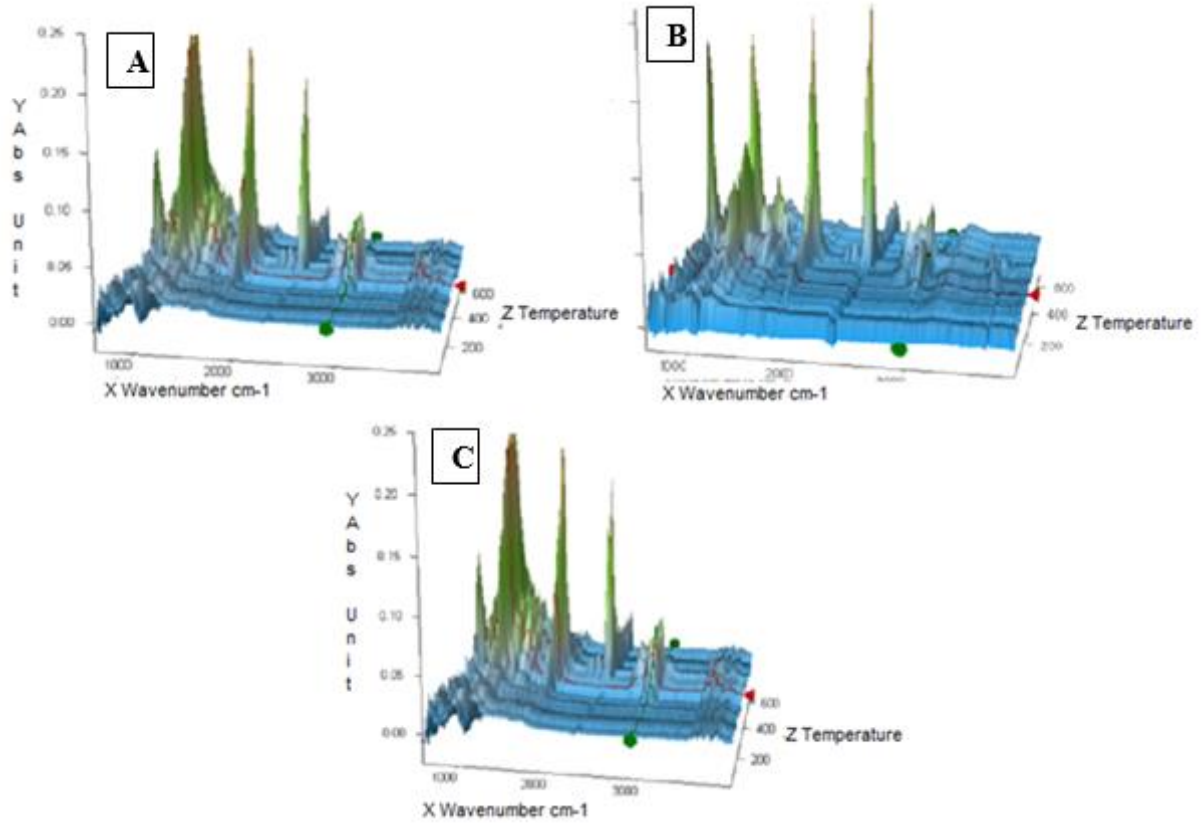


**Figure 4.6 (2)** 3D FT-IR Spectrum: (A) polyHEMA + 0.1% ZnO, (B) poly(HEMA-co-AAc) + 0.1% ZnO, (C) Crosslinked copolymer + 0.1% ZnO.

From the 3D FT-IR (Fig 4.6 (2)) spectra of gases evolved during thermal decomposition of polymer and copolymer samples, has been extracted the spectra at the temperatures of maximum decomposition. In Figure 4.6 (3) are shown as example the spectra of polyHEMA and poly(HEMA-co-AAc), both with the addition of 0.1% of ZnO.

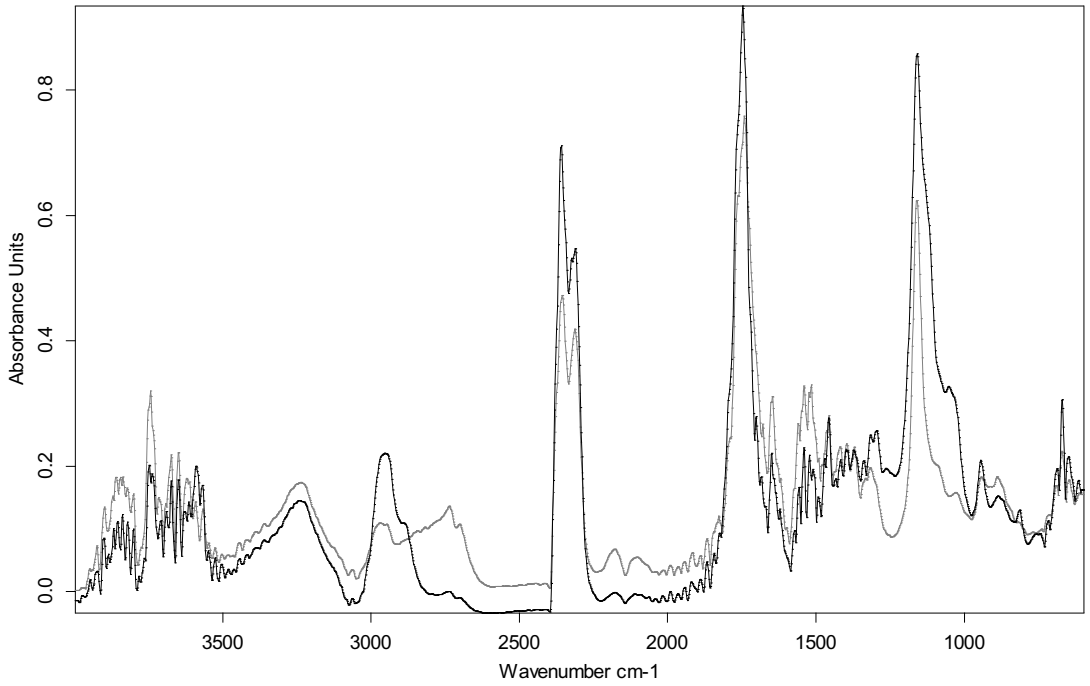


**Figure 4.6 (3)** The FTIR spectra of the evolved gases from pHEMA+0.1% ZnO at 289°C (grey) and from p(HEMA-co-AAc)+0.1% ZnO at 414°C (black).

It can be concluded that the degradation of pHEMA and p(HEMA-co-AAc) runs via depolymerization process to HEMA which is followed by the side chain scission reactions, water elimination and decarboxylation. In the spectra presented in Fig 4.6 (2), the characteristic absorption bands for HEMA are at 1701 $cm^{-1}$, 1643 $cm^{-1}$ and 1162 $cm^{-1}$. Instead, the peaks at 2357, 2311 and 670 $cm^{-1}$ belong to carbon dioxide, while the peak at 1747 $cm^{-1}$ is associated to another carbonyl specie. Finally, the spectrum regions at 3800-3600 $cm^{-1}$ and 1600-1400 $cm^{-1}$ are characteristic of water evaporation.

# 5 Drug Uptake and Release

Before starting to charge the samples with drugs (drug uptake experiments), the most appropriate concentration of the solution with drug had to be determined.

To this purpose, the maximum solubility reported in the datasheet of both the commercial drugs has been taken into account as a reference to set the starting concentration of the uptake solutions.

| Drug | Maximum solubility |
|---|---|
| Ibuprofen | 100 mg/mL |
| Diclofenac | 50 mg/mL |

Then, pure polyHEMA samples were selected to make the first trial of drug absorption and to find the best time of uptake, from 1 h up to 4 h.

During this time, the concentration of the solution was measured each hour, in order to monitor the drug uptake process and chose the proper time of uptake. Moreover, also the integrity of the sample was monitored for all the time, to see if it remained intact.

It has been found that the drug absorpion continued to increase during time, but at the end of the trial, the sample appeared too soft. This was due to the swelling property of the polymer, which is at the basis of the mechanism by which the drug can be effectively absorbed within the sample itself.

From a study made on some properties of Poly(2-hydroxyethyl methacrylate), among them the swelling ratio, it has been taken the graph below that shows the swelling profile of the polymer during time in a solution at 37 °C (pH 7.4) (Dijana Takić Miladinov, August 2016).

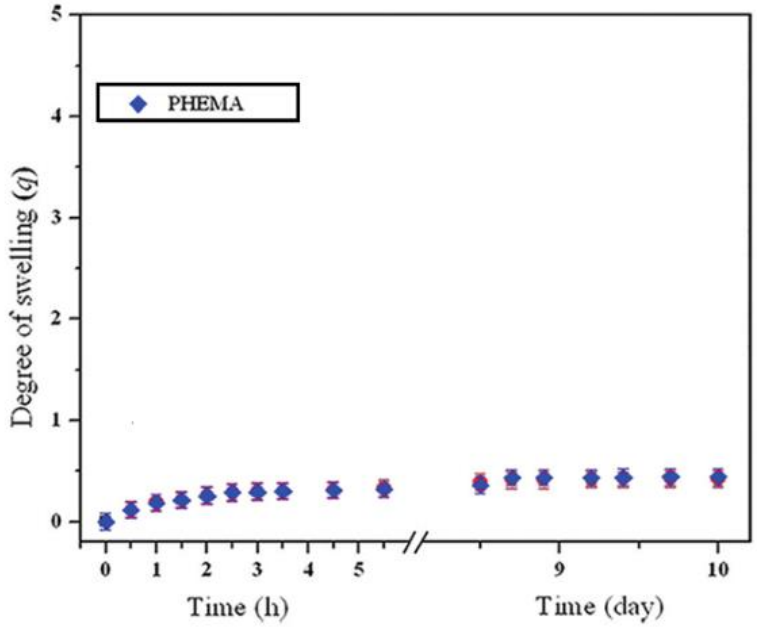


**Figure 5** Swelling rate of polyHEMA in buffer at 37°C (pH 7.4).

From Figure 5 it is possible to notice that the swelling profile already reaches the plateau after 4 hours. That means that after this time, the material does not absorb the solution (in the case of this thesis work, the drug inside water) anymore.
Hence, if the polymer is kept in the solution for too long, there is a risk that its meshes would widens excessivelly or that the hydrolysis process would start.
This fact should lead to the leakage of drug from the sample and consequently to the failure of the uptake process.

For that reason, considering the evidence that the drug absorption continued up to all 4 hours but also that after that time might start the hydrolysis degradation, it has been choosen 4 hours of immersion as standard time of uptake, both for ibuprofen and diclofenac sodium salts drugs.

For what concern the release, the time of study has been set at 2 weeks (336 hours). After that period, the samples have been dried in oven and then analyzed with different cheracterization thechniques as FESEM, XRD and also IR spectroscopy.

### *5.1 Calibration curves*

The concentration of the drug solution both during the uptake and the release experiments has been evaluated by means of UV-Vis spectroscopy.

This technique provides the absorbance of the solution, from which the concentration can be determined according to the Lambert-Beer Law.
To do that, it is necessary to know the equation of the calibration line for each drug in each solvent used.

In analytical chemistry, a calibration curve is a general method for determining the concentration of a substance in an unknown sample by comparing it to a set of standard samples of known concentration (Translations, 2019).

For this study, the calibration lines have been derived including two different standards: ibuprofen in artificial urine and diclofenac in artificial urine; both used used to analyze their release trend in different conditions.

For each standard, a series of test-tubes at different concentrations near the expected concentration of the analyte in the unknown samples have been prepared. The concentrations of the standards should lie within the working range of the technique used.

At first, 7 samples of 1 mL each at a different concentration of Diclofenac in urine have been prepared: starting from the most concentrate solution (3600 μg/mL), the following 6 serial dilutions have been made until reaching the lowest concentration 0,0036 μg/mL.
The dilutions, with a dilution factor of 10, were made by taking 100 μL from the previous solution more concentrated and adding 900 μL of bidistilled water.
The concentration of the first test-tube has been chosen taking into account the highest amount of diclofenac adsorbed by the samples previously loaded with the drug. This value was converted in the maximum concentration achievable durign the potential release of the drug in solution.This quantity

was estimated before the construction of the calibration curves, simply weighting the samples before and after the uptake of diclofenac.

The same dilutions, starting from the same concentration, were made concerning the cases of ibuprofen in artificial urine.

Once the series of all the standards were ready, a 96-well quartz plate has been prepared for the UV-Vis spectroscopy.
Firstly 100 μL of artificial urine and 100 μL of water have been inserted, to be used as background.
For each concentration, two plate's wells were filled with 100 μL of solutions, in order to have all data in duplicate, to be averaged at the end.

Firstly, the UV-Vis analysis has been made on the drugs Ibuprofen and Diclofenac to evaluate the presence of an absorbance peaks and to obtain a calibration curve. UV-Vis absorbance spectra were collected in the range 200–800 nm by means of a UV-VIS spectrometer microplate reader (Multiskan™ FC Microplate Photometer, from ThermoFischer Scientific). The software used to control the microplate reader is SkanIt RE. All of the UV spectra have been background subtracted.

Every substance is able to absorb the radiation at a specific wavelength. That is the reason why the spectrum is made for diclofenac in urine and for ibuprofen in both water and urine, in order to discover their specific absorbtion wavelength.
From the absorbance obtained by the spectrum, for each standard it has been created the graph Absorbance-Wavelength, from which it was possible to see the absorbtion peaks of both the drugs.

After that, a second series of scans have been collected at the wavelength, for which Ibuprofen and Diclofenac has an absorbance's peak to obtain a calibration line.
Each concentration is associated with an absorbance, and it is possible to chart the calibration line (Abs-Conc graph).

It is important to specify that the Lambert-Beer Law is particularly good to describe the absorption behavior of diluted solutions, with the maximum concentration associated with an absorbance value of 3; hence, beyond this limit, it is possible to notice some variance from the proportionality between absorbance and concentration. These problems may result from the fact that at high concentrations, the distance between ions or molecules decreases to the point that each particle influence the distribution of electrical charges of the surrounding particles. This changes their ability to absorb at their precise wavelength (n.d., s.d.).

The calibration line has an equation of the type: y=a+b*x, where the "a" parameter is the intercept and the "b" parameter is the slope. In accordance with the Lambert-Beer Law, this equation can be used to calculate the concentration of an absorbing specie knowing its absorbance:

$$A=a+b*C$$

- A: Absorbance:
- C: Concentration;
- a: Extinction coefficient;
- b: Length of the beam in the absorbing medium.

*5.2 Diclofenac*

Figure 5.2 (1) shows the absorbance spectrum of Diclofenac in simulated urine for wavelengths between 200 and 800 nm. The background, composed by pure artificial urine and quartz of the 96-well plate, has been already subtracted:

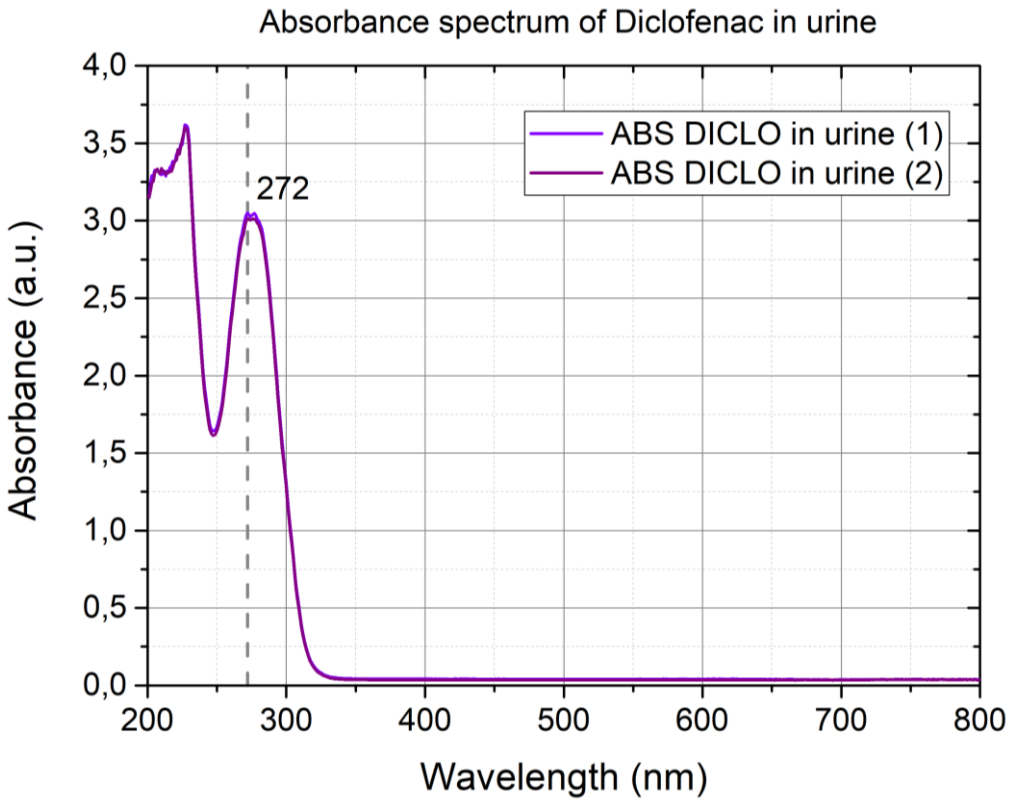


**Figure 5.2 (1)** Diclofenac absorbance spectrum in urine.

The Diclofenac has a peak of absorbance at 272 nm, thus the next scan of the 7 samples with different concentrations in artificial urine have been made at this wavelength.
In Tables 5.2 are reported the recorded absorbance values. The concentrations with absorbance around or higher than 3 have been highlighted in red, as these do not respect the Lambert-Beer Law and cannot be represented in the calibration curves.

| **272nm** | |
|---|---|
| CONC [µg/ml] | ABS DICLO in urine |
| 3600 | 3,540 |
| 360 | 2,967 |
| 36 | 0,332 |
| 3,60 | 0,024 |
| 0,360 | 0,002 |
| 0,036 | N/A |
| 0,0036 | 0,000 |

**Table 5.2** Mean Absorbance of Diclofenac in urine at each concentration. N/A means that the absorbance resulted to be less than the instrument resolution.

The absorbance values obtained have been interpolated with the software Origin8 to obtain a calibration curve of the drug (Figure 5.2 (2)).
In table 5.2 it has been indicated as N/A the absorbance values related to a concentration resulted to be negative, which means that the absorbance detected was less than the instrument resolution.
In the calibration curve these values shall be replaced by 0.

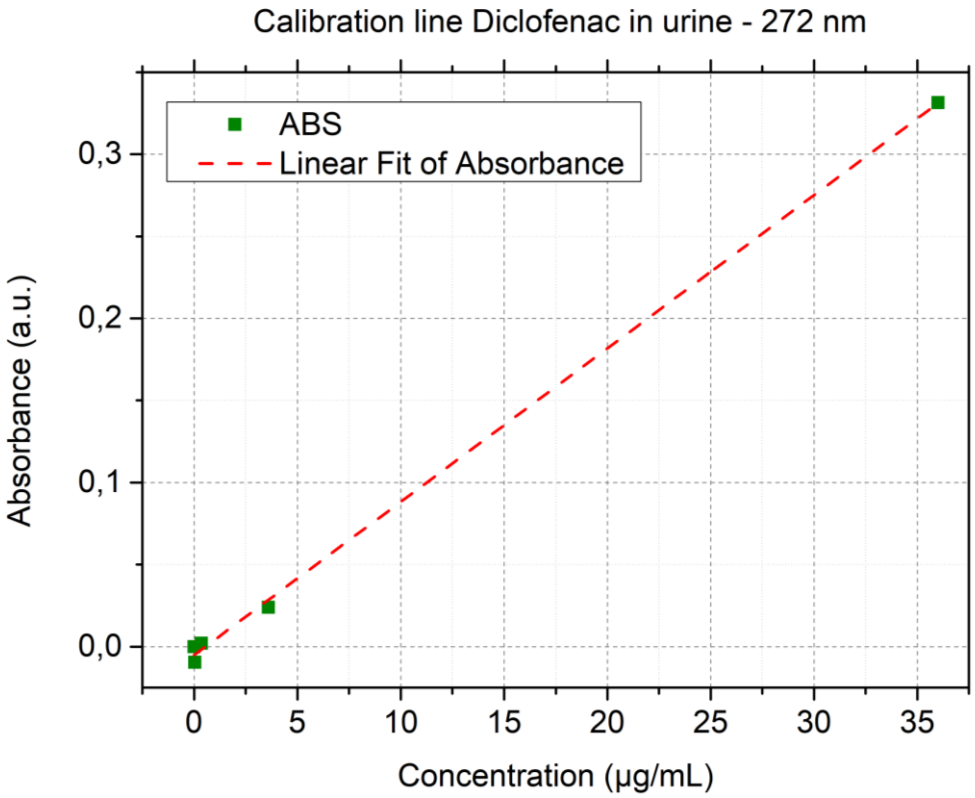


**Figure 5.2 (2)** Diclofenac calibration line in artificial urine.

| Equation y= a + b*x | | | |
|---|---|---|---|
| Adj. R-Square 0.99872 | | | |
| **DICLO in Urine** | | Value | Standard Error |
| Abs | Intercept | -0.00511 | 0.0027 |
| Abs | Slope | 9.34E-03 | 1.67E-04 |

The equation of the calibration curve in artificial urine is the following one:

$$y = -0.00511 + 0.00934x$$

- $y$: Absorbance (A) of the sample;
- $x$: Concentration (C) of the sample.

### *5.2.1 Uptake Diclofenac in water*

Before starting with the uptake of Diclofenac, it was necessary to determine all the process parameters, such as: concentration of the solution with drug, method to measure the drug absorbed by the sample.

Regarding the starting concentration of the solution, the datasheet of Diclofenac Sodium Salt has been taken into account, in which the maximum solubility indicated in water had a value of 50 mg/mL. Hence, it has been decided to take this value, preparing 1 mL of drug solution. However, at this concentration the solution looked cloudy, indicating the not perfect dissolution of the drug in water. For that reason, there were some tests preparing different concentrations in the same volume, in order to choose the highest one that did not show saturation.
At the end, the maximum concentration chosen for the Diclofenac uptake was 10 mg/mL.

Regarding the analysis method of the uptake, to measure the effective amount of drug absorbed, a precision scale was used. Therefore, before beginning the uptake, all the samples were weighed.

After having determined all the process parameters, the samples were loaded with drug. For each material of the two classes, the drug loading experiments were performed in triplicate. A solution of 10 mL with 100 mg of drug was prepared, in order to immerse three samples (of the same material) at once.

The solution was prepared in a small vessel and put on the heating magnetic stirrer. The temperature was increased up to 37 °C in order to further support the solubility. To avoid the evaporation of the solvent, a gas-tight cap was put on the vessel and the samples were soaked under magnetic stirring conditions.to avoid the creation of concentration gradients.

When 4 hours have passed, the samples were removed and, after several rounds of drying in the oven at 50 °C, were weighted again.

In the Table 5.2.1 (1) below, the weights before and after the uptake of the samples used to study the release in physiologic urine have been reported, together with the total amount absorbed by each.

| **DICLO uptake weight Physiologic release** | PRE-UPTAKE | | POST-UPTAKE | | Uptake (mg) | |
|---|---|---|---|---|---|---|
| | Sample 1 (mg) | Sample 2 (mg) | Sample 1 (mg) | Sample 2 (mg) | Sample 1 (mg) | Sample 2 (mg) |
| PolyHEMA pure | 313 | 425.1 | 320.4 | 438.0 | 7.4 | 12.9 |
| PolyHEMA + 0.1% ZnO | 357 | 298.4 | 366.6 | 307.5 | 9.6 | 9.1 |
| PolyHEMA + 1% ZnO | 329.5 | 393.1 | 332.9 | 402.0 | 3.35 | 8.9 |
| Poly(HEMA-co-Aac) pure | 384.5 | 311.2 | 397.9 | 397.9 | 13.4 | 86.7 |
| Poly(HEMA-co-Aac) + 0.1% ZnO | 354.2 | 350.5 | 366.0 | 366.0 | 11.8 | 15.5 |
| Poly(HEMA-co-Aac) + 1% ZnO | 327.3 | 293.5 | 340.8 | 340.8 | 13.5 | 47.3 |

**Table 5.2.1 (1)** Weights before and after the uptake. Samples used for release in physiologic urine.

Other 2 samples for each material have been prepared and loaded with drug, in order to study the release in alkaline (Sample 3) and acid (Sample 4) urine. The amounts of drug absorbed have been reported in Table 5.2.1 (2).

| DICLO uptake weight Alkaline/acid release | PRE-UPTAKE | | POST-UPTAKE | | Uptake (mg) | |
|---|---|---|---|---|---|---|
| | Sample 3 (mg) | Sample 4 (mg) | Sample 3 (mg) | Sample 4 (mg) | Sample 3 (mg) | Sample 4 (mg) |
| PolyHEMA pure | 363.8 | 237.3 | 375.2 | 249.6 | 11.4 | 12.3 |
| PolyHEMA + 0.1% ZnO | 267.8 | 342.6 | 275.1 | 357.0 | 7.3 | 14.4 |
| PolyHEMA + 1% ZnO | 328.4 | 306.1 | 338.1 | 320.3 | 9.7 | 14.2 |
| Poly(HEMA-co-Aac) pure | 432.4 | 293.4 | 447.5 | 305.7 | 15.1 | 12.3 |
| Poly(HEMA-co-Aac) + 0.1% ZnO | 337.1 | 335.2 | 347.9 | 350.1 | 10.8 | 14.9 |
| Poly(HEMA-co-Aac) + 1% ZnO | 294.4 | 303.9 | 305.1 | 317.4 | 10.7 | 13.5 |

**Table 5.2.1 (2)** Weights before and after the uptake. Samples used to study the release in alkaline/acid urine.

### *5.2.2 Diclofenac Release in physiologic artificial urine*

The release in artificial urine at physiological pH (around 7.3) was carried out including the first 2 samples of each material, previously loaded with Diclofenac; thus in total 12 samples were analyzed.

First of all, 12 falcons filled with 50 mL of artificial urine have been prepared and put inside a MultiTherm™ Vortex incubator, in order to maintain the temperature at 37 °C and keep the solutions stirred at 200 rpm. From each falcon, 100 µL were collected at each time step and then inserted in the 96-well quartz plate, to be used as background.

Then, each sample has been put inside 1 falcon and the release analyses started.

It has been decided to control the release trend by collecting the solution from each Falcon every hour, during the first 6 hours. Then, the follow-up has continued measuring the concentrations after 24 h, 48h, 168 h (1 week) and 336 h (2 weeks).

Even in this case, to prepare the quartz plate for the following UV-Vis analysis it has been taken 200 µL from each falcon, in order to fill 2 wells and to have duplicate data.

Firstly, the UV-Vis absorbance spectra were collected in the range 200–800 nm, in order to evaluate the trend of the absorbance peak of Diclofenac. In the following is reported as an example, the graph that collects all the spectra of poly(HEMA) + 1% ZnO, sample 1:

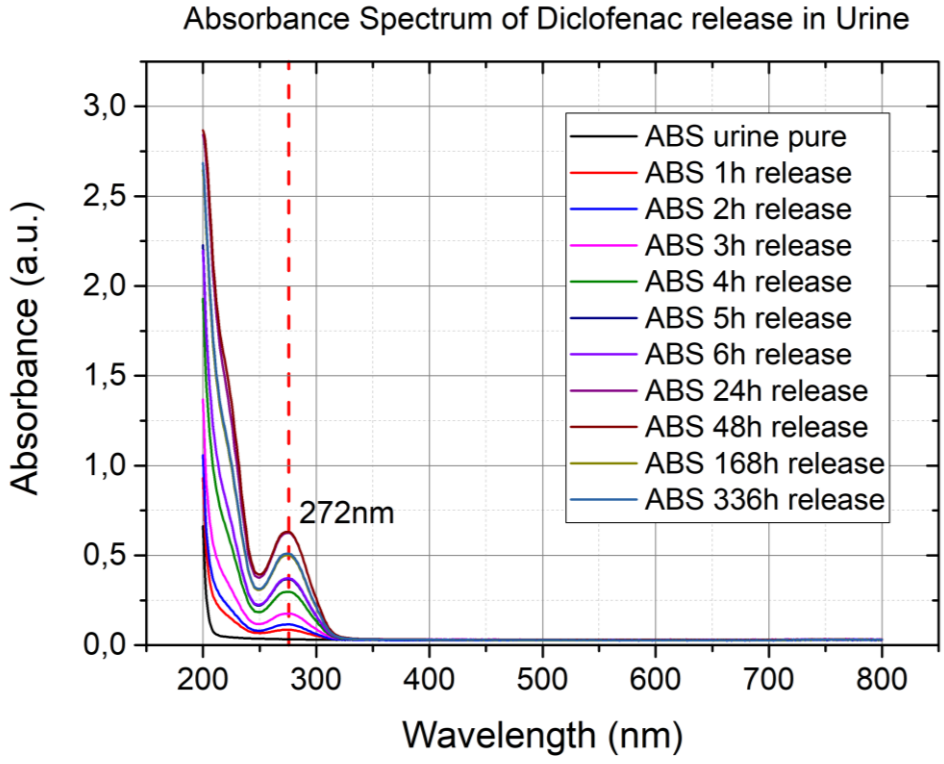


**Figure 5.2.2 (1)** Spectrum of sample 1, poly(HEMA) + 1% ZnO.

Then, the second series of scans have been collected at 272 nm (Diclofenac characteristic wavelength) to obtain the absorbances.

The amount of drug released from each material of polyHEMA and poly(HEMA-co-AAc) has been evaluated using the calibration line equation of Diclofenac in artificial urine:

$$y = -0.00511 + 0.00934x$$

The results of the release test are reported in Table 5.2.2 (1):

| Release time [Hours] | pHEMA pure | pHEMA 0.1% ZnO | pHEMA 1% ZnO | copHEMA pure | copHEMA 0.1% ZnO | copHEMA 1% ZnO |
|---|---|---|---|---|---|---|
| 0 | 0.547± 0.000 | 0.547± 0.000 | 0.547± 0.000 | 0.547± 0.000 | 0.547± 0.000 | 0.547± 0.000 |
| 1 | 18.963±12.848 | 17.464±0.107 | 22.228±4.229 | 8.577±1.713 | 8.818±1.713 | 13.395±0.268 |
| 2 | 4.857±4.470 | 23.995±0.589 | 28.170±7.602 | 14.600±1.954 | 13.957±1.954 | 20.622±0.054 |
| 3 | 17.437±1.793 | 28.706±2.248 | 33.283±8.324 | 19.123±3.587 | 16.500±3.587 | 24.798±0.964 |
| 4 | 26.216±2.382 | 34.942±1.633 | 40.643±12.313 | 22.175±4.122 | 21.024±4.122 | 26.885±0.214 |
| 5 | 32.426±3.667 | 37.994±1.258 | 43.507±13.517 | 25.681±4.309 | 23.781±4.309 | 30.419±0.161 |
| 6 | 32.185±4.390 | 38.797±2.115 | 44.203±11.215 | 27.100±4.764 | 25.199±4.764 | 32.346±0.054 |
| 24 | 56.329±6.317 | 51.216±0.187 | 55.660±14.855 | 39.974±5.327 | 38.770±5.327 | 43.240±0.509 |
| 48 | 59.460±1.579 | 52.340±2.382 | 56.784±2.168 | 41.099±1.044 | 39.894±1.044 | 44.364±0.294 |
| 168 | 62.057±4.818 | 51.645±1.900 | 53.599±14.615 | 40.135±4.845 | 38.663±4.845 | 43.748±0.910 |
| 336 | 60.156±3.078 | 51.645±1.847 | 53.572±14.588 | 40.001±4.925 | 38.529±4.925 | 43.641±1.017 |

**Table 5.2.2 (1)** Diclofenac release's concentrations [µg/mL].

From each absorbance values, the background of pure artificial urine was subtracted (as explained above) and the mean of the 2 samples for each material has been calculated.

In red are highlighted the maximum value of release; it can be observed that the maximum release is reached after 2 days of immersion in physiologic urine; only the polyHEMA pure has continued to release Diclofenac, reaching the maximum value after 1 week.

Knowing the amount of drug uptaken by each sample (see Table below):

| | Uptake (mg) | |
|---|---|---|
| | Sample 1 (mg) | Sample 2 (mg) |
| PolyHEMA pure | 7.4 | 12.9 |
| PolyHEMA + 0.1% ZnO | 9.6 | 9.1 |
| PolyHEMA + 1% ZnO | 3.35 | 8.9 |
| Poly(HEMA-co-Aac) pure | 13.4 | 86.7 |
| Poly(HEMA-co-Aac) + 0.1% ZnO | 11.8 | 15.5 |
| Poly(HEMA-co-Aac) + 1% ZnO | 13.5 | 47.3 |

and comparing it with the relative concentration, it was possible to calculate the % Release. Also in this case, the percentages of the samples owned to the same material have been mediated (Table 5.2.2 (2)):

| **Release time [Hours]** | **pHEMA pure** | **pHEMA 0.1% ZnO** | **pHEMA 1% ZnO** | **copHEMA pure** | **copHEMA 0.1% ZnO** | **copHEMA 1% ZnO** |
|---|---|---|---|---|---|---|
| 0 | 0±0 | 0±0 | 0±0 | 0±0 | 0±0 | 0±0 |
| 1 | 0.239±0.191 | 0.187±0.006 | 0.490±0.288 | 0.072±0.005 | 0.079±0.006 | 0.107±0.005 |
| 2 | 0.039±0.034 | 0.257±0.013 | 0.642±0.411 | 0.124±0.001 | 0.125±0.007 | 0.164±0.011 |
| 3 | 0.191±0.069 | 0.308±0.032 | 0.752±0.472 | 0.161±0.009 | 0.147±0.003 | 0.198±0.022 |
| 4 | 0.272±0.050 | 0.374±0.027 | 0.938±0.620 | 0.187±0.010 | 0.188±0.006 | 0.215±0.017 |
| 5 | 0.334±0.054 | 0.407±0.024 | 1.007±0.670 | 0.217±0.007 | 0.213±0.008 | 0.243±0.019 |
| 6 | 0.330±0.046 | 0.416±0.034 | 1.000±0.630 | 0.228±0.009 | 0.225±0.009 | 0.258±0.019 |
| 24 | 0.581±0.095 | 0.548±0.017 | 1.266±0.808 | 0.339±0.001 | 0.348±0.030 | 0.345±0.029 |
| 48 | 0.637±0.188 | 0.560±0.011 | 1.174±0.560 | 0.356±0.057 | 0.358±0.040 | 0.354±0.028 |
| 168 | 0.646±0.128 | 0.552±0.006 | 1.222±0.784 | 0.341±0.005 | 0.347±0.030 | 0.350±0.032 |
| 336 | 0.631±0.141 | 0.552±0.005 | 1.221±0.783 | 0.340±0.004 | 0.345±0.028 | 0.349±0.033 |

**Table 5.2.2 (2)** Diclofenac %released amount in physiologic urine.

In order to obtain more precise percentage values, it has been made the normalization of the % Release as compared with each maximum value within each sample. The 2 different normalized values obtained for each material have been mediated, and the standard error has been calculated (Table 5.2.2 (3)):

| Release time [Hours] | Normalized % Release ± Standard Error | | | | | |
|---|---|---|---|---|---|---|
| | pHEMA pure | pHEMA 0.1% ZnO | pHEMA 1% ZnO | copHEMA pure | copHEMA 0.1% ZnO | copHEMA 1% ZnO |
| 0 | 0±0 | 0±0 | 0±0 | 0±0 | 0±0 | 0±0 |
| 1 | 30.629±24.545 | 32.949±1.083 | 35.238±20.700 | 19.501±1.285 | 22.142±1.788 | 30.199±1.556 |
| 2 | 7.290±6.307 | 45.298±2.321 | 44.195±28.276 | 33.274±0.060 | 35.091±2.081 | 46.487±3.200 |
| 3 | 27.448±9.982 | 54.283±5.691 | 52.351±32.831 | 43.499±2.319 | 41.583±0.745 | 55.884±6.146 |
| 4 | 40.906±7.552 | 66.011±4.843 | 63.486±41.940 | 50.443±2.603 | 52.941±1.692 | 60.601±4.809 |
| 5 | 50.543±8.230 | 71.745±4.290 | 67.890±45.174 | 58.458±1.927 | 59.871±2.131 | 68.567±5.258 |
| 6 | 50.114±7.001 | 73.310±5.947 | 69.496±43.745 | 61.669±2.541 | 63.419±2.658 | 72.912±5.328 |
| 24 | 87.805±14.380 | 96.625±2.937 | 87.356±55.726 | 91.108±0.217 | 97.320±8.424 | 97.463±8.101 |
| 48 | 93.276±27.551 | 98.594±1.853 | 91.801±43.806 | 94.210±15.115 | 100.000±11.093 | 100.000±7.803 |
| 168 | 96.887±19.130 | 97.310±0.980 | 84.057±53.931 | 91.516±1.385 | 97.059±8.276 | 98.603±9.081 |
| 336 | 94.033±20.956 | 97.313±0.879 | 84.019±53.887 | 91.202±1.157 | 96.749±7.793 | 98.360±9.303 |

**Table 5.2.2 (2)** Diclofenac normalized % released amount.

The releases of both pure PolyHEMA and Poly(HEMA-co-AAc) is shown in Figure 5.2.2 (2), instead Figure 5.2.2 (3) shows in the same graph, the releases of polymers and copolymers with 0.1% and 1% of ZnO. It is also shown in both, the enlargement of the release on the first 48 hours.

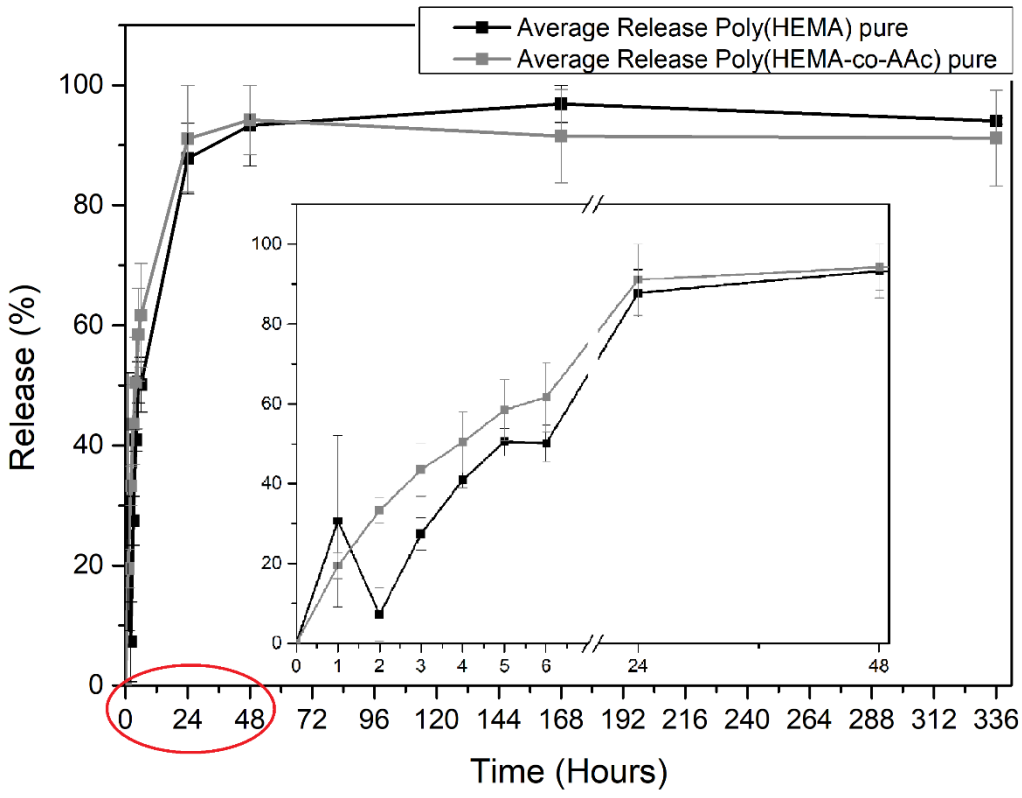


**Figure 5.2.2 (2)** Comparison between the pure pHEMA and copolymer release.

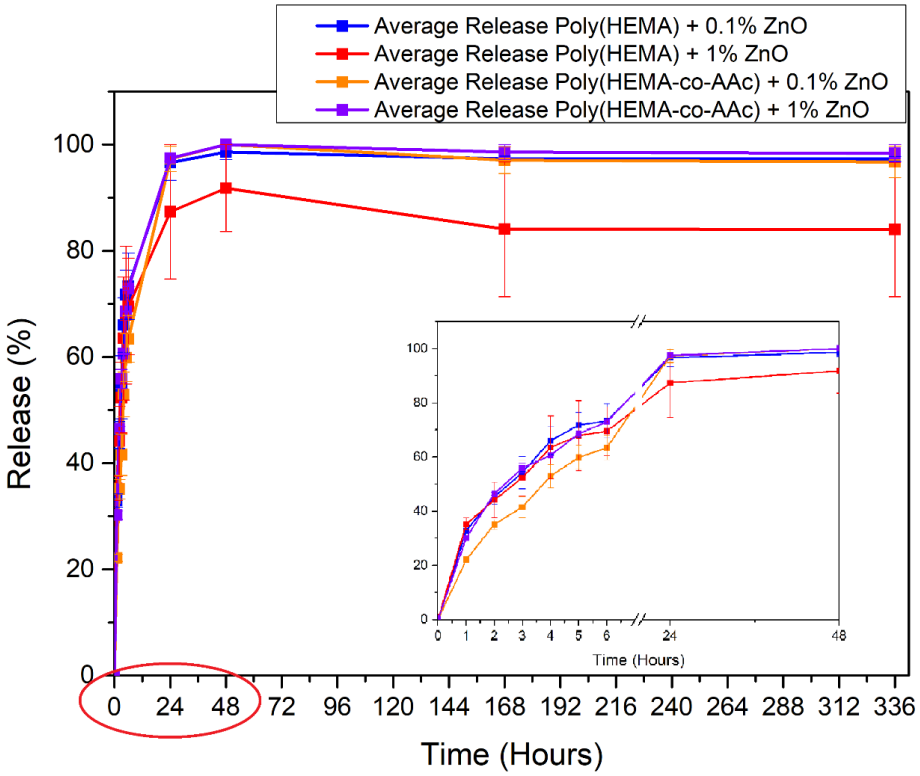


**Figure 5.2.2 (3)** Comparison between materials with 0.1% and 1% ZnO. Enlargement of 2 days release.

Then, the data of each single release curve have been interpolated with the software Origin8 in order to find the best fitting curve for each material (Figure 5.2.2 (4)). The release profile followed a pseudo-first-order kinetic law (see the red fitting curve), characterized by the following equation:

$$y = A * ( 1 - e^{-k(x-x_c)} ).$$

In Table 5.2.2 (3), the release rate constants of each material have been reported in ascending order.

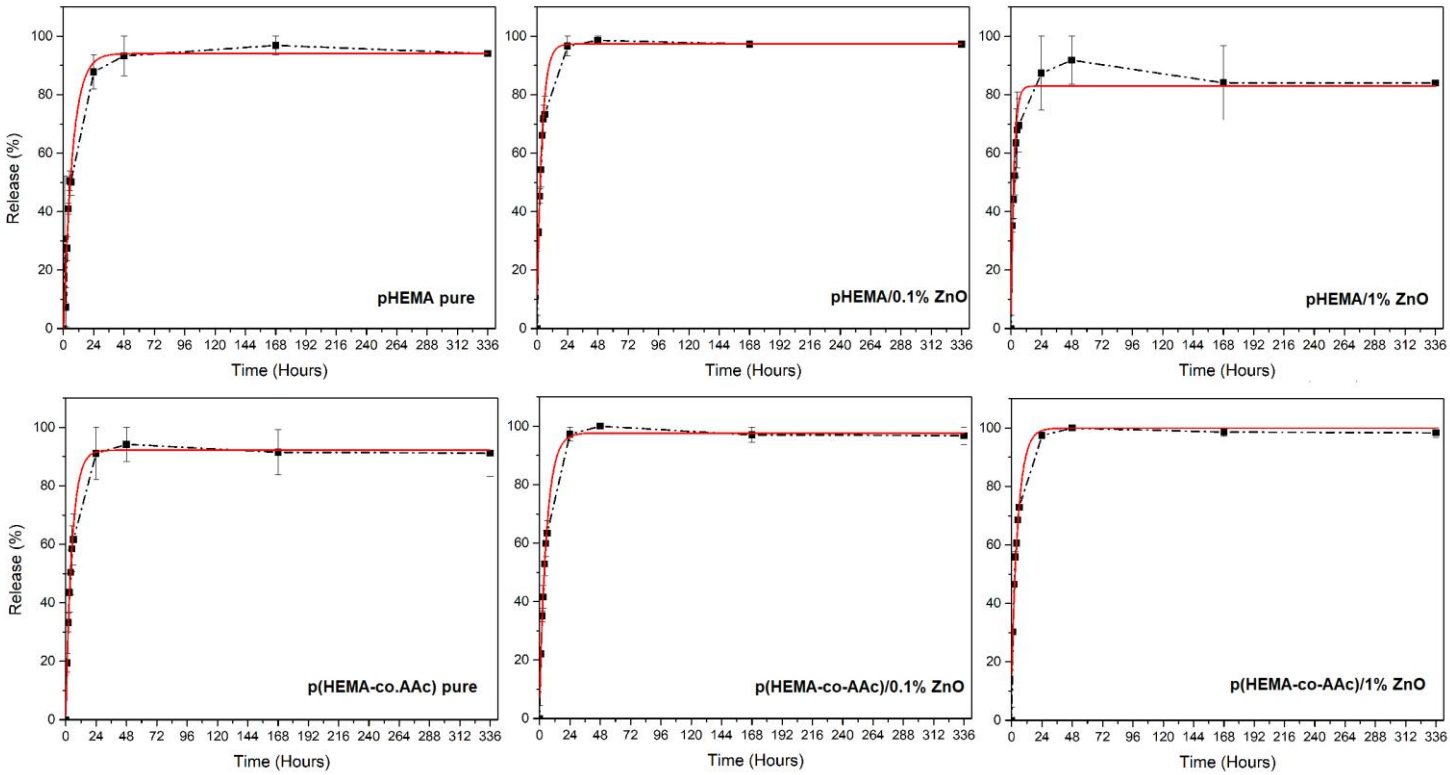


**Figure 5.2.2 (4)** Fitting lines of Diclofenac release graphs in physiologic urine.

| Material | pH | K ($hours^{-1}$) | $R^2$ |
|---|---|---|---|
| PolyHEMA pure | 7.3 | 0.14309±0.01281 | 0.99318 |
| Poly(HEMA-co-AAc)+0.1% ZnO | 7.3 | 0.17754±0.01098 | 0.99768 |
| Poly(HEMA-co-AAc)+1% ZnO | 7.3 | 0.19311±0.0097 | 0.99779 |
| Poly(HEMA-co-AAc) pure | 7.3 | 0.20617±0.00883 | 0.99705 |
| PolyHEMA+0.1% ZnO | 7.3 | 0.26086±0.0275 | 0.99601 |
| PolyHEMA+1% ZnO | 7.3 | 0.42743±0.07401 | 0.94473 |

**Table 5.2.2 (3)** Kinetic parameters of Diclofenac released from pure pHEMA and copolymer and from ZnO/polymer and ZnO/copolymer systems.

The material with the lowest burst release is the polyHEMA pure, which is the only one that has reached the maximum release (96% of the total amount of drug absorbed) after 1 week.

All the other samples have reached the maximum value after 48 hours; in particular the other 2 materials with a low burst release are the two copolymer composites, but they show an important burst delivery after that time with 100% Diclofenac.

By contrast, the two fastest materials are the polymer/ZnO composites with 1% and 0.1% of powder. However, it can be noticed that even if the first has the highest kinetic constant, its maximum release reaches only 91%.

### *5.2.3 Diclofenac Release in alkaline and acid artificial urine*

In general, urine is characterized by different parameters which define its nature. These include for instance density (between 1007 and 1035), temperature (between 32,5 and 37,5 °C) and molecules content as creatine, urea, sodium, potassium and chloride. In urine, these molecules have a significantly higher concentration than in other body fluids. Especially, urea is very important because affects another relevant parameter to control, which is the pH.
It is the final product of the cataboism of proteins, made by liver and it forms the main nitrogen part of urine. Urea contains two amine groups, which are released from its process of distruction, thus the pH value of urine increases, becoming more basic.
In physiologic condition, the normal value of urine pH is between 4.5 and 7.5, with tendency to keep a pH value slightly acid.
Contrary, in pathological conditions, the urine pH can reach the value of 9. For these reasons, it was considered useful to test the drug release from all materials both in alkaline and acid urine (Fabio Manoni, 2016).

In order to do that, 600 mL of artificial urine, previously prepared, has been taken from the stock, 50 mL for each sample.
Then, using the pHmeter and adding sodium hydroxide drop by drop, the pH has reached the value of 9.4.
For the release in alkaline urine, a third sample of each material previously loaded with drugs, has been used. These samples have been cut in half, in order to analyze 2 indipendent release for each material to be averaged.
Concerning the maximum amount of drug in each piece of the same sample, it has been considered the half of that in the one-piece sample.
The same procedure has been done to test the release of drugs from samples in acid urine. In this case, hydrogen chloride has been added in the same volume collected from the stock of artificial urine, up to reach a pH of around 5.2.
Then, for this release study have been used the samples 4, always cut in half.

The release and analysis have been made in the same way as explained for physiological urine.
Therefore, are still given below the results of the release test in alkaline urine through concentrations (Table 5.2.3 (1)) and the normalized % release values (Table 5.2.3 (2)).

| Release time [Hours] | pHEMA pure | pHEMA 0.1% ZnO | pHEMA 1% ZnO | copHEMA pure | copHEMA 0.1% ZnO | copHEMA 1% ZnO |
|---|---|---|---|---|---|---|
| 0 | 0.067±0.001 | 0.067±0.001 | 0.067±0.001 | 0.067±0.001 | 0.067±0.001 | 0.067±0.001 |
| 1 | 19.899±0,027 | 21.452±0.080 | 16.500±0.161 | 29.535±0.401 | 30.820±0.669 | 18.106±0.054 |
| 2 | 29.990±0,161 | 26.190±0.054 | 23.459±0.535 | 35.317±0.723 | 32.640±0.348 | 26.029±0.642 |
| 3 | 36.040±0,161 | 29.883±0.107 | 25.922±0.161 | 36.896±1.445 | 32.212±0.187 | 28.010±0.428 |
| 4 | 40.777±0,401 | 34.648±0.803 | 28.090±0.080 | 39.305±0.642 | 33.363±0.321 | 30.793±0.803 |
| 5 | 43.588±0,696 | 36.334±0.401 | 29.964±0.294 | 41.072±0.642 | 32.319±0.080 | 31.730±0.027 |
| 6 | 48.700±0,294 | 37.458±0.241 | 30.900±0.161 | 41.446±0.910 | 33.818±0.401 | 33.416±0.107 |
| 24 | 61.414±0,535 | 44.043±0.027 | 35.531±0.883 | 45.435±0.027 | 37.458±0.187 | 38.904±0.134 |
| 48 | 66.808±0,308 | 47.670±0.120 | 37.900±0.602 | 48.446±0.147 | 39.907±0.308 | 40.670±0.294 |
| 168 | 72.201±0,080 | 51.297±0.214 | 40.269±0.321 | 51.457±0.268 | 42.357±0.428 | 42.437±0.455 |
| 336 | 76.859±2,168 | 55.526±0.268 | 44.712±0.321 | 54.000±1.686 | 48.085±0.642 | 48.352±0.428 |

**Table 5.2.3 (1)** Diclofenac release's concentrations [µg/mL] in alkaline pH.

To study the release in alkaline urine, it has been used the group of materials named as Sample 4. The amount of drug absorbed by each sample has been reported below:

| DICLO uptake weight for alkaline release study | Uptake (mg) |
|---|---|
| | Sample 3 |
| PolyHEMA pure | 11.4 |
| PolyHEMA + 0.1% ZnO | 7.3 |
| PolyHEMA + 1% ZnO | 9.7 |
| Poly(HEMA-co-Aac) pure | 15.1 |
| Poly(HEMA-co-Aac) + 0.1% ZnO | 10.8 |
| Poly(HEMA-co-Aac) + 1% ZnO | 10.7 |

Knowing these quantities, it was possible to obtain from the concentration values, the % of Diclofenac released by each sample, normalized by the total amount of drug absorbed. The results are reported below in Table 5.2.3(2):

| Release time [Hours] | Normalized % Release ± Standard Error | | | | | |
|---|---|---|---|---|---|---|
| | pHEMA pure | pHEMA 0.1% ZnO | pHEMA 1% ZnO | copHEMA pure | copHEMA 0.1% ZnO | copHEMA 1% ZnO |
| 0 | 0±0 | 0±0 | 0±0 | 0±0 | 0±0 | 0±0 |
| 1 | 25.912±0.766 | 38.634±0,042 | 37.264±0.268 | 54.725±0.965 | 64.089±0.535 | 37.450±0.442 |
| 2 | 39.045±0.892 | 47.168±0,324 | 52.462±0.820 | 65.424±0.705 | 67.883±0.183 | 53.848±1.806 |
| 3 | 46.934±1.533 | 53.821±0,452 | 58.337±0.419 | 68.309±0.544 | 66.997±0.505 | 57.925±0.373 |
| 4 | 53.112±2.021 | 62.394±1,145 | 62.829±0.631 | 72.821±1.084 | 69.387±0.259 | 63.705±2.225 |
| 5 | 56.731±0.695 | 65.441±1,039 | 67.023±1.140 | 76.096±1.187 | 67.227±1.065 | 65.628±0.526 |
| 6 | 60.846±4.751 | 67.465±0,759 | 69.111±0.137 | 76.775±0.712 | 70.332±0.105 | 69.118±0.834 |
| 24 | 79.989±2.953 | 79.321±0,334 | 79.456±1.405 | 84.219±2.580 | 77.909±0.651 | 80.463±0.436 |
| 48 | 94.012±2.547 | 92.387±0,831 | 90.714±0.724 | 95.369±2.482 | 88.091±0.286 | 87.765±0.164 |
| 168 | 97.006±1.324 | 96.194±0,729 | 95.357±0.795 | 97.684±1.813 | 94.046±0.143 | 93.882±0.488 |
| 336 | 100.000±0.100 | 100.000±0,626 | 100.000±0.867 | 100.000±1.143 | 100.000±0.001 | 100.000±0.812 |

**Table 5.2.3 (2)** Diclofenac normalized % released amount in alkaline pH.

In conditions of alkaline pH, it can be noticed that in all the materials, the release increase continuously until the end of the period covered by study, although getting slower after 48 hours. Besides, all the samples reach the 100% of release at the end of the period of study.

Also in this case, the trend release of both pure PolyHEMA and Poly(HEMA-co-AAc) are shown in Figure 5.2.3 (1). Instead, Figure 5.2.3 (2) shows the release profiles of the other composites, with the enlargement on the first 48 hours of release.

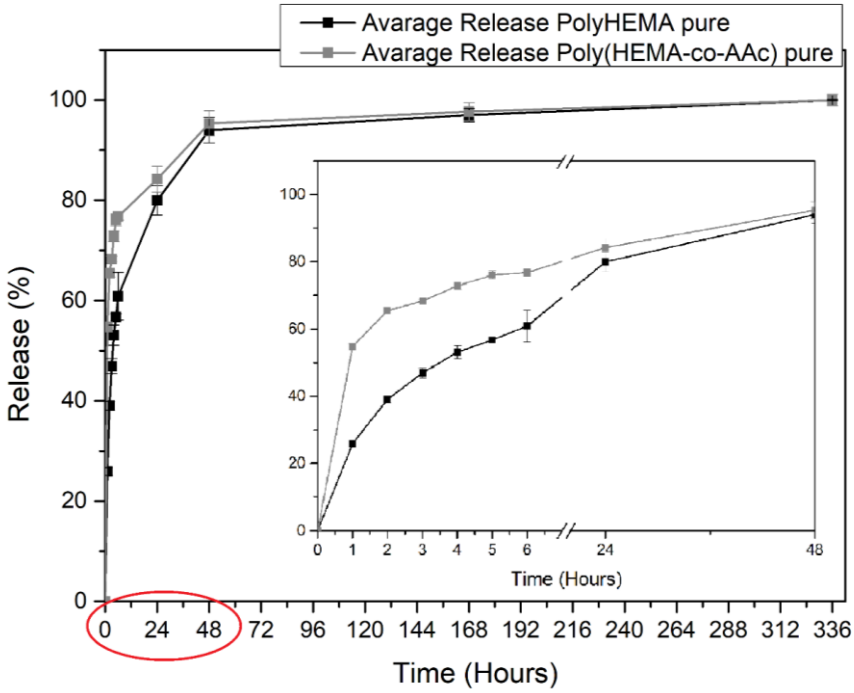


**Figure 5.2.3 (1)** Comparison of pure pHEMA and copolymer release at pH 9.4.

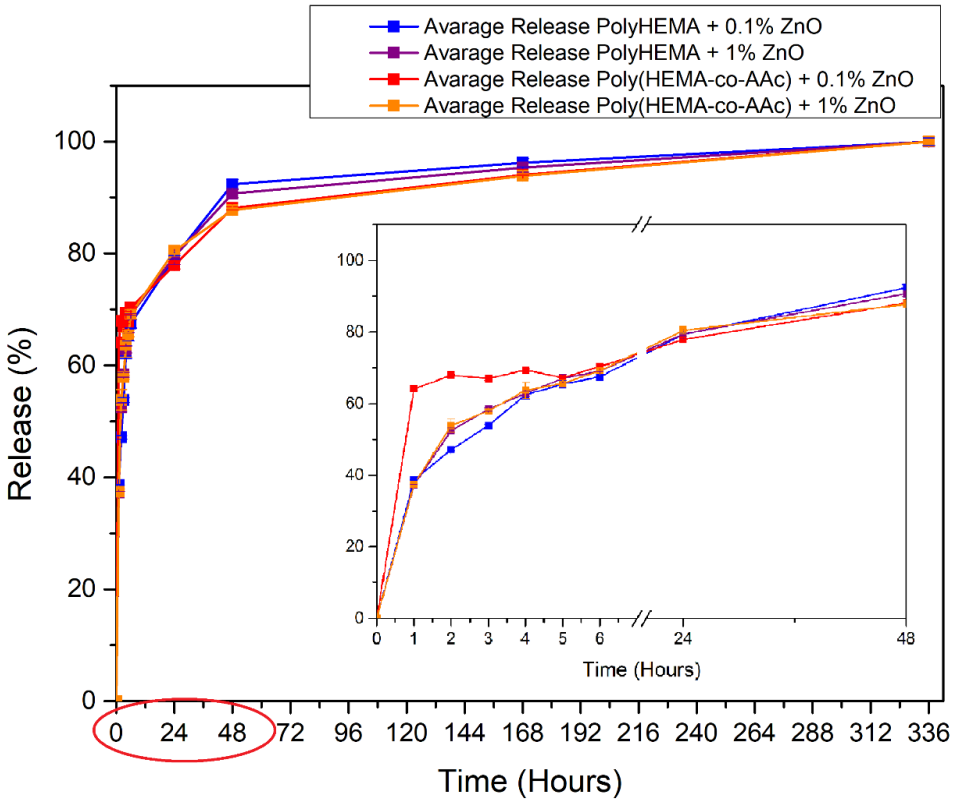


**Figure 5.2.3 (2)** Comparison between materials with 0.1% and 1% ZnO at pH

Using always the same exponential equation, the fitting curves for each material have been found and they have been shown in graphs of Figure 5.2.3 (3) (red line).
In Table 5.2.3 (3), the kinetic parameters of the release profiles have been reported in ascending order.

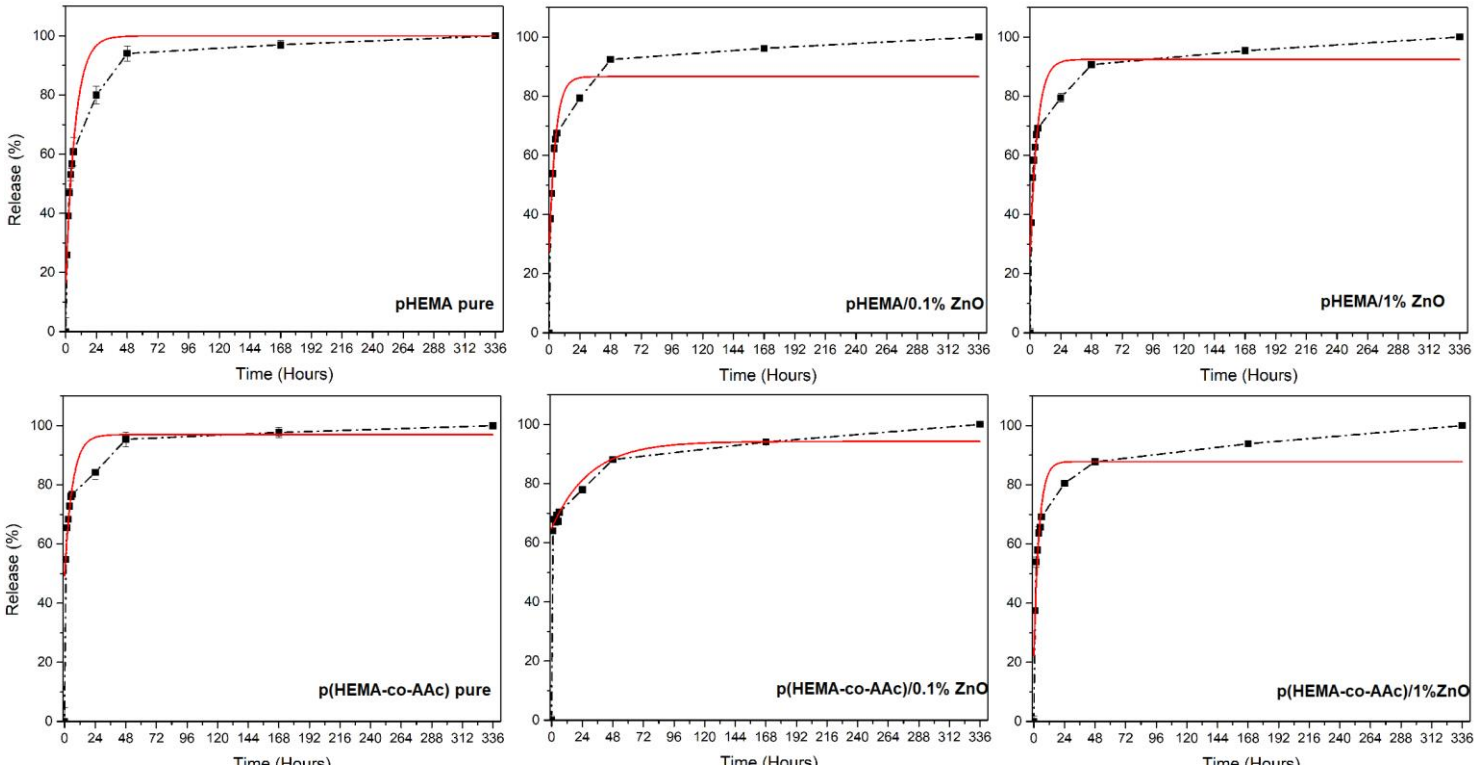


**Figure 5.2.3 (3)** Fitting curves of Diclofenac release graphs in alkaline urine.

| Material | pH | K ($hours^{-1}$) | $X^2$ |
|---|---|---|---|
| Poly(HEMA-co-AAc)+0.1% ZnO | 9.4 | 0,03357±0,01681 | 0,89801 |
| PolyHEMA pure | 9.4 | 0,13524±0,01365 | 0,99534 |
| Poly(HEMA-co-AAc) pure | 9.4 | 0,16431±0,04301 | 0,87325 |
| PolyHEMA+1% ZnO | 9.4 | 0,17794±0,0261 | 0,9499 |
| PolyHEMA+0.1% ZnO | 9.4 | 0,20583±0,0651 | 0,9455 |
| Poly(HEMA-co-AAc)+1% ZnO | 9.4 | 0,24221±0,05158 | 0,94299 |

**Table 5.2.3 (3)** Kinetic parameters of Diclofenac released in alkaline urine from pure pHEMA and copolymer and from ZnO/polymer and ZnO/copolymer systems.

For initial analysis, it can be noticed that in alkaline conditions, the sample with the lowest kinetic constant release is the poly(HEMA-co-AAc) with 0.1% of powder. Although it is the one with the lowest burst release, it still reaches the 100% of drug release until 2 weeks.
Concerning the other materials, the two fastest samples are, in order, the copolymer/1% and the polymer/0.1%; both reaching around 90% of drug release within 48 hours. The same data have been reported also for the release study in acid urine.

| Release time [Hours] | pHEMA pure | pHEMA 0.1% ZnO | pHEMA 1% ZnO | copHEMA pure | copHEMA 0.1% ZnO | copHEMA 1% ZnO |
|---|---|---|---|---|---|---|
| 0 | 13.342±2.516 | 13.342±2.516 | 13.342±2.516 | 13.342±2.516 | 13.342±2.516 | 13.342±2.516 |
| 1 | N.A. | N.A. | N.A. | N.A. | N.A. | N.A. |
| 2 | N.A. | N.A. | N.A. | N.A. | N.A. | N.A. |
| 3 | 0.440±0.482 | N.A. | N.A. | N.A. | N.A. | N.A. |
| 4 | 4.830±0.001 | 1.403±0.374 | 3.625±0.027 | N.A. | N.A. | 1.645±0.027 |
| 5 | 7.373±0.455 | 4.562±0.428 | 8.015±0.669 | N.A. | N.A. | 2.983±0.027 |
| 6 | 9.675±0.080 | 7.100±0.133 | 9.728±0.08 | N.A. | N.A. | 4.294±0.107 |
| 24 | 17.624±0.535 | 12.94±0.401 | 18.507±0.509 | 0.146±0.134 | 7.667±0.010 | 9.862±0.268 |
| 48 | 20.997±0.161 | 15.937±0.080 | 18.641±0.642 | 1.725±0.161 | 10.504±0.054 | 13.877±0.161 |
| 168 | 22.201±0.455 | 16.955±0.508 | 19.578±0.562 | 2.367±0.642 | 10.076±0.268 | 13.636±0.134 |
| 336 | 21.050±0.268 | 16.446±0.214 | 19.551±0.642 | 1.323±0.08 | 7.747±0.241 | 12.806±0.054 |

**Table 5.2.3 (4)** Diclofenac concentrations release [µg/mL]. pH 5.2.

In this case the group of materials named as Sample 4 has been used. The amount of drug absorbed by each sample has been reported below:

| **DICLO uptake weight. Acid release study** | Uptake (mg) Sample 4 |
|---|---|
| PolyHEMA pure | 12.3 |
| PolyHEMA + 0.1% ZnO | 14.4 |
| PolyHEMA + 1% ZnO | 14.2 |
| Poly(HEMA-co-Aac) pure | 12.3 |
| Poly(HEMA-co-Aac) + 0.1% ZnO | 14.9 |
| Poly(HEMA-co-Aac) + 1% ZnO | 13.5 |

Knowing these quantities, it was possible to obtain from the concentration values, the % of Diclofenac released by each sample, normalized by the total amount of drug absorbed. The results are reported below in Table 5.2.3(5):

| **Release time [Hours]** | **Normalized % Release ± Standard Error** | | | | | |
|---|---|---|---|---|---|---|
| | **pHEMA pure** | **pHEMA 0.1% ZnO** | **pHEMA 1% ZnO** | **copHEMA pure** | **copHEMA 0.1% ZnO** | **copHEMA 1% ZnO** |
| 0 | 0±0 | 0±0 | 0±0 | 0±0 | 0±0 | 0±0 |
| 1 | N.A. | N.A. | N.A. | N.A. | N.A. | N.A. |
| 2 | N.A. | N.A. | N.A. | N.A. | N.A. | N.A. |
| 3 | 1.938±2.130 | N.A. | N.A. | N.A. | N.A. | N.A. |
| 4 | 21.764±0.446 | 8.352±2.461 | 18.512±0.693 | N.A. | N.A. | 11.855±0.330 |
| 5 | 33.180±1.370 | 26.855±1.720 | 37.503±1.126 | N.A. | N.A. | 21.496±0.056 |
| 6 | 43.602±1.255 | 41.966±2.048 | 49.653±1.082 | N.A. | N.A. | 30.942±0.413 |
| 24 | 79.368±0.785 | 76.317±0.079 | 91.891±2.760 | 4.984±4.301 | 72.991±0.372 | 71.054±1.107 |
| 48 | 94.600±1.216 | 94.071±2.348 | 91.891±2.760 | 76.668±14.021 | 100±0.100 | 100±0.110 |
| 168 | 100±0.100 | 100±0.100 | 97.084±2.916 | 100±0,100 | 95.912±2.059 | 98.266±0.173 |
| 336 | 94.880±3.150 | 97.050±1.648 | 96.537±2.900 | 59.353±12.714 | 73.744±1.918 | 92.292±0.682 |

**Table 5.2.3 (5)** Diclofenac normalized % released amount in acid pH.

From data reported on Table 5.2.3 (4) it is possible to notice that the release of Diclofenac in acid solution starts not earlier than 2 hours, in some cases also after 6 hours. Furthermore, even after the release process has begun, the final amount of drug released is very low (few tens of micrograms).

In order to explain the slow release, the chemical characteristics of Diclofenac should be considered. The drug used in these release studies is in the salt form, meaning that it is characterized by a pKa value equal to 4 at 25°C.

The acid dissociation constant (pKa) is a quantity used in order to define the capacity of a chemical substance to dissociate in ions when it is put in a solution with a certain pH. Therefore, from low pKa value it is possible to determine how strong is an acid.
This dimension also depends on other physical quantities, as for instance the temperature, and in particular pKa increases with increasing of the latter.
Hence, the pKa value of Diclofenac sodium salt at 37°C should be higher than 4.

Usually, when the solution pH changes, as in this study, the balance of the dissolution reaction shifts, in accordance with the solute value of pKa. In particular, two conditions may occur and they are reported below:

$$HA + H_2O \rightarrow A^- + H_3O^+$$

pH>pKa → $[A^-]$>[HA] → dissociation of acid

pH<pKa → [HA]> $[A^-]$ → acid does not dissociate.

Comparing the maximum concentrations of drug released in different conditions of pH (Table 5.2.2(1), Table 5.2.3 (1) and Table and5.2.3 (4)), it can be noticed that these values are higher in case of alkaline pH, while they are lower in conditions of acid pH.
In case of physiologic pH, the values (still elevated) stay in the middle with respect to the other two conditions.
These differences occurred because in the first two studies (at pH 7 and 9.4), the solution had a pH>>pKa, which means that the drug was able to dissociate completely and easily get free in the solution.
By contrast, when the urine pH was 5, at 37 °C happened the case pKa>pH, which means that the Diclofenac was not able to dissociate, and the higher amount of drug absorbed during the uptake stayed inside the samples.

Explained the reason for the slow release at acid pH, Figure 5.2.3 (4) and (5) show the trend release of all the materials with the enlargement on the first 48 hours of release.

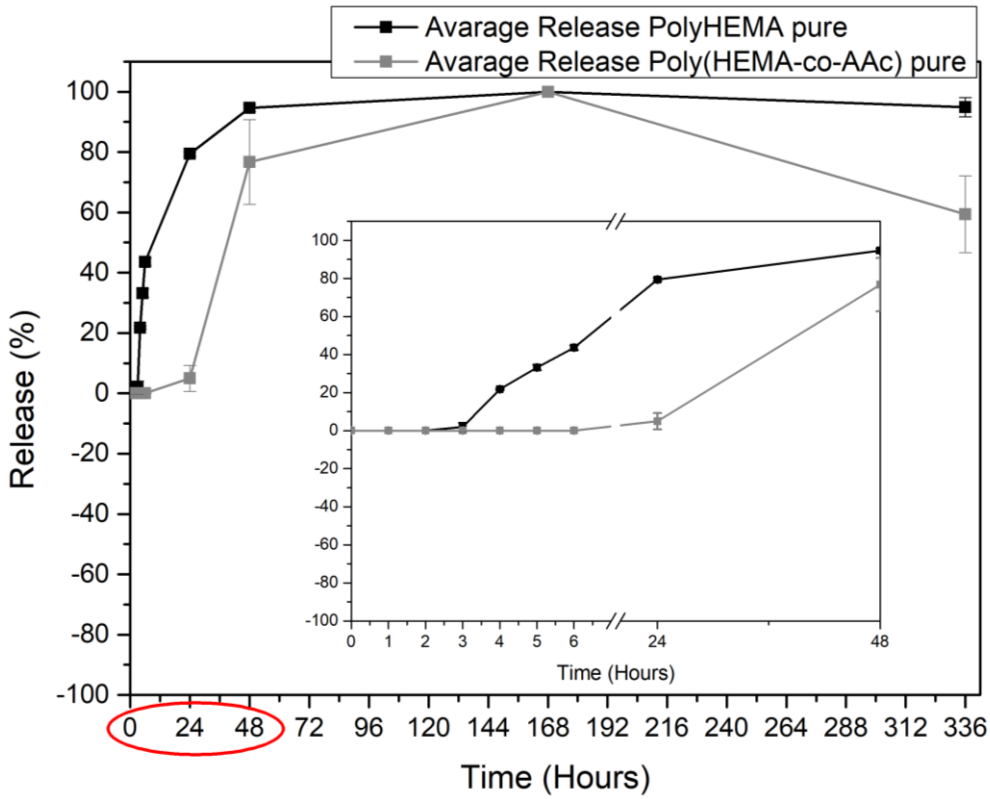


**Figure 5.2.3 (4)** Confrontation of pure pHEMA and copolymer release. pH 5.2.

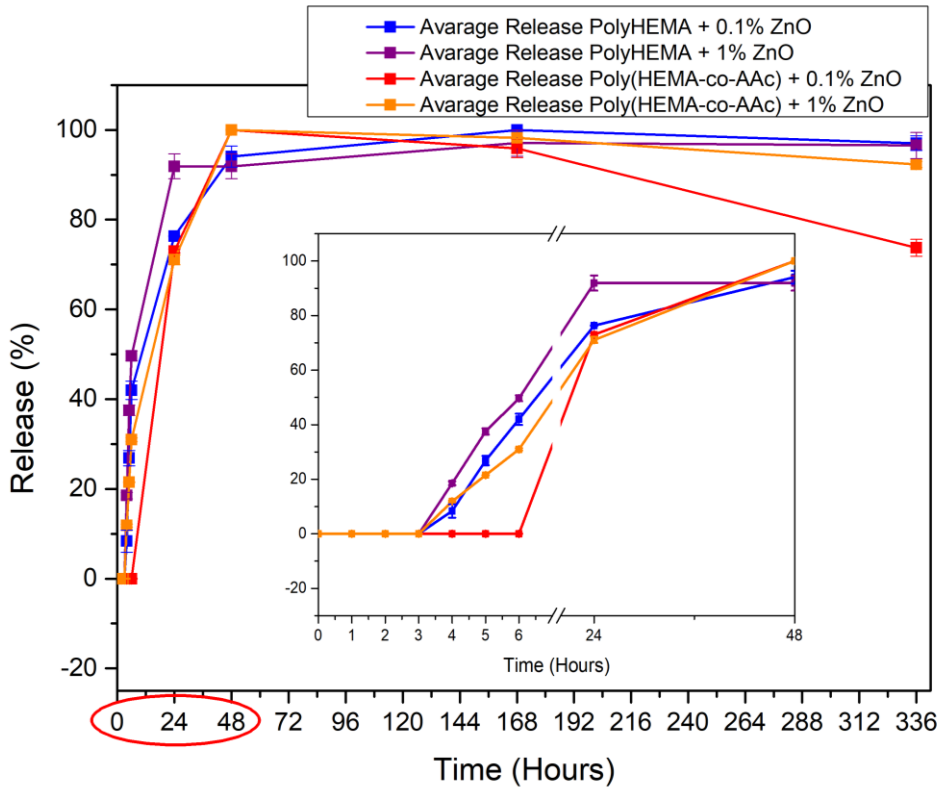


**Figure 5.2.3 (5)** Comparison between materials with 0.1% and 1% ZnO. pH 5.2.

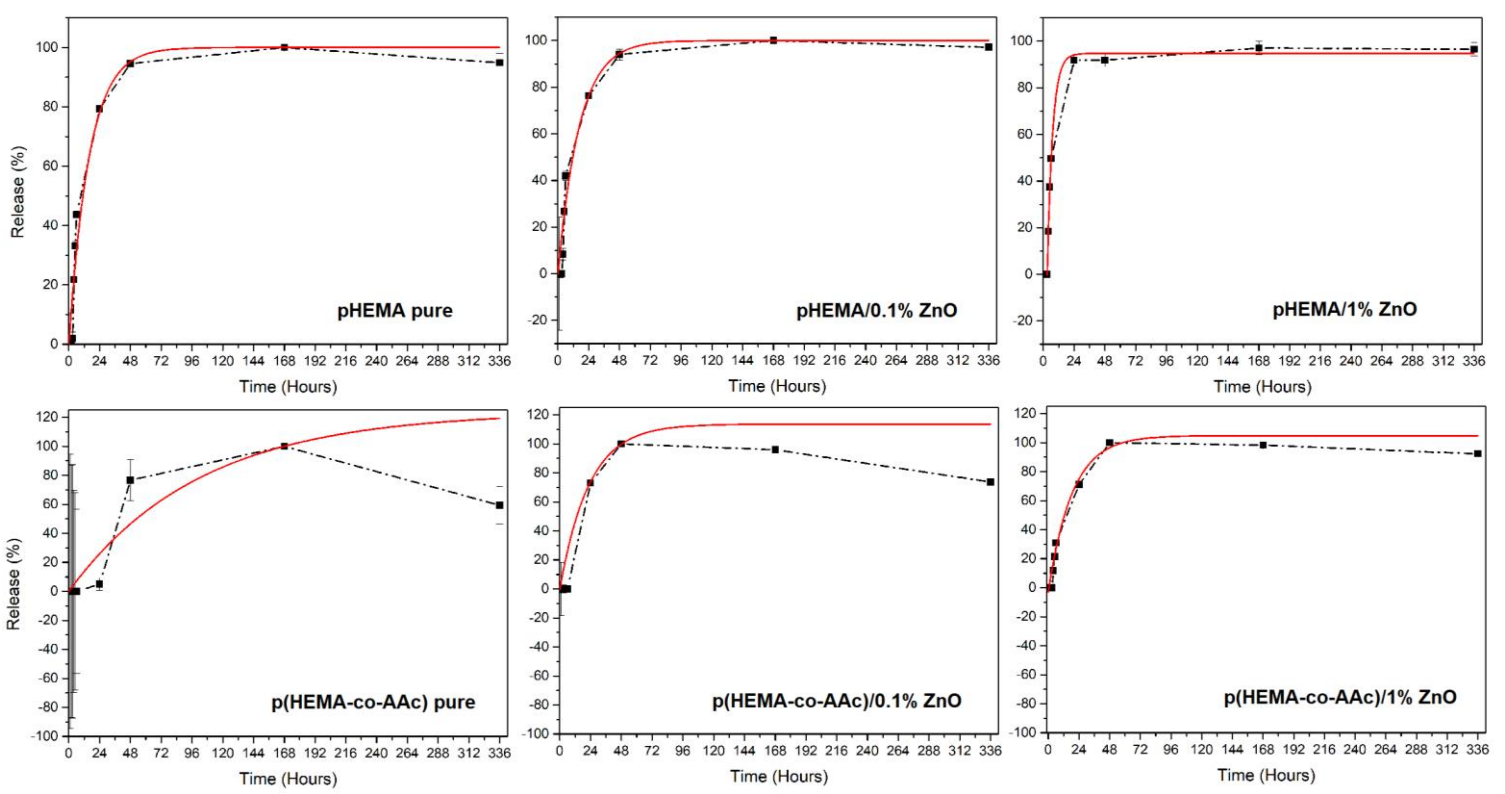


**Figure 5.2.3 (6)** Fitting curves of Diclofenac release graphs in acid urine.

| Material | pH | K ($hours^{-1}$) | $R^2$ |
|---|---|---|---|
| Poly(HEMA-co-AAc) pure | 5.2 | 0.0098±0.00602 | 0.99987 |
| Poly(HEMA-co-AAc)+0.1% ZnO | 5.2 | 0.04385±0.00865 | 0.99724 |
| Poly(HEMA-co-AAc)+1% ZnO | 5.2 | 0.05327±0.00589 | 0.99214 |
| PolyHEMA+0.1% ZnO | 5.2 | 0.05999±0.00122 | 0.99933 |
| PolyHEMA pure | 5.2 | 0.06323±0.0068 | 0.99895 |
| PolyHEMA+1% ZnO | 5.2 | 0.24013±0.01065 | 0.99784 |

**Table 5.2.3 (6)** Kinetic parameters of Diclofenac released in alkaline urine from pure pHEMA and copolymer and from ZnO/polymer and ZnO/copolymer systems. Acid pH.

From Table 5.2.3 (6) it can be seen that the sample with the lowest initial burst release is the pure poly(HEMA-co-AAc); despite this, it still shows the 100% of drug release after 168 hours, as the other material with a lower kinetic constant. However, this value is not stable, and it falls to 60% at the end of the release study.
The only two materials which reach the maximum release within 48 hours keeping a low initial burst release are the other copolymer with 0.1% and 1% of ZnO.

By contrary, the polymer composite made by poly(HEMA) with 1% of ZnO is the sample with the highest kinetic constant (0,24013±0,01065). Even if it does not get free all the drug absorbed (maximum release 97% after 168 hours), it is the unique material that keeps stable this value of burst delivery until the end of the study.

*5.3 Ibuprofen*

Figure 5.3 (1) shows the absorbance spectrum of Ibuprofen in urine for wavelengths between 200 and 800. The background, composed by urine and quartz of the 96-well plate, has been already subtracted:

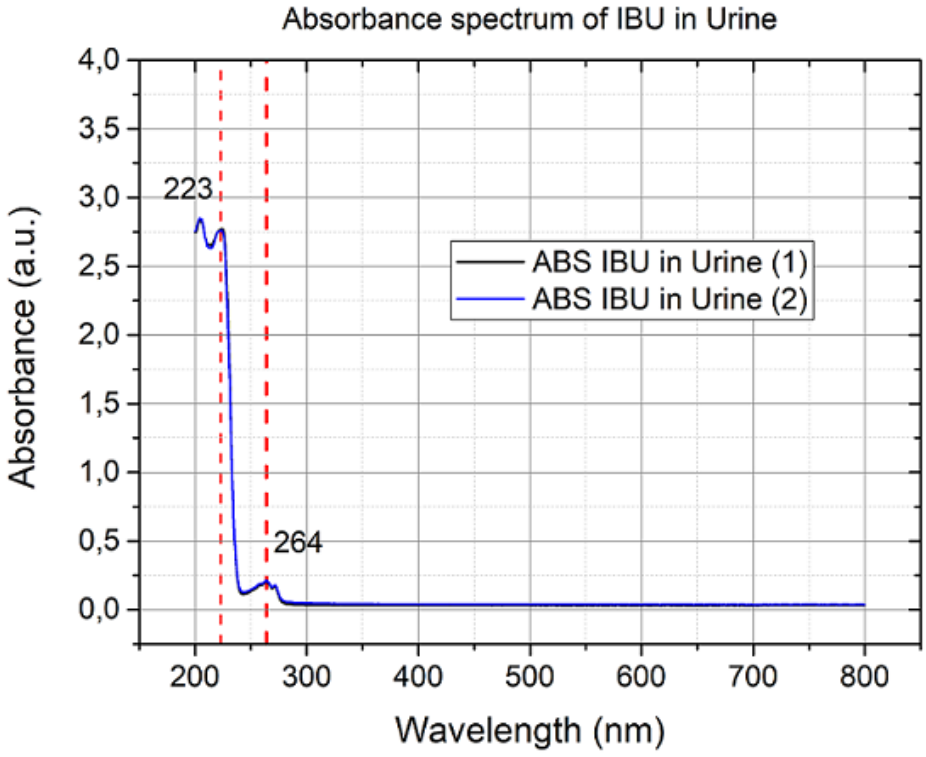


**Figure 5.3 (1)** Ibuprofen absorbance spectrum in urine.

In this case, it can be seen that Ibuprofen has 2 peaks of absorbance: at 223 nm and at 264 nm. Hence, the next scan of the 7 series with different concentrations and the urine have been made at these wavelengths (Table 5.3):

| **223nm** | | **264nm** |
|---|---|---|
| CONC [µg/ml] | ABS IBU in urine | ABS IBU in urine |
| 3600 | 3.540 | 3.023 |
| 360 | 2.967 | 2.347 |
| 36 | 0.332 | 0.262 |
| 3,60 | 0.024 | 0.041 |
| 0,360 | 0.002 | 0.039 |
| 0,036 | N.A. | 0.011 |
| 0,0036 | 0.000 | 0.003 |

**Table 5.3** Mean Absorbance of Ibuprofen in urine measured at 223nm and 264 nm.

Also in this case, it has been highlighted in red the concentrations with absorbance around and higher than 3, in order not to consider them in the calibration line. Therefore, 2 different calibration lines with their respective equations have been obtained, one for each wavelength. They have been shown in Figure 4.3 (2) and (3):

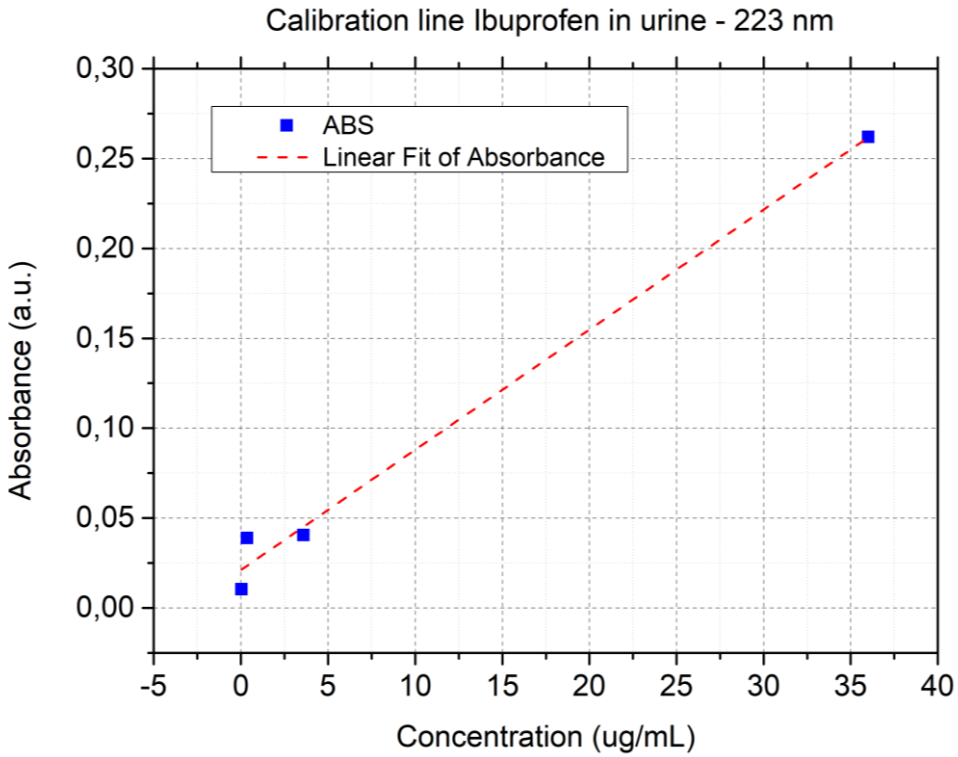


**Figure 5.3 (2)** Ibuprofen calibration line in urine, at 223 nm.

| Equation y= a + b*x | | | |
|---|---|---|---|
| Adj. R-Square 0.9861 | | | |
| **IBU in Urine – 223 nm** | | Value | Standard Error |
| Absorbance | Intercept | 0.0212100 | 0.008260000 |
| Absorbance | Slope | 0.0066800 | 0.000456755 |

This calibration line at 223 nm is defined by the following equation:

$$ABS = 0.02121 + 0.00668C$$

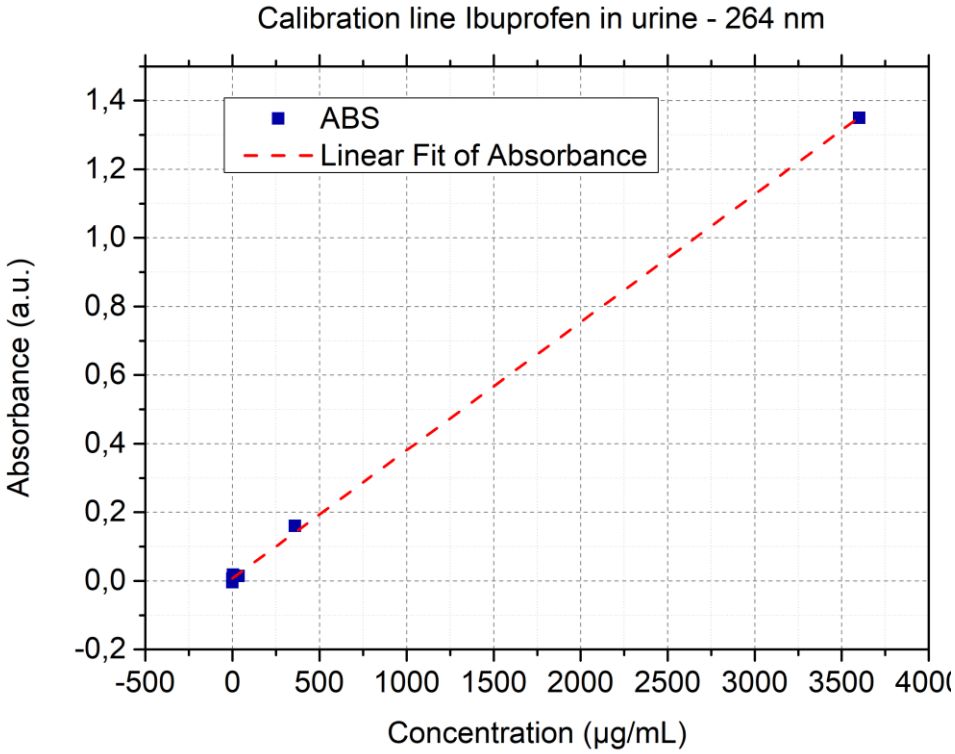


**Figure 5.3 (3)** Ibuprofen calibration line in urine, at 264 nm.

| Equation y= a + b*x | | | |
|---|---|---|---|
| Adj. R-Square 0.99948 | | | |
| **IBU in Urine – 264 nm** | | Value | Standard Error |
| Absorbance | Intercept | 0.0072200 | 0.004770000 |
| Absorbance | Slope | 0.0003734 | 0.000003491 |

This calibration line is defined by the equation:

$$ABS = 0.0072200 + 0.0003734C$$

Even if the calibration lines of both the wavelengths have been obtained, only the equation of that at 223 nm has been next used, because its peak was more relevant.

### *5.3.1 Ibuprofen uptake in water*

At the same time with Diclofenac, also Ibuprofen has been loaded in the same way inside the samples, in order to study the release trend and to compare the behavior of the two drugs.
For the uptake of Ibuprofen, it has been used the same process parameters of Diclofenac:

- Starting concentration: 10 mg/mL;
- Time: 4h;
- Measure of absorption: balance.

It has been prepared 10 mL of solution in a falcon of 50 mL, but in this case each single sample has been put inside a different volume.

In the same way, after 4 hours the samples were removed and, after several rounds of drying in the oven at 50°C, were weighted.

The weights of samples and the amounts of drug absorbed during the uptake have been reported in Table 5.3.1 (1) and (2).

| **IBU uptake weight Physiologic release** | PRE-UPTAKE | | POST-UPTAKE | | Uptake (mg) | |
|---|---|---|---|---|---|---|
| | Sample 1 (mg) | Sample 2 (mg) | Sample 1 (mg) | Sample 2 (mg) | Sample 1 (mg) | Sample 2 (mg) |
| PolyHEMA pure | 271 | 283.9 | 284.6 | 298.7 | 13.6 | 14.8 |
| PolyHEMA + 0.1% ZnO | 330.5 | 275.7 | 348.6 | 289.7 | 18.1 | 14.0 |
| PolyHEMA + 1% ZnO | 399.3 | 407.4 | 412.4 | 433.6 | 13.1 | 26.2 |
| Poly(HEMA-co-Aac) pure | 361.5 | 320.3 | 389.1 | 339.9 | 27.6 | 19.6 |
| Poly(HEMA-co-Aac) + 0.1% ZnO | 340 | 361.3 | 347.2 | 364.1 | 7.2 | 2.8 |
| Poly(HEMA-co-Aac) + 1% ZnO | 285.3 | 339.9 | 295.6 | 348.5 | 10.3 | 8.6 |

**Table 5.3.1 (1)** Weights before and after the Ibuprofen uptake. Samples used for release in physiologic urine.

| **IBU uptake weight Alkaline/acid release** | PRE-UPTAKE | | POST-UPTAKE | | Uptake (mg) | |
|---|---|---|---|---|---|---|
| | Sample 3 (mg) | Sample 4 (mg) | Sample 3 (mg) | Sample 4 (mg) | Sample 3 (mg) | Sample 4 (mg) |
| PolyHEMA pure | 350.5 | 311.8 | 407.6 | 325.5 | 57.1 | 13.7 |
| PolyHEMA + 0.1% ZnO | 350.4 | 386.8 | 361.8 | 407.8 | 11.4 | 21.0 |
| PolyHEMA + 1% ZnO | 307.3 | 291 | 317 | 305.2 | 9.7 | 14.2 |
| Poly(HEMA-co-Aac) pure | 400.1 | 317.2 | 414.9 | 332.4 | 14.8 | 15.2 |
| Poly(HEMA-co-Aac) + 0.1% ZnO | 321.2 | 338.8 | 378.1 | 353 | 56.9 | 14.2 |
| Poly(HEMA-co-Aac) + 1% ZnO | 330 | 340.1 | 359.8 | 358.8 | 29.8 | 18.7 |

**Table 5.3.1 (2)** Weights before and after the Ibuprofen uptake. Samples used for release in alkaline/acid urine.

### *5.3.2 Ibuprofen release in physiologic artificial urine*

As in case of Diclofenac, the release in artificial urine at physiological pH (around 7.3) has been investigated including the first 2 samples of each material, previously loaded with Ibuprofen.

The preparation of the falcons and the quartz plate have been made in the same way, and the measure of the drug amount released has been obtained by UV-Vis analysis, monitoring the solution with the same follow-up (every hour until 6 hours, 24h, 48h, 168h, 336h).

In Figure 5.3.2 (1), the graph which collects all the UV-Vis absorbance spectra in the range 200–800 nm is reported, in order to evaluate the trend of the absorbance peak of Ibuprofen. It is possible to observe the increasing trend of the solution concentration, illustrating that the sample is releasing the drug over the time.
The sample held as example is the poly(HEMA) + 1% ZnO:

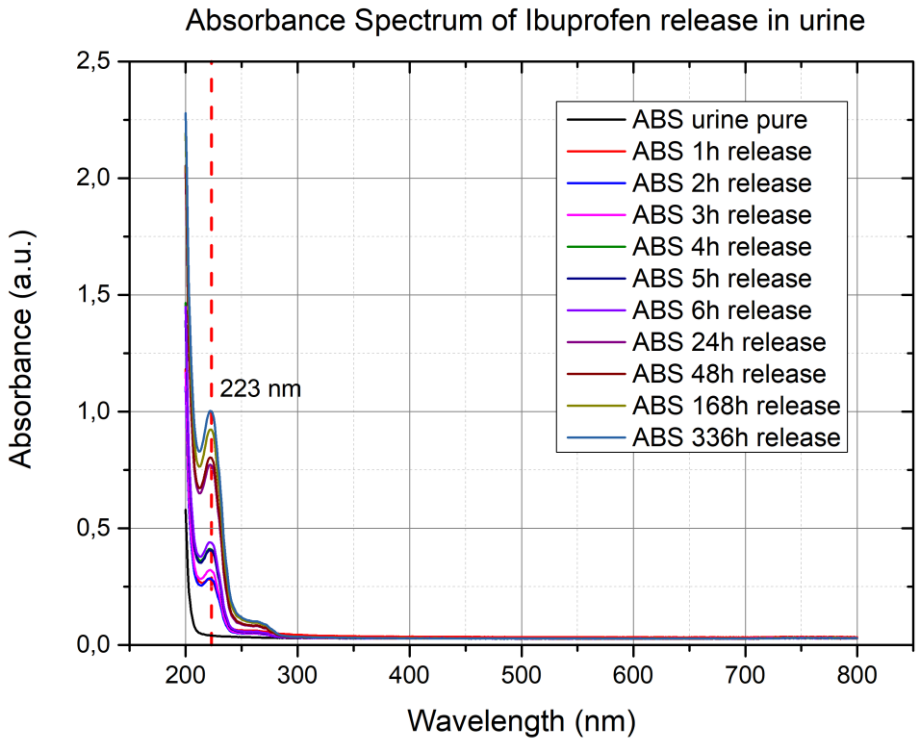


**Figure 5.3.2 (1)** Spectrum of sample 1, poly(HEMA) + 1% ZnO.

Then, the second series of scans have been collected at 223 nm, the Ibuprofen characteristic wavelength, to obtain the absorbances.
The calibration line equation of Ibuprofen in urine used to obtaine the concentration is:

$$y = -0.00511 + 0.00934x$$

The concentrations of the release test are reported in Table 5.3.2 (1):

| Release time [Hours] | pHEMA pure | pHEMA 0.1% ZnO | pHEMA 1% ZnO | copHEMA pure | copHEMA 0.1% ZnO | copHEMA 1% ZnO |
|---|---|---|---|---|---|---|
| 0 | 2.963±0.150 | 2.963±0.150 | 2.963±0.150 | 2.963±0.150 | 2.963±0.150 | 2.963±0.150 |
| 1 | 31.031±1.123 | 32.753±0.150 | 71.001±6.437 | 22.835±9.319 | 22.985±0.561 | 71.001±4.266 |
| 2 | 35.036±2.058 | 35.747±0.524 | 77.963±14.371 | 32.266±9.094 | 29.160±4.566 | 80.171±3.481 |
| 3 | 40.650±2.208 | 41.548±2.208 | 90.463±16.542 | 39.639±11.302 | 38.142±7.111 | 86.346±4.341 |
| 4 | 54.909±2.919 | 53.936±3.368 | 109.437±16.729 | 43.531±13.398 | 38.442±6.138 | 89.302±2.358 |
| 5 | 52.963±1.422 | 50.942±2.545 | 107.678±16.916 | 48.434±12.987 | 41.548±6.025 | 92.858±3.892 |
| 6 | 57.379±0.973 | 54.422±2.283 | 114.115±16.841 | 52.214±15.719 | 44.430±6.886 | 95.103±3.293 |
| 24 | 110.485±4.528 | 107.978±8.533 | 211.608±19.274 | 102.588±18.713 | 76.952±8.870 | 144.055±2.545 |
| 48 | 120.066±9.469 | 120.103±5.838 | 245.440±21.295 | 121.937±22.193 | 88.928±8.421 | 152.701±5.052 |
| 168 | 134.475±5.314 | 139.452±11.564 | 241.922±22.343 | 136.832±28.780 | 96.076±7.260 | 157.753±7.260 |
| 336 | 143.120±3.106 | 144.692±12.013 | 239.939±22.156 | 141.286±34.132 | 97.948±5.389 | 158.427±4.790 |

**Table 5.3.2 (1)** Ibuprofen release concentrations [µg/mL].

In red are highlighted the maximum value of release; it can be observed that the relase continues to increase until 2 weeks. Just the polyHEMA with 1% of ZnO reaches the maximum release after 2 days.

Knowing the amount of drug uptaken by each sample (Table 5.3.1 (1)) and comparing it with the concentrations, it has been obtained the % release of each sample.

In the following Table 5.3.2 (2) are reported the values of % Release already normalized, on the basis of the maximum value within each sample. The 2 different normalized values obtained for each material have been mediated, and the standard error has been calculated (Table 5.3.2 (2)):

| Release time [Hours] | Normalized % Release ± Standard Error | | | | | |
|---|---|---|---|---|---|---|
| | **pHEMA pure** | **pHEMA 0.1% ZnO** | **pHEMA 1% ZnO** | **copHEMA pure** | **copHEMA 0.1% ZnO** | **copHEMA 1% ZnO** |
| 0 | 0±0 | 0±0 | 0±0 | 0±0 | 0±0 | 0±0 |
| 1 | 21.709±1.256 | 22.802±1.997 | 28.918±0.114 | 15.420±2.910 | 23.506±0.720 | 44.717±4.274 |
| 2 | 24.460±0.907 | 24.847±1.701 | 31.493±3.123 | 22.512±1.067 | 29.604±3.033 | 50.461±3.986 |
| 3 | 28.382±0.927 | 28.787±0.864 | 36.548±3.569 | 27.633±1.408 | 38.659±5.133 | 54.361±4.666 |
| 4 | 38.339±1.208 | 37.340±0.772 | 44.330±2.970 | 30.171±2.283 | 39.020±4.119 | 56.175±3.486 |
| 5 | 37.002±0.191 | 35.304±1.172 | 43.602±3.109 | 33.910±1.104 | 42.208±3.829 | 58.444±4.530 |
| 6 | 40.096±0.190 | 37.742±1.556 | 46.247±2.849 | 36.251±2.475 | 45.110±4.548 | 59.842±4.204 |
| 24 | 77.165±1.489 | 74.651±0.301 | 86.183±0.375 | 73.387±4.238 | 78.303±4.747 | 90.474±1.633 |
| 48 | 83.788±4.797 | 83.245±2.877 | 100±0.1 | 87.237±5.073 | 90.593±3.613 | 95.851±0.251 |
| 168 | 93.923±1.675 | 96.380±0.010 | 98.518±0.555 | 97.205±2.795 | 97.978±2.022 | 98.977±1.023 |
| 336 | 100±0.1 | 100±0.1 | 97.711±0.549 | 99.584±0.416 | 100±0.1 | 99.456±0.544 |

**Table 5.3.2 (2)** Ibuprofen normalized % released amount.

From these normalized values of concentration, it can been seen that not all the samples have released the 100% of drug; both copolymer and copolymer/1% ZnO have reached 99% of release, that however is very close to the maximum value.

The release profiles of both pure PolyHEMA and Poly(HEMA-co-AAc) have been shown in Figure 5.3.2 (2), instead Figure 5.3.2 (3) shows in the same graph, the releases of polymers and copolymers with 0.1% and 1% of ZnO. Both figures also show the enlargement on the first 48 hours of the period of study.

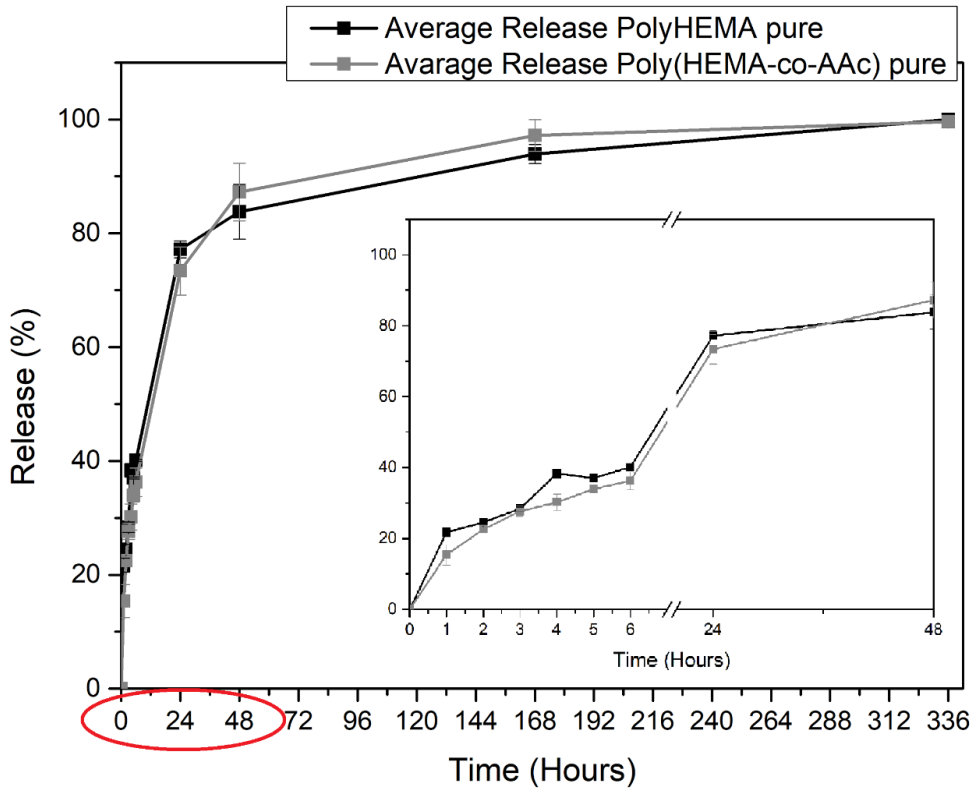


**Figure 5.3.2 (2)** Comparison of pure pHEMA and copolymer release of ibuprofen.

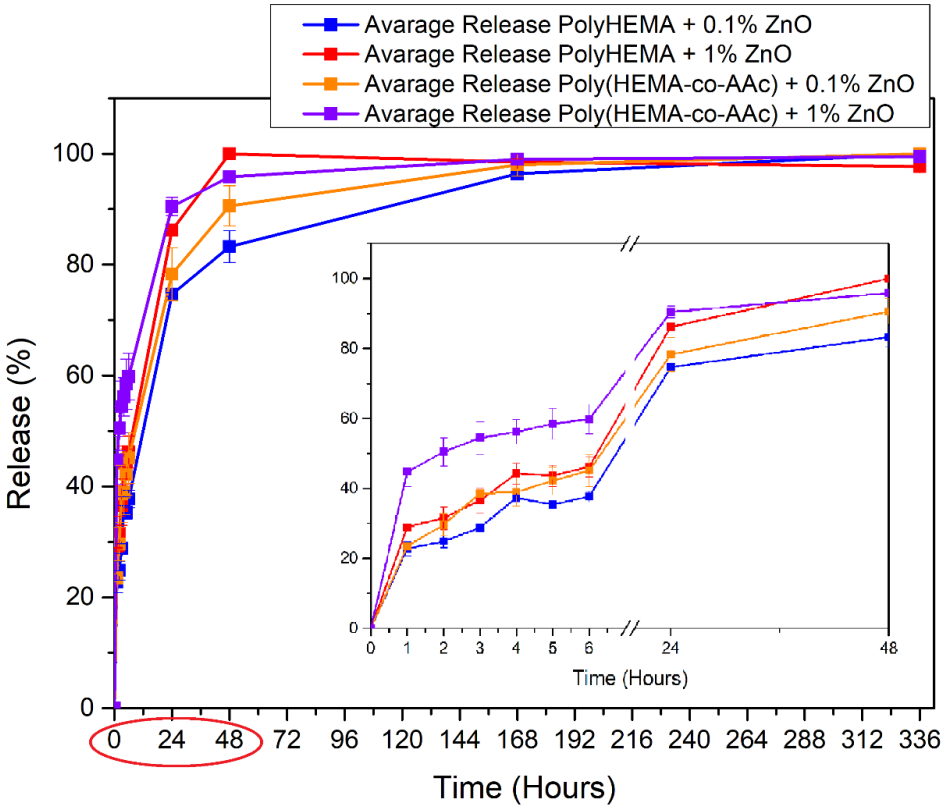


**Figure 5.3.2 (3)** Comparison between composites with different amount of ZnO. Enlargement on the first 2 days of release in the same graph.

By using the equation of MnMolecular model,

$$y = A * ( 1 - e^{-k(x-x_c)} )$$

all the fitting curves have been shown together with the corresponding release profiles, in Figure 5.3.2 (4).
Using the software Origin, the kinetic parameters have been obtained from the exponential curves and have been reported in Table 5.3.2 (3) in ascending order.

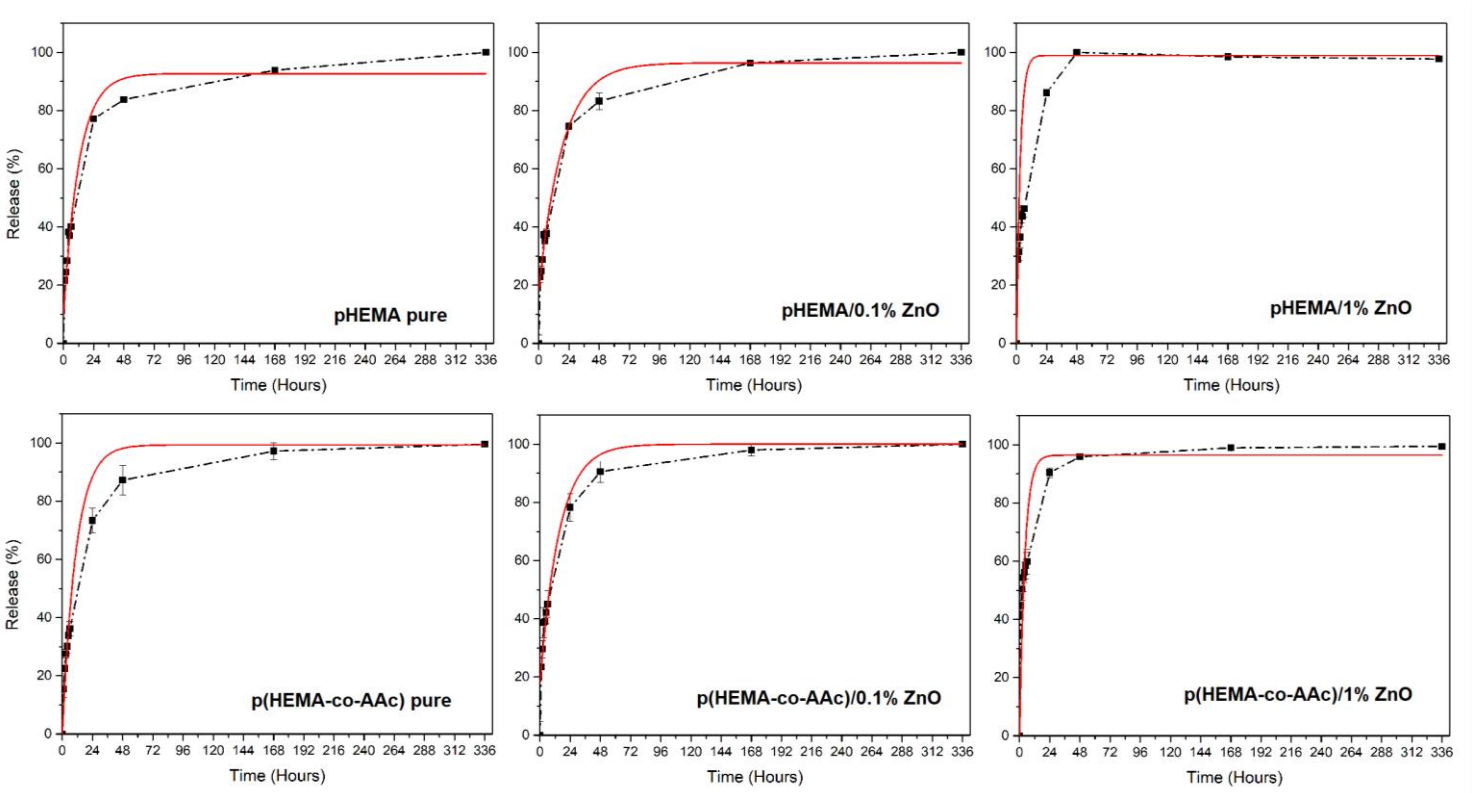


**Figure 5.3.2 (4)** Fitting lines of Ibuprofen release in physiologic urine.

| Material | pH | K ($hours^{-1}$) | $R^2$ |
|---|---|---|---|
| PolyHEMA+0.1% ZnO | 7.3 | 0.05347±0.00238 | 0.99607 |
| Poly(HEMA-co-AAc)+0.1% ZnO | 7.3 | 0.06545±0.01174 | 0.99792 |
| PolyHEMA pure | 7.3 | 0.08106±0.01598 | 0.9679 |
| Poly(HEMA-co-AAc) pure | 7.3 | 0.09213±0.00747 | 0.99844 |
| Poly(HEMA-co-AAc)+1% ZnO | 7.3 | 0.24138±0.04917 | 0.9991 |
| PolyHEMA+1% ZnO | 7.3 | 0.34038±0.029 | 0.99595 |

**Table 5.3.2 (3)** Kinetic parameters of Ibuprofen released from pure pHEMA and copolymer and from ZnO/polymer and ZnO/copolymer systems.

The material with the lowest burst release during the first hours of the study is the polyHEMA with 0.1% of ZnO; that sample also reaches the 100% of drug released at the end of the period of study. The second material with the lowest kinetic rate is the composite made by poly(HEMA-co-AAc) with 0.1% of ZnO; it has a kinetic constant similare to the first, but it reaches the 90% of release after 48 hours.

By contrast, the polyHEMA with 1% has the highest kinetic constant and it reaches the maximum release as really as 2 days.

### *5.3.3 Ibuprofen Release in alkaline and acid artificial urine*

From the 600 mL of artificial urine previously taken from the stock and adjusted to pH 9.4, 50 mL were used for each of the 6 samples, in the same way as Diclofenac.

The same procedure has been followed to test the release in urine at pH 5.2.

The release and analysis have been made in the same way as explained for physiological urine, using again the third sample loaded with Ibuprofen, diveded in half.
Concerning the maximum amount of drug in each piece of the same sample, it has been considered the half of that in the one-piece sample.
Therefore, are still given below the results of the release test through concentrations (Table 5.3.3 (1)) and the normalized % release values (Table 5.3.3 (2)).

| Release time [Hours] | pHEMA pure | pHEMA 0.1% ZnO | pHEMA 1% ZnO | copHEMA pure | copHEMA 0.1% ZnO | copHEMA 1% ZnO |
|---|---|---|---|---|---|---|
| 0 | 0.067±0.001 | 0.067±0.001 | 0.067±0.001 | 0.067±0.001 | 0.067±0.001 | 0.067±0.001 |
| 1 | 16.398±1.834 | 36.234±2.433 | 62.805±4.603 | 19.579±1.871 | 14.939±1.946 | 68.082±6.587 |
| 2 | 22.686±0.262 | 49.033±0.262 | 72.049±0.299 | 27.588±0.075 | 21.301±0.898 | 71.451±2.246 |
| 3 | 29.160±1.123 | 62.281±2.433 | 85.972±2.545 | 33.015±1.160 | 25.567±1.347 | 80.246±2.882 |
| 4 | 31.855±0.449 | 68.569±0.037 | 89.452±0.187 | 36.720±0.524 | 29.310±0.374 | 82.828±1.198 |
| 5 | 38.442±2.320 | 79.310±4.716 | 102.551±5.501 | 43.569±2.807 | 34.175±1.497 | 89.864±3.967 |
| 6 | 38.666±0.374 | 81.518±0.561 | 102.738±0.075 | 45.927±0.299 | 35.597±0.449 | 90.575±1.010 |
| 24 | 52.961±1.809 | 96.973±1.260 | 106.628±1.310 | 59.722±1.834 | 52.524±1.272 | 135.167±4.921 |
| 48 | 86.588±3.431 | 153.186±2.239 | 161.887±2.582 | 96.481±3.518 | 87.249±2.320 | 157.463±6.877 |
| 168 | 120.216±5.052 | 209.400±3.219 | 217.147±3.855 | 133.240±5.202 | 121.975±3.368 | 179.759±8.832 |
| 336 | 127.102±0.187 | 202.476±0.711 | 231.181±0.973 | 155.246±5.352 | 138.666±0.524 | 199.781±4.903 |

**Table 5.3.3 (1)** Ibuprofen release's concentrations [μg/mL] in alkaline urine.

| Release time [Hours] | Normalized % Release ± Standard Error | | | | | |
|---|---|---|---|---|---|---|
| | pHEMA pure | pHEMA 0.1% ZnO | pHEMA 1% ZnO | copHEMA pure | copHEMA 0.1% ZnO | copHEMA 1% ZnO |
| 0 | 0±0 | 0±0 | 0±0 | 0±0 | 0±0 | 0±0 |
| 1 | 12.904±1.462 | 17.891±1.139 | 27.159±1.877 | 12.585±0.772 | 10.779±1.444 | 34.018±2.462 |
| 2 | 17.848±0.180 | 24.217±0.214 | 31.167±0.261 | 17.794±0.662 | 15.359±0.590 | 35.814±2.003 |
| 3 | 22.944±0.917 | 30.756±1.093 | 37.184±0.944 | 21.266±0.014 | 18.442±1.041 | 40.155±0.457 |
| 4 | 25.063±0.390 | 33.866±0.137 | 38.694±0.082 | 23.669±0.478 | 21.136±0.190 | 41.499±1.618 |
| 5 | 30.248±1.870 | 39.162±2.191 | 44.350±2.193 | 28.035±0.842 | 24.650±1.173 | 44.959±0.882 |
| 6 | 30.421±0.250 | 40.262±0.419 | 44.441±0.219 | 29.625±1.214 | 25.670±0.227 | 45.377±1.619 |
| 24 | 41.670±1.455 | 47.892±0.548 | 46.122±0.497 | 38.479±0.536 | 37.881±0.996 | 45.100±1.278 |
| 48 | 68.129±2.785 | 75.654±0.887 | 70.023±0.885 | 62.145±0.464 | 62.927±1.879 | 67.512±1.746 |
| 168 | 94.588±4.114 | 103.415±1.226 | 93.924±1.272 | 85.812±0.393 | 87.973±2.761 | 89.923±2.214 |
| 336 | 100±0.01 | 100±0.1 | 100±0.1 | 100±0.1 | 100±0.1 | 100±0.1 |

**Table 5.3.3 (2)** Ibuprofen normalized % released amount in alkaline urine.

Also in this case, the trend of the releases of both pure PolyHEMA and Poly(HEMA-co-AAc) in 2 weeks and in 48 hours have been shown together in Figure 5.3.3 (1), instead Figure 5.3.3 (2) the releases of the other composites during the same two period of time.

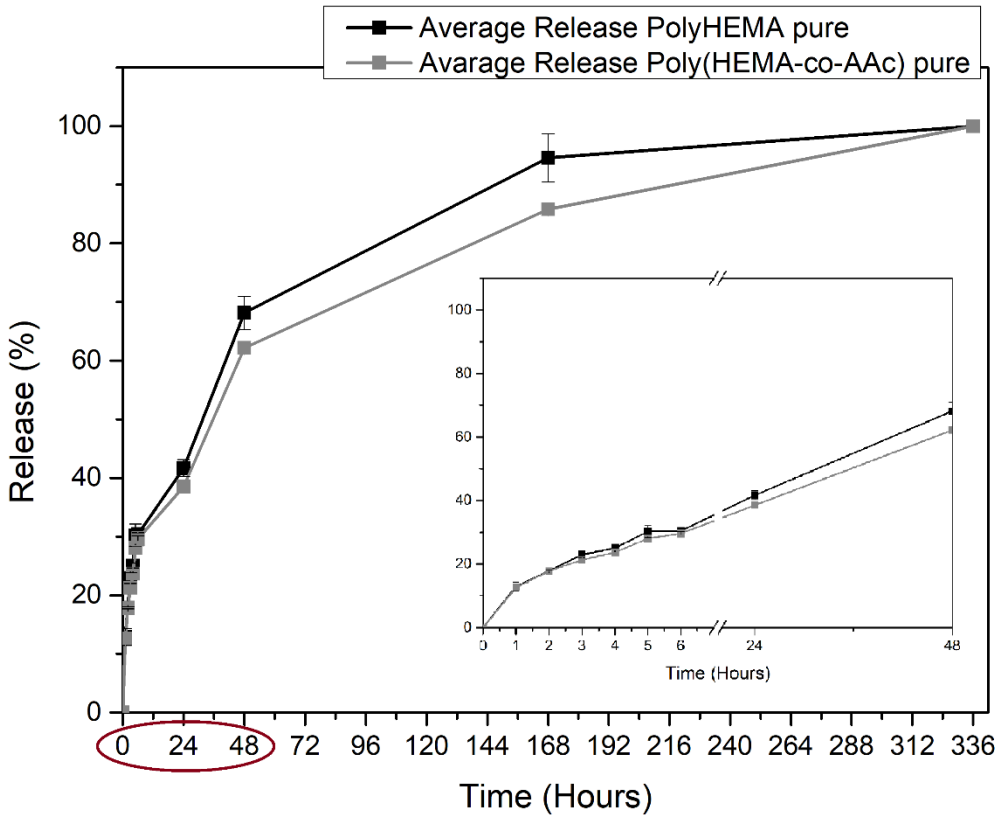


**Figure 5.3.3 (1)** Comparison of Ibuprofen release from pHEMA and p(HEMA-co-AAc) both pure, in alkaline urine.

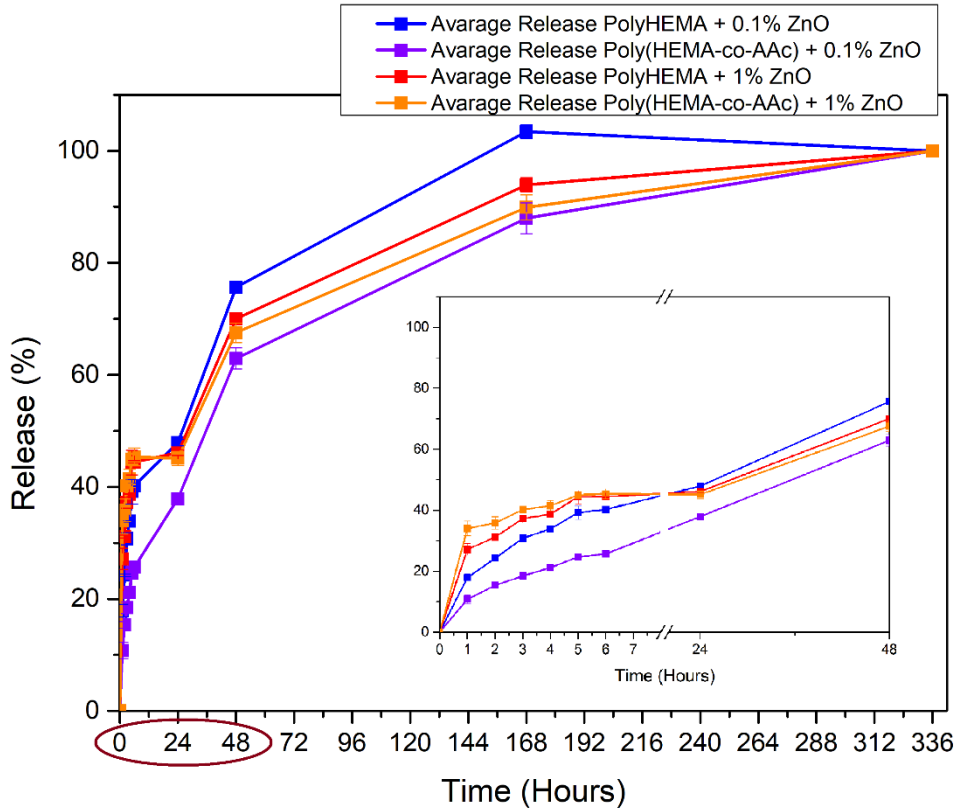


**Figure 5.3.3 (2)** Release trend comparison between composites with different amount of ZnO. Enlargement on the first 2 days of Ibuprofen release in alkaline urine.

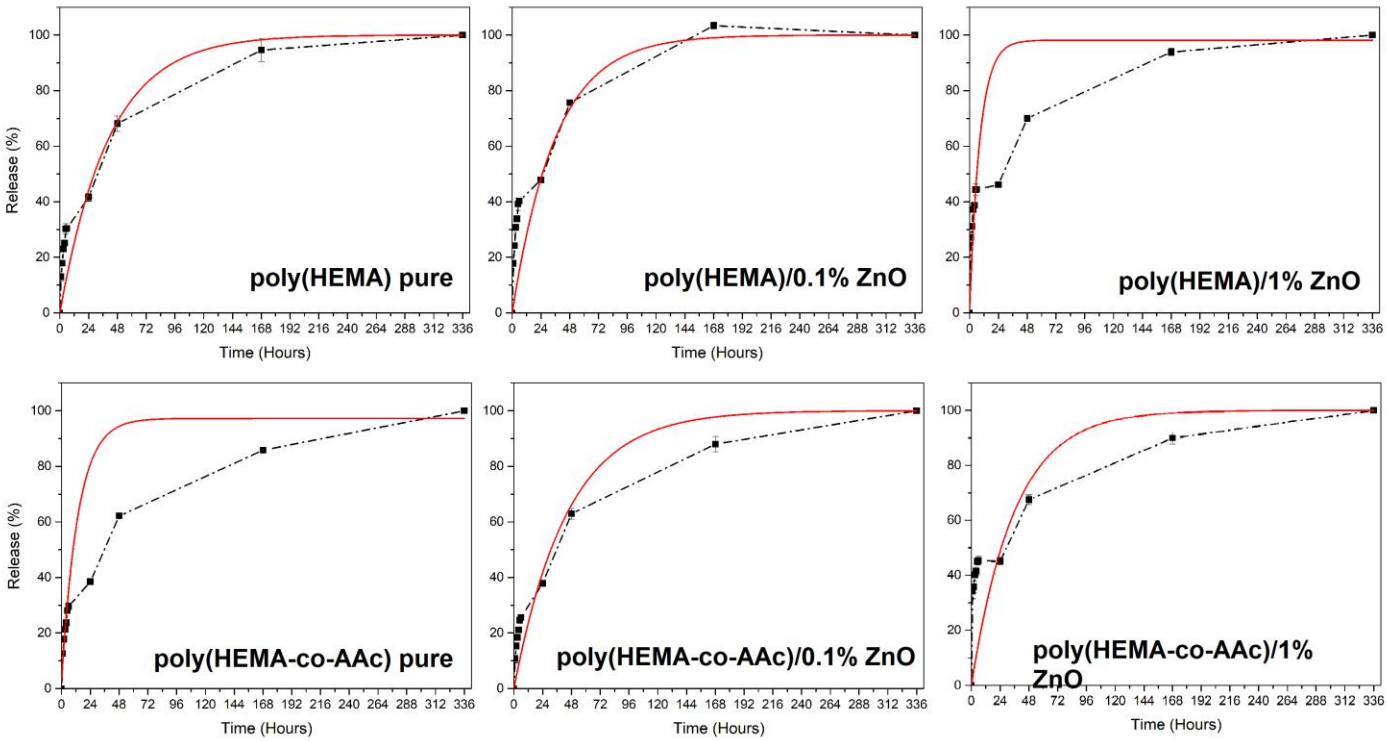


**Figura 5.3.3 (3)** Fitting lines of Ibuprofen release in alkaline urine.

| Material | pH | K ($hours^{-1}$) | $R^2$ |
|---|---|---|---|
| Poly(HEMA-co-AAc)+0.1% ZnO | 9.4 | 0.0225 0.01069 | 0.98044 |
| PolyHEMA pure | 9.4 | 0.02424±0.01602 | 0.971988 |
| PolyHEMA+0.1% ZnO | 9.4 | 0.02758±0.02069 | 0.90217 |
| Poly(HEMA-co-AAc)+1% ZnO | 9.4 | 0.02786±0.02077 | 0.98155 |
| Poly(HEMA-co-AAc) pure | 9.4 | 0.07285±0.01464 | 0.97568 |
| PolyHEMA+1% ZnO | 9.4 | 0.11711±0.01671 | 0.96968 |

**Table 5.3.3 (3)** Kinetic parameters of Ibuprofen released from pure pHEMA and copolymer and from ZnO/polymer and ZnO/copolymer systems.

All the samples reach the 100% of drug released after 14 days, but the material with the lowest kinetic parameter is the poly(HEMA-co-AAc)/0.1% ZnO.

By contrary, the fastest sample is the copolymer with 1% of powder, which has a kinetic constant of 0.14286±0.03112.

The same data have been found also for the release study in acid pH and have been reported below in the same order.

| Release time [Hours] | pHEMA pure | pHEMA 0.1% ZnO | pHEMA 1% ZnO | copHEMA pure | copHEMA 0.1% ZnO | copHEMA 1% ZnO |
|---|---|---|---|---|---|---|
| 0 | 14.714±3.518 | 14.714±3.518 | 14.714±3.518 | 14.714±3.518 | 14.714±3.518 | 14.714±3.518 |
| 1 | 0.717±1.198 | N.A. | N.A. | N.A. | 0.455±0.112 | N.A. |
| 2 | 20.178±3.743 | 18.981±0.449 | 3.524±14.334 | 18.831±1.497 | 19.355±1.422 | 17.558±1.946 |
| 3 | 13.591±1.048 | 32.865±1.759 | 34.25±4.341 | 32.678±2.021 | 27.701±2.433 | 32.865±2.957 |
| 4 | 19.692±3.855 | 42.521±1.01 | 45.066±2.433 | 45.552±1.123 | 38.367±0.898 | 45.403±1.572 |
| 5 | 26.802±1.46 | 50.68±2.283 | 58.314±6.25 | 55.133±4.042 | 43.12±4.079 | 55.058±4.266 |
| 6 | 34.924±3.817 | 58.951±0.599 | 63.591±1.422 | 59.175±1.497 | 46.413±0.711 | 64.714±1.796 |
| 24 | 72.274±2.769 | 112.805±0.487 | 134.362±8.046 | 90.051±3.406 | 86.234±4.678 | 122.648±9.132 |
| 48 | 86.683±3.256 | 134.287±4.229 | 140.088±9.132 | 95.178±5.913 | 114.377±5.801 | 149.07±7.186 |
| 168 | 91.885±0.374 | 140.275±0.037 | 132.79±1.46 | 93.644±0.861 | 120.627±0.599 | 150.68±5.501 |
| 336 | 107.716±1.385 | 154.609±1.048 | 131.219±4.828 | 88.292±2.171 | 121.376±2.171 | 149.183±4.229 |

**Table 5.3.3 (4)** Ibuprofen normalized % released amount in acid urine.

| Release time [Hours] | Normalized % Release ± Standard Error | | | | | |
|---|---|---|---|---|---|---|
| | pHEMA pure | pHEMA 0.1% ZnO | pHEMA 1% ZnO | copHEMA pure | copHEMA 0.1% ZnO | copHEMA 1% ZnO |
| 0 | 0±0 | 0±0 | 0±0 | 0±0 | 0±0 | 0±0 |
| 1 | 0.652±1.103 | N.A. | N.A. | N.A. | 0,372±0.087 | N.A. |
| 2 | 18.781±3.716 | 12.279±0,374 | 1.868±10.099 | 19.328±2.182 | 15.912±1.398 | 11.713±1.722 |
| 3 | 12.607±0.811 | 21.250±0,994 | 21.408±1.365 | 33.382±0.942 | 22.721±1.669 | 21.763±1.162 |
| 4 | 18.238±3.344 | 27.508±0,840 | 32.369±3.798 | 46.670±2.720 | 31.520±1.193 | 30.204±2.153 |
| 5 | 24.869±1.035 | 32.771±1,254 | 37.267±2.376 | 56.299±2.237 | 35.365±2.839 | 36.476±1.490 |
| 6 | 32.382±3.128 | 38.133±0,646 | 45.583±3.920 | 60.628±3.572 | 38.126±1.135 | 43.039±2.774 |
| 24 | 67.075±1.709 | 72.963±0,18 | 90.416±5.765 | 92.066±0.382 | 70.766±2.819 | 81.264±3.072 |
| 48 | 80.448±1.989 | 86.841±2,147 | 94.006±5.994 | 97.228±2.772 | 93.866±3.407 | 98.866±1.134 |
| 168 | 85.313±0.749 | 90.733±0,591 | 93.738±5.977 | 95.891±4.109 | 99.061±0.939 | 99.976±0.024 |
| 336 | 100±0.100 | 100±0,100 | 90.470±5.769 | 90.308±0.822 | 99.657±0.343 | 99.013±0.833 |

**Table 5.3.3 (5)** Ibuprofen normalized % released amount in acid urine.

As in case of Diclofenac released in acid urine, also in Table 5.3.3(4) it can be noticed that the release started only after 2 hours, and the maximum concentrarion values are lower than the other 2 release conditions.

The reason why that happens lies in the pKa value of Ibuprofen sodium salt, which is the same of Diclofenac.

Also in this case, the trend of the releases of both pure PolyHEMA and Poly(HEMA-co-AAc) in 2 weeks and in 48 hours have been shown together in Figure 5.3.3 (4), instead Figure 5.3.3 (5) the releases of the other composites during the same two period of time.

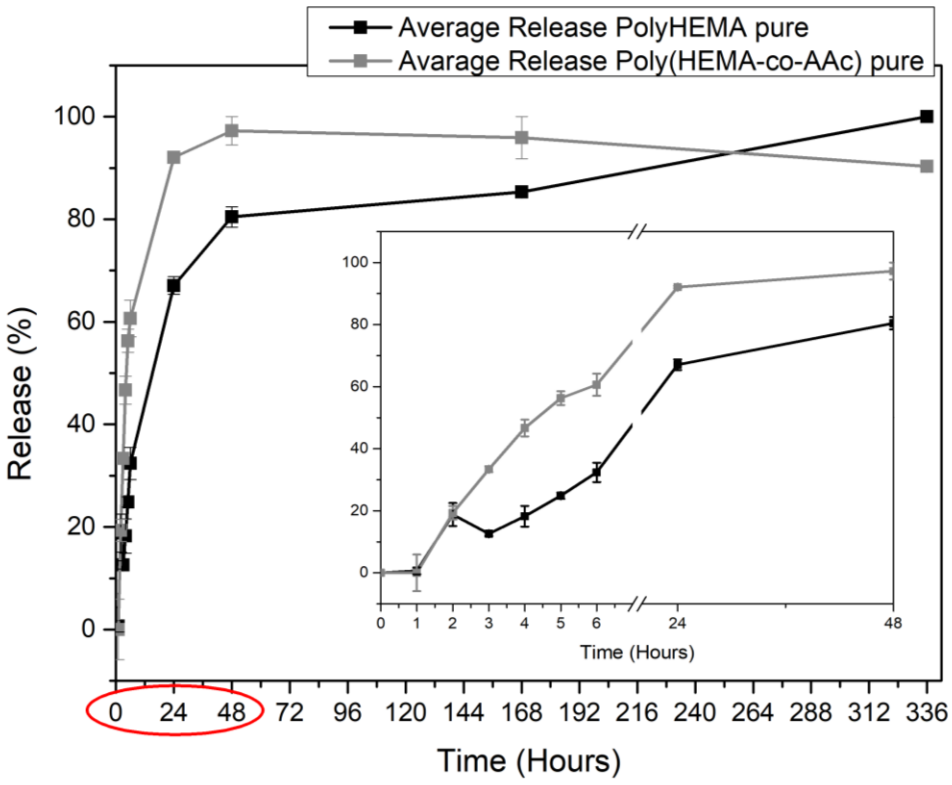


**Figure 5.3.3 (4)** Comparison of Ibuprofen release from pHEMA and p(HEMA-co-AAc) both pure, in acid urine.

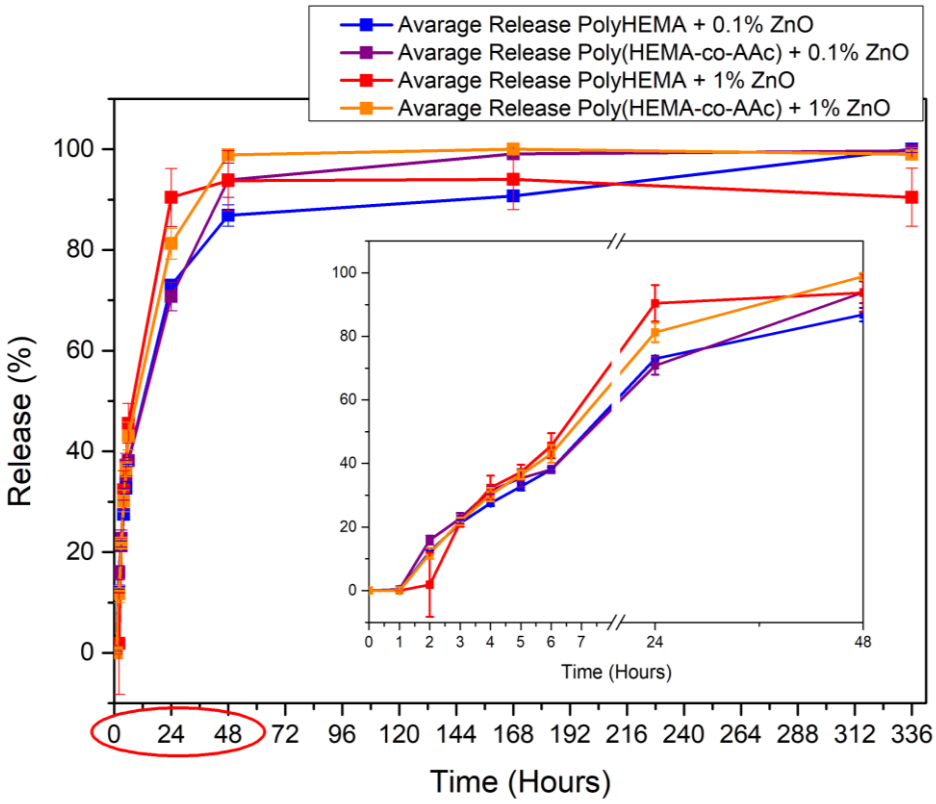


**Figure 5.3.3 (5)** Release trend comparison between composites with different amount of ZnO. Enlargement on the first 2 days of Ibuprofen release in acid urine.

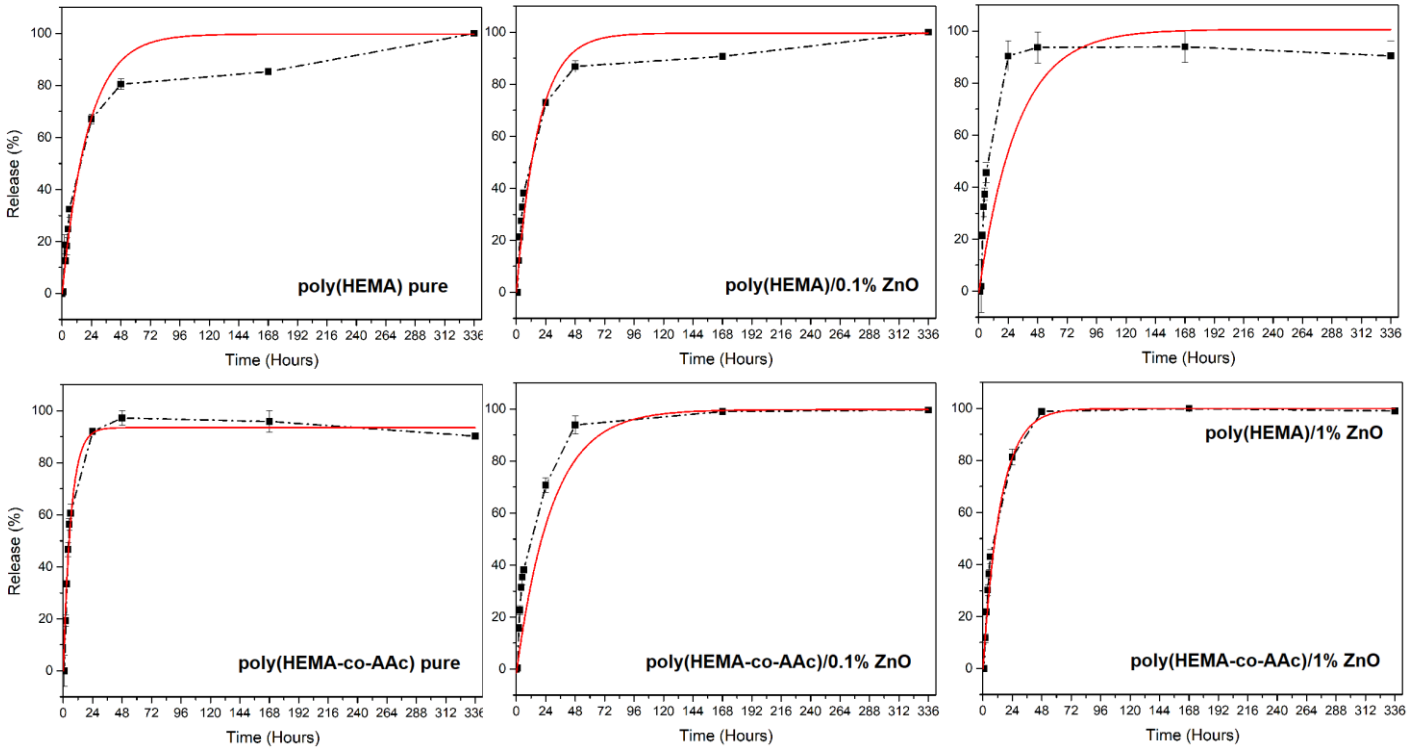


**Figure 5.3.3 (6)** Fitting lines of Ibuprofen release in acid urine.

| Material | pH | K ($hours^{-1}$) | $R^2$ |
|---|---|---|---|
| PolyHEMA+1% ZnO | 5.2 | 0.03194±0.01845 | 0,.60916 |
| Poly(HEMA-co-AAc)+0.1% ZnO | 5.2 | 0.03446±0.01306 | 0.98157 |
| PolyHEMA pure | 5.2 | 0.04722±0.01002 | 0.99892 |
| PolyHEMA+0.1% ZnO | 5.2 | 0.05614±0.00302 | 0.99821 |
| Poly(HEMA-co-AAc)+1% ZnO | 5.2 | 0.06963±0.01187 | 0.99968 |
| Poly(HEMA-co-AAc) pure | 5.2 | 0.15814±0.01081 | 0.99917 |

**Table 5.3.3 (6)** Kinetic parameters of Ibuprofen released from pure pHEMA and copolymer and from ZnO/polymer and ZnO/copolymer systems.

The two samples which have similar kinetic constant and with the lowest burst release are, in order, the composites polymer/1% ZnO and copolymer/0.1% ZnO. Both have a constant of release around 0.03, but the main difference lies on the maximum value of drug released. In case of the polymer composite, the maximum burst delivery reaches the 94% as really as 48 hours, but this value does not hold stady until 2 weeks. Opposite, the poly(HEMA-co-AAc) with 0.1% of powder reaches almost

the 100% of drug released after 1 week and that the value sligtly increases and stays stable until the end of the study.

Concerning the other samples, their kinetic constant are slightly higher than the lowest.

The unique material with highest burst release is the pure copolymer. In this case, the maximum release of 97% is still reached after 48 hours and it does not stay stable.

*5.4 Characterization of post release samples*

After the release study, IR analysis and also XRD pattern have been obtained, in order to evaluate possible residues of drug inside the samples. Previously, images by FESEM and EDX analysis have been acquired in order to see if some encrostations and deposition of salts occurred at the end of the immersion in urine and eventually to find the composition.
Besides, these analysis were taken also as a prelimiary study on the degradation behavior of in the investigated composite samples after 2 weeks.

The samples considered for these characterizations are those used for the release in physiologic urine.

*5.4.1 FESEM and EDX characterization*

After 2 weeks of immersion in artificial urine, it would be useful to see the conditions of samples' surface by FESEM, in order to verify if some salt inclusions have been formed.
In the following are shown the images of polyHEMA/1% and poly(HEMA-co-AAc)/1% as examples, whereas the other samples have shown similar results.

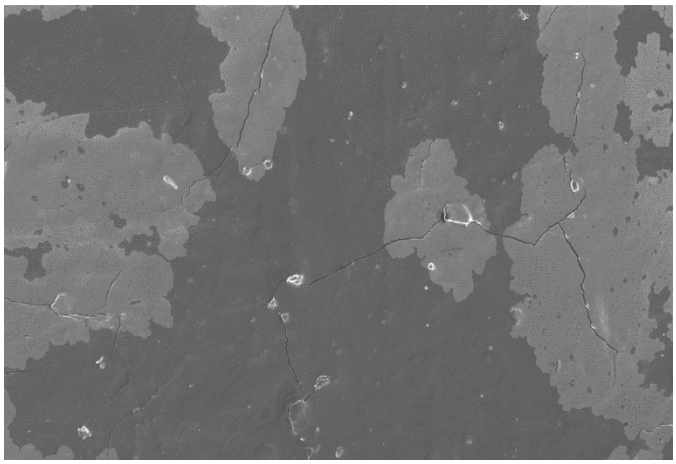

In Figure 5.4.1 (1), which represents the FESEM image of the polyHEMA sample with 1% of ZnO, it is possible to notice that some encrustations and depositions of salts occurred at the end of the release study.

**Figure 5.4.1 (1)** FESEM image of the surface of polyHEMA/1% ZnO after 2 weeks of immersion in urine.

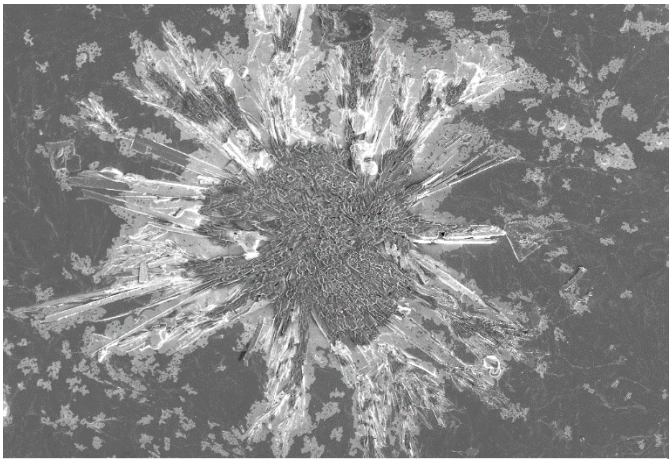

In order to verify the composition of the deposits that have been detected, it has been made the EDX analysis on these points.
From the table which reports the % atomic weight of the elements detected from the inclusions, there is a little amount of sodium, which is part of the urine composition. It has also been detected Zn, demonstrating that there is still ZnO powder left in the sample.

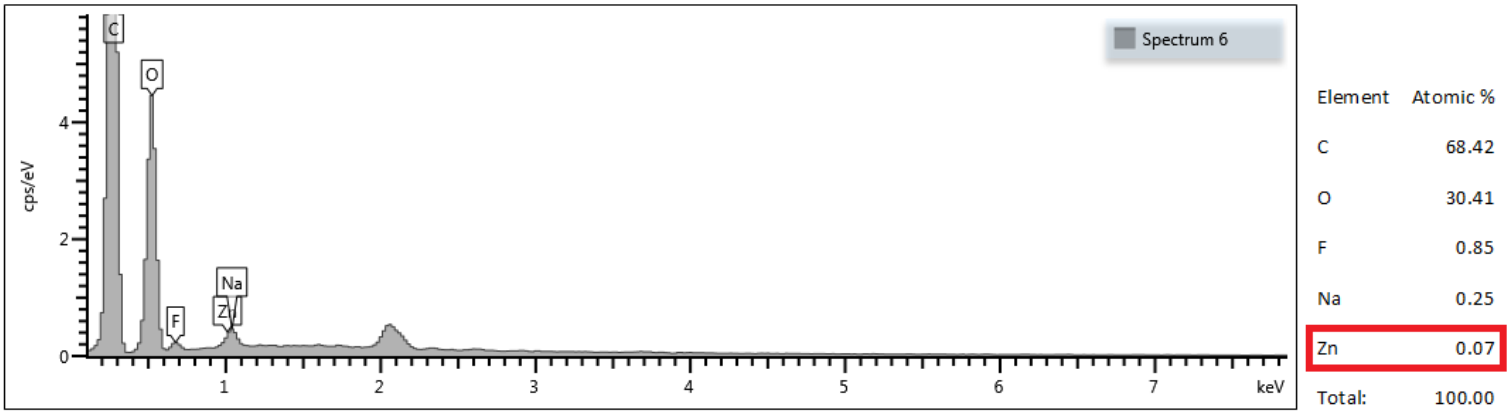


**Figure 5.4.1 (2)** EDX spectrum of PolyHEMA + 1% ZnO after immersion in artificial urine for 2 weeks. Table with % atomic weight of each element.

The same results have been reported also for the sample poly(HEMAA-co-AAc) with 1% of ZnO, in order to analyze different material, but always with the same percentage of powder.
Figure 5.4.1(3) shows the appearance of the sample surface at the end of the release study performed in artificial urine for 2 weeks.

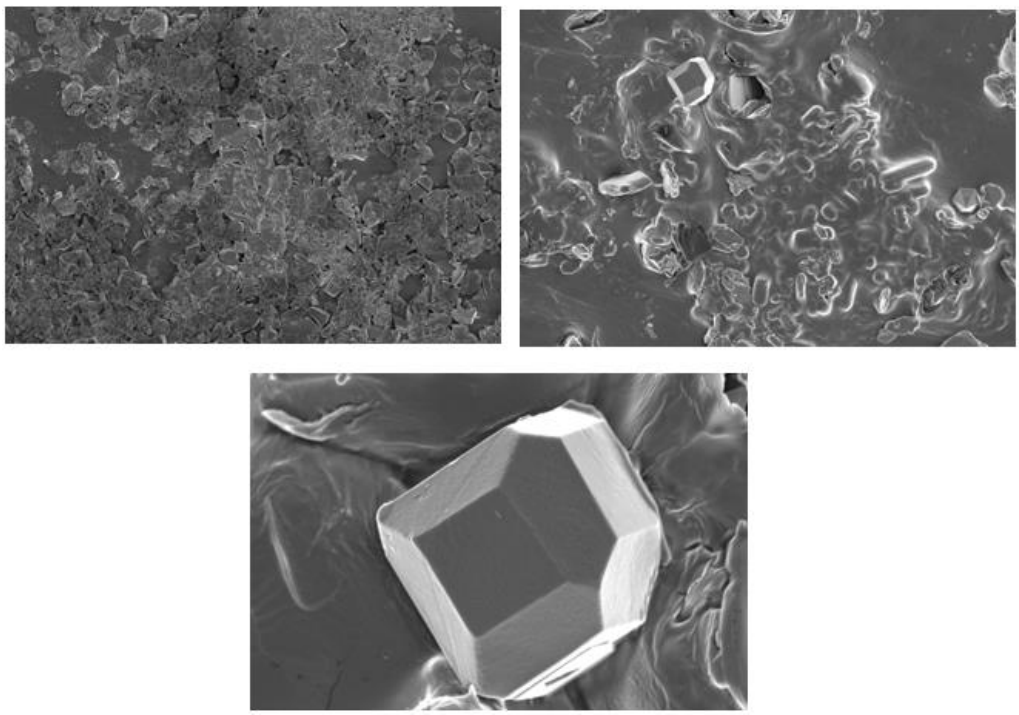

**Figure 5.4.1 (3)** FESEM images of the poly(HEMA-co-AAc)/1% ZnO surface after 2 weeks of immersion in urine.

On the top of this sample can be seen that there are a lot of salt depositions. Even in this case, the EDX analysis has been made in order to identify the elements forming the crystals.

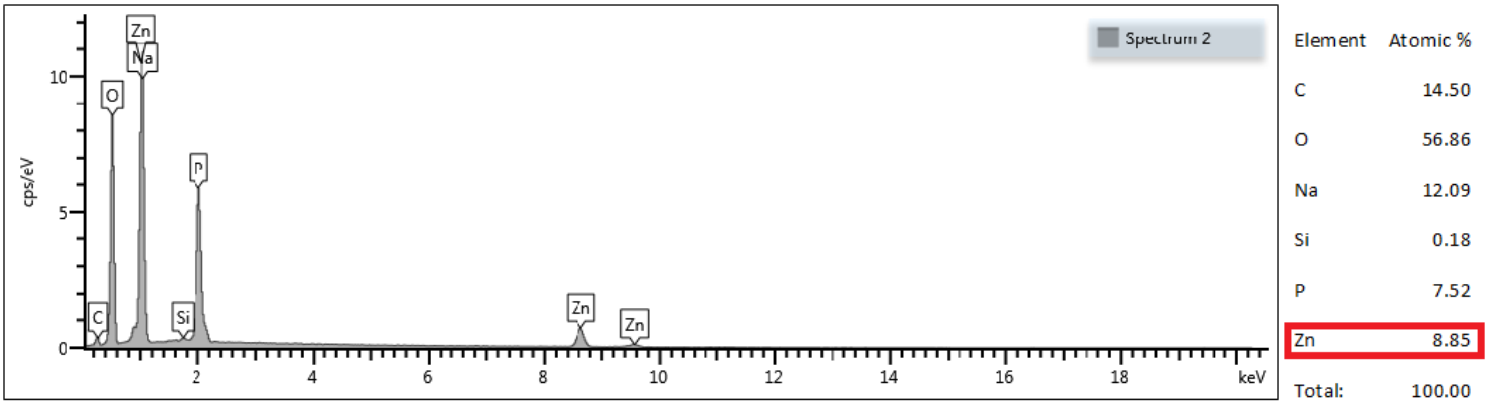


**Figure 5.4.1 (4)** EDX spectrum of encrustations on the top of Poly(HEMA-co-AAc) + 1% ZnO sample Table with % atomic weight of each element.

From the $Na_2HPO_4$ salt dissolved in water during the formulation of the artificial urine, an high percentage of phosphorus and sodium are precipitated and have covered the composite surface. Also in this case, Zn has been detected, indicating that some amount of ZnO is still inside the sample.

In order to verify if the amount of ZnO inside the sample could influence the deposition of salts on the surface, the FESEM image of pure poly(HEMA) has been reported below as an example.

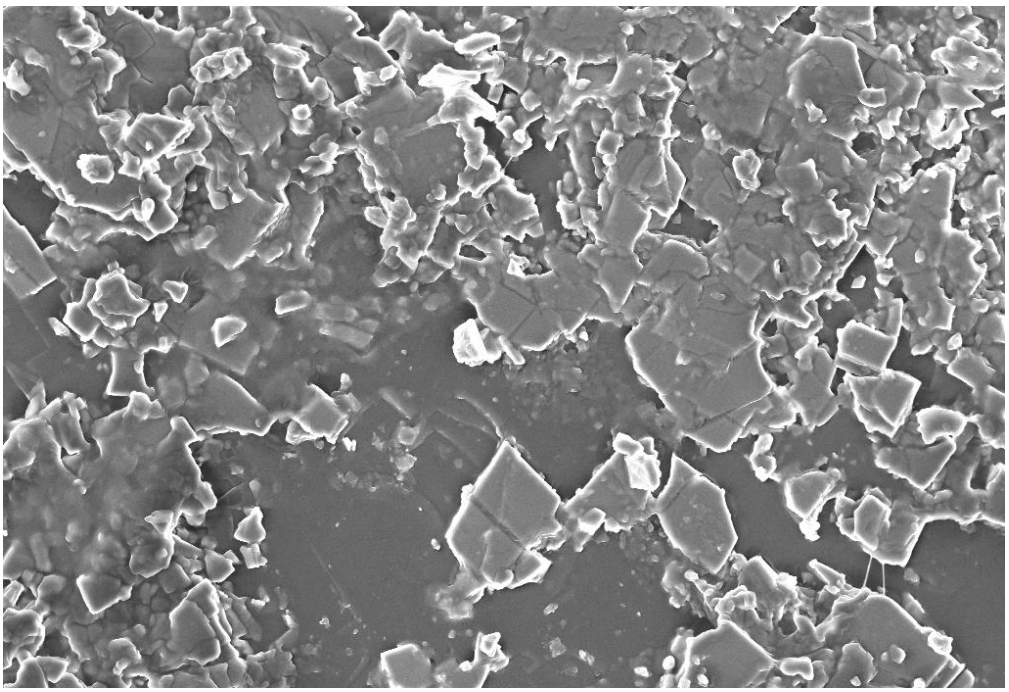

**Figure 5.4.1 (5)** Salt depositions on the polyHEMA pure sample on the surface after 2 weeks of immersion in urine.

From Figure 5.4.1(5) it can be seen that also in the material without ZnO the same encrustations largely cover the surface. This evidence may suggest that the presence of ZnO in the formulation of the material does not inhibit the precipitation of salts.

### *5.4.2 Infrared Spectroscopy characterization*

For this qualitative analysis, the spectra that have been collected for each sample are listed below:

- Polymer/copolymer without drug;
- Polymer/copolymer after the uptake (both for Diclofenac and Ibuprofen);
- Drug powder;
- Polymer/copolymer after the release study.

By bringing together all these spectra in the same graph and comparing the curves together, it has been possible to evaluate residues of drug that may be present inside the materials. This has resulted in a validation of the data obtained from the study of the release; in particular, this analysis allowed to verify the % normalized release for each sample tested in physiologic urine.

As an illustration, the spectra of both Diclofenac and Ibuprofen released from the polyHEMA/0.1% ZnO have been reported.

From Table 5.2.2 (2) for Diclofenac and Table 5.3.2 (2) for Ibuprofen, it can be noticed that for the first, the maximum percentage of drug released is 98.5%, while for the latter case, the maximum release is 100%. It is possible to verify these results by checking the spectra obtained from IR analysis.

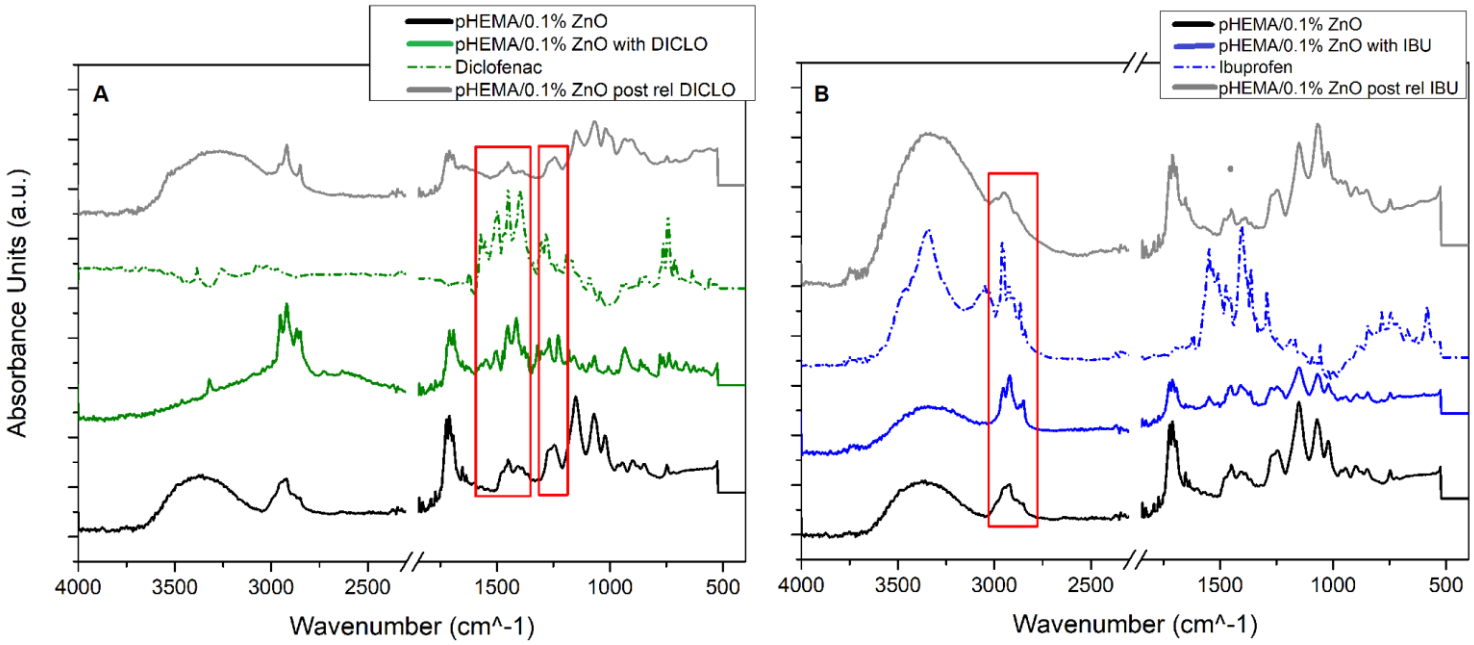


**Figure 5.4.3 (1)** IR analysis of the samples in case of (A) Diclofenac release and (B) Ibuprofen release.

Panel A of Figure 5.3.4 (1) represents the case of Diclofenac uptake and release. The red box highlights the characteristic peaks of Diclofenac drug that are found also in the spectrum of the sample after the uptake, confirming the successful drug uptake. The same aspect can be observed comparing the curves reported in graph B, which represents the analysis in the case of Ibuprofen.

Thereafter, looking the grey curve, which represents the sample after the release, it is possible to notice that the shape of the peaks around the wavenumbers 1250 $cm^{-1}$ and 1500 $cm^{-1}$ becomes different from the spectrum of polyHEMA/0.1% before the release (green curve), and it becomes again similar to the spectrum of the bare sample (black curve).

Looking the graph (B), which reports the same spectra but in case of Ibuprofen, in the red box is highlighted the distinctive peak of the drug around 2750 $cm^{-1}$. It can be noticed that the grey spectrum has lost the spikes acquired from the spectrum of the drug, and it has almost reacquired the same shape of the spectrum of the polymer/0.1% untouched (black line). This means that all the Ibuprofen absorbed during the uptake has been completely delivered, validating the 100% of maximum release obtained during the study.

In the same way, all the graphs of the other samples have been analyzed, comparing them with the maximum release obtained during the period of study. All the data can be considered valid, having had the correct feedback with respect to UV-Vis results.

The spectra of the other samples, both for the two drugs, have been reported in the appendix.

### *5.4.3 X-Ray Diffractometry Characterization*

Also XRD analysis has been made in order to verify the data acquired during the release study, as well as to check the presence of ZnO powders in the composite. For this qualitative analysis, the pattern that have been collected for each material are listed below:

- Polymer/copolymer without drug (black);
- Polymer/copolymer after the uptake (both for Diclofenac and Ibuprofen);
- Polymer/copolymer after the release study (grey).

Comparing the curve of the untouched sample and the one after the uptake is possible to indentify the peaks associated to the drug. Afterwards, by matching the last curve mentioned with the pattern of the sample after the release study near the spikes previously identified, it is possible to determine if some drug has left inside the material. Figure 5.4.3 (1) and (2) reported below, show the XRD patterns of the study about Diclofenac and Ibuprofen, in order.

The red box highlights the peaks associated to the drugs.

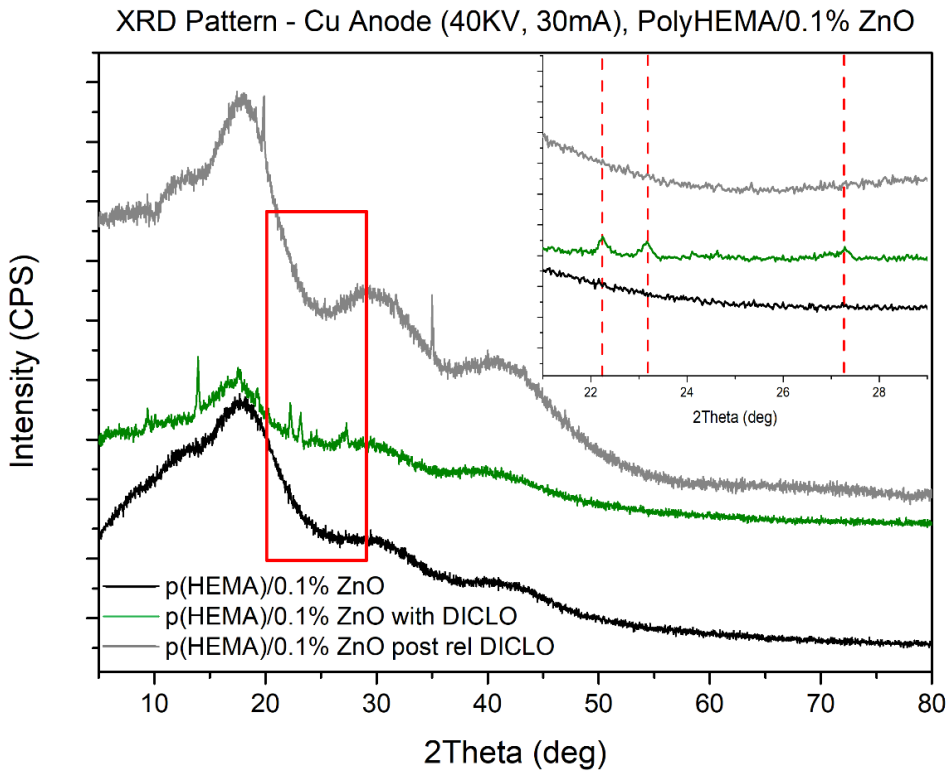


**Figure 5.4.3 (1)** XRD pattern of samples used to study the Diclofenac release in physiologic urine. Enlargement on the main peaks of the drug.

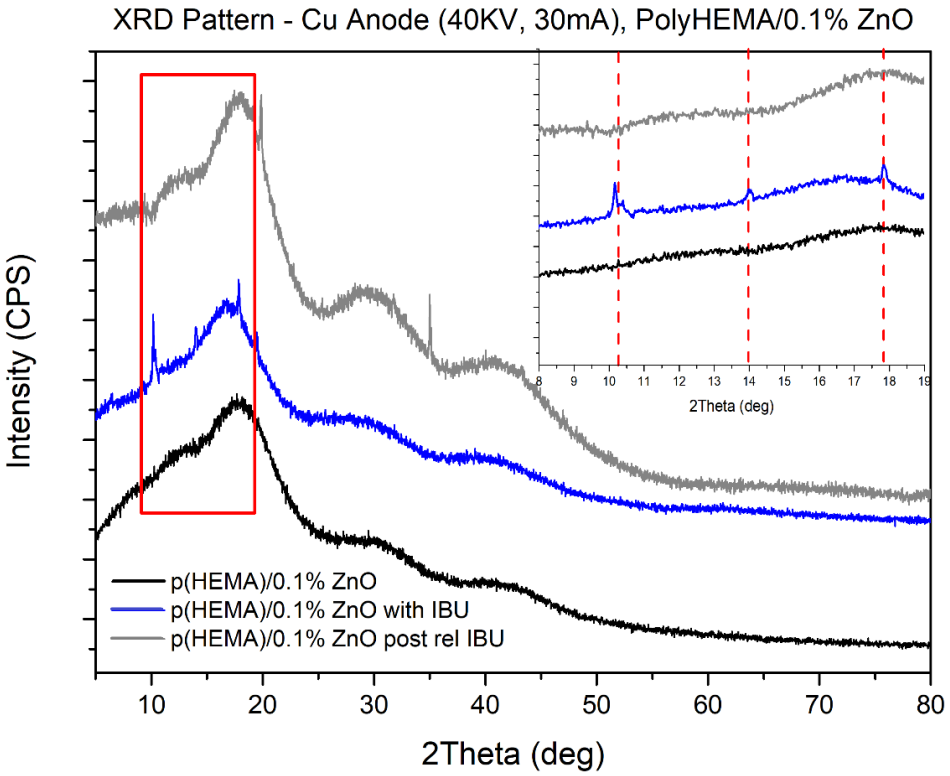


**Figure 5.4.3 (2)** XRD pattern of samples used to study the Ibuprofen release in physiologic urine. Enlargement to highlight the main peaks of the drug.

In both graphs, comparing the two patterns before and after the release, it is possile to notice that near the angles associated to each drug (red box), the spikes that were detected in the second pattern, completely disappear in the grey curve. Therefore, from this qualitative analysis it might be concluded that, both for Diclofenac and Ibuprofen, the release after 2 weeks in physiologic urine has been total.

By the contrary, the XRD analysis can be more useful to start an initial study about the degradation of ZnO powder. Actually, noting the peaks near the typical angles of ZnO, which are 31.82°, 34.54° and 36.42° and matching the patterns of the sample pre and post release (black and grey curves), it is possible to imagine if the powder started the degradation process during the period of study in urine at 37°C.

For the investigation, the graphs of polyHEMA with 1% of ZnO for both the drugs have been reported in Figure 5.4.3 (3) and (4), because in these cases the peaks were high enough to be visible.

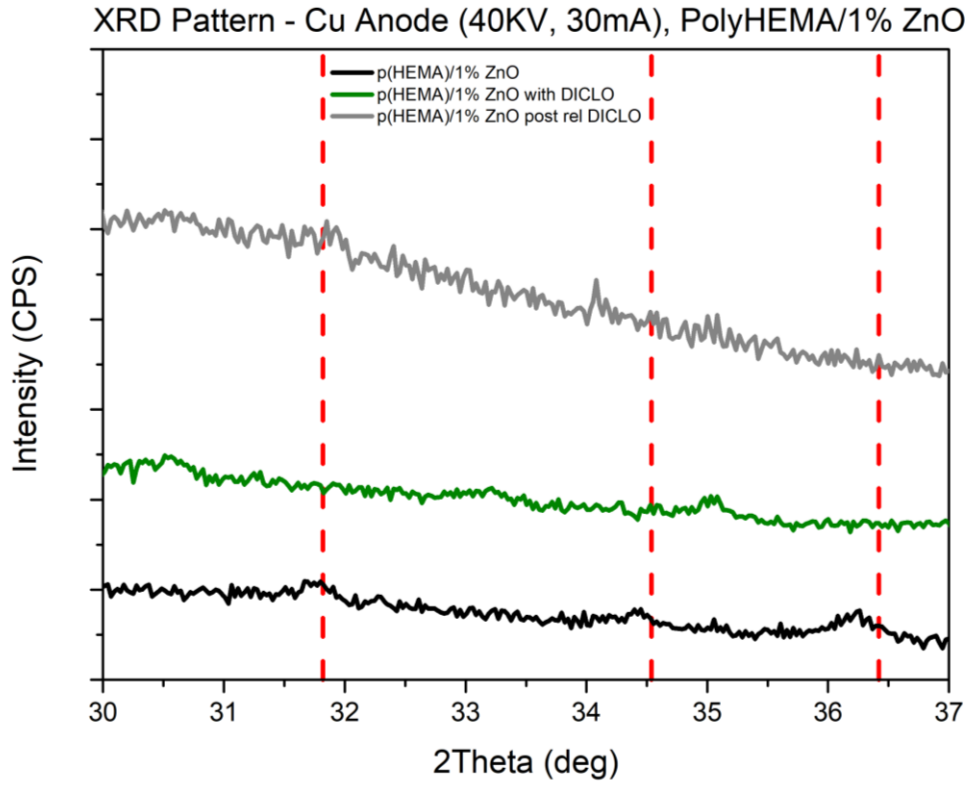


**Figure 5.4.3 (3)** XRD pattern of polyHEMA/1% in the Diclofenac release study. Enlargement on typical angles of ZnO.

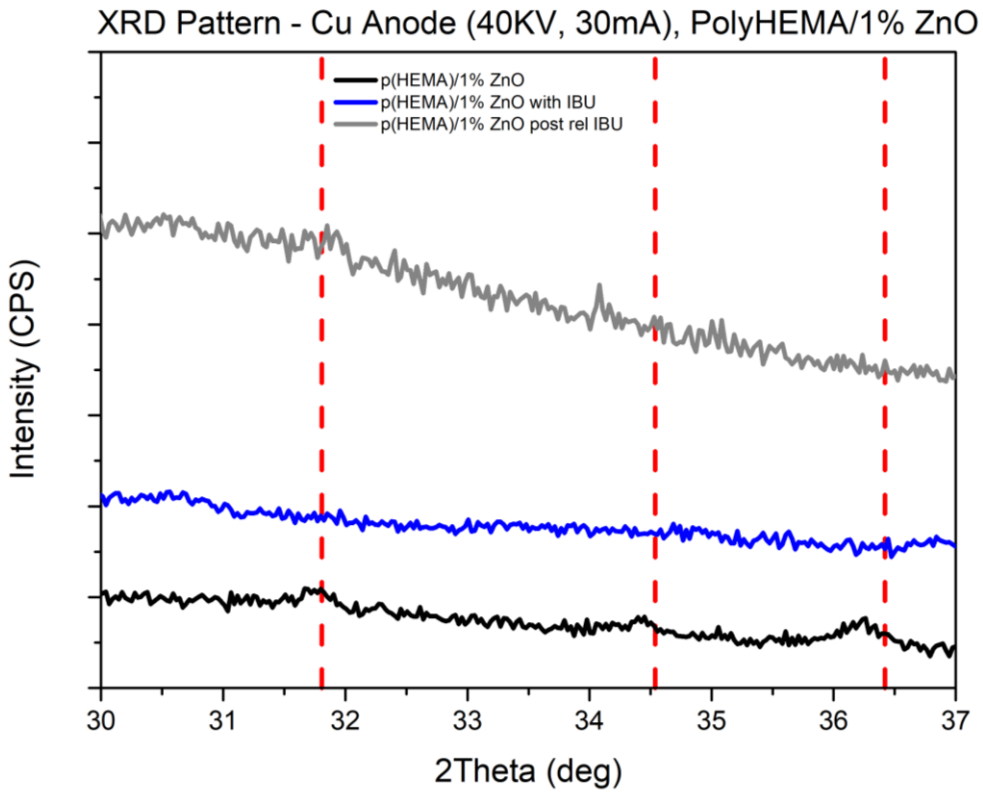


**Figure 5.4.3 (4)** XRD pattern of polyHEMA/1% in the Ibuprofen release study. Enlargement on typical angles of ZnO.

Comparing the peaks near the angles indicated by the red lines, it is possible to notice that the shape of the peaks found in the black curve is almost the same of those in the grey curve. That evidence shows that the degradation of ZnO has not already begun and confirms the data obtained by the EDX, in which significant amounts of Zn had been found.

# 6 Conclusion

In this Master thesis, the study was focused on the formulation of new innovative and smart materials, acceptable in the field of ureteral stent applications. The main goal of this work was to obtain materials with multifunctional properties, such as anti-bacterial effects, drug elution and biodegradability.
First of all, ZnO powder with flower-like crystalline structure and a relatively high surface area (16 $m^2g^{-1}$) has been successfully synthetized by low-cost hydrothermal process.
Then, ZnO/polymer composites were fabricated, combining different percentages of the inorganic ZnO powder during the polymerization process of both Poly(2-hydroxyethyl methacrylate) and poly(HEMA-co-AAc). These polymers have been chosen because of their high swelling ability that allows them to store a large amount of water.

After the synthesis, the morphology analysis and other characterization results pointed out the correct integration of ZnO inside the samples.
Furthermore, thermal analysis such as TGA and DSC have shown that copolymer has a higher stability than the simple polyHEMA. This stability was even more improved thanks to the addition of ZnO powders.

These results have been afterwards verified during the absorption of two different drugs: Diclofenac and Ibuprofen, both in salt form.
Actually, looking at conditions of each sample after 4 hours of uptake in water, it was possible to notice that the copolymer samples resulted more rigid and intact. These practice evidence suggest that the composites made by copolymer may be most appropriate for the application discussed in this thesis work.

Then, the work continued with the study of drug release in urine at three different pH conditions (7.3, 9.4, 5.2). These different values of pH have been chosen with the aim to test the behavior of the same stock of materials in different physiologic or pathologic conditions. Actually, the normal pH value of urine in the body can vary between 4.5 and 7.5, depending on the protein catabolism. Contrary, in pathological conditions the urine pH can reach the value of 9, also due to the increase of the urea destruction process, which produces ammonium.
For these reasons, it was considered useful to test the release of drug in all materials both in neutral, alkaline and acid urine.

During the drug delivery, from each sample the normalized values of drug released have been obtained, compared to the total amount of drug absorbed.
In particular, it has been obtained that the maximum amount of the released drug was always reached between 48 hours, from materials with high burst release, and 336 hours (14 days) from the start of the experiment for materials with slow release rates.

Then, these data have been used to track the fitting curves of release, which allow to describe the release trend by pseudo-first-order kinetic model. From the different fitting curves, the kinetic constants have been derived, in order to compare the different burst release.
Comparing the different kinetic parameters, the presence of ZnO appears not to affect the release performance over time. For that reason, it is possible to conclude that the addition of ZnO in the formulation of the material is useful for its antibacterial properties, but it does not affect the storage or the release of the drugs.

The positive aspect to include the powder inside the polymer matrix is that it is possible to shield the direct contact between cells and ZnO, decreasing the toxic effects of zinc. In this way, the amount of ZnO to be included in the composite can be properly optimized in order to increase the antibacterial effect.

On the other hand, what may influence the release trend is the type of material, whether polymer or copolymer. Actually, observing the kinetic parameters for each drug and pH condition, the material that in general has always a slow initial burst release is the poly(HEMA-co-AAc) with 0.1% of ZnO.

The samples have been characterized also at the end of the period of release study (FESEM, EDX, IR Spectroscopy, XRD). These different analyses have been used to preliminary examine the degradation properties after two weeks of immersion in artificial urine, as well as to verify the data of the maximum release collected.

By FESEM, it has been possible to notice the salt depositions on the surface, which have occurred equally in all the samples.
On the other hand, from the IR analysis it was possible to detect the residues of drug remained inside the samples that had not reached 100% of release.
Finally, by the XRD pattern it has been tried to make a qualitative assessment of the degradation process of ZnO.

In conclusion, in this Master thesis it has been deeply studied the behavior of new composite materials, based on the incorporation of ZnO into polyHEMA or poly(HEMA-co-AAc). In particular, it has been found that the amount of ZnO inside the formulation does not negatively affect its ability to storage or release drug. On the other hand, depending on the type of material (polymer or copolymer), the stability of the composite in organic fluids can change during time, thereby also influencing the release rate.
The material which has always shown the best release trend, characterized by low kinetic constant and burst release combined with good stability at the end of the study, is the poly(HEMA-co-AAc) with 0.1% of ZnO.
This material satisfies the multifunctional requirements needed in the field of ureteral stent applications.

# Appendix

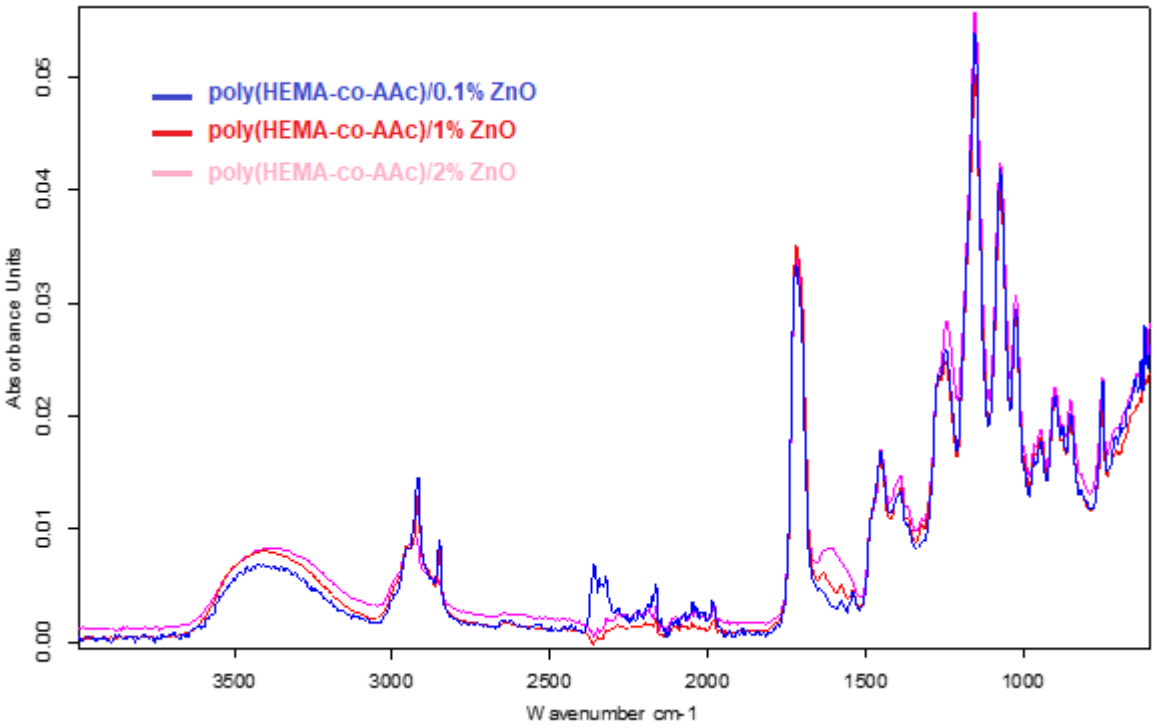


**Figure 1** Comparison of FT-IR spectra of poly(HEMA-co-AAc) samples with different percentages of ZnO.

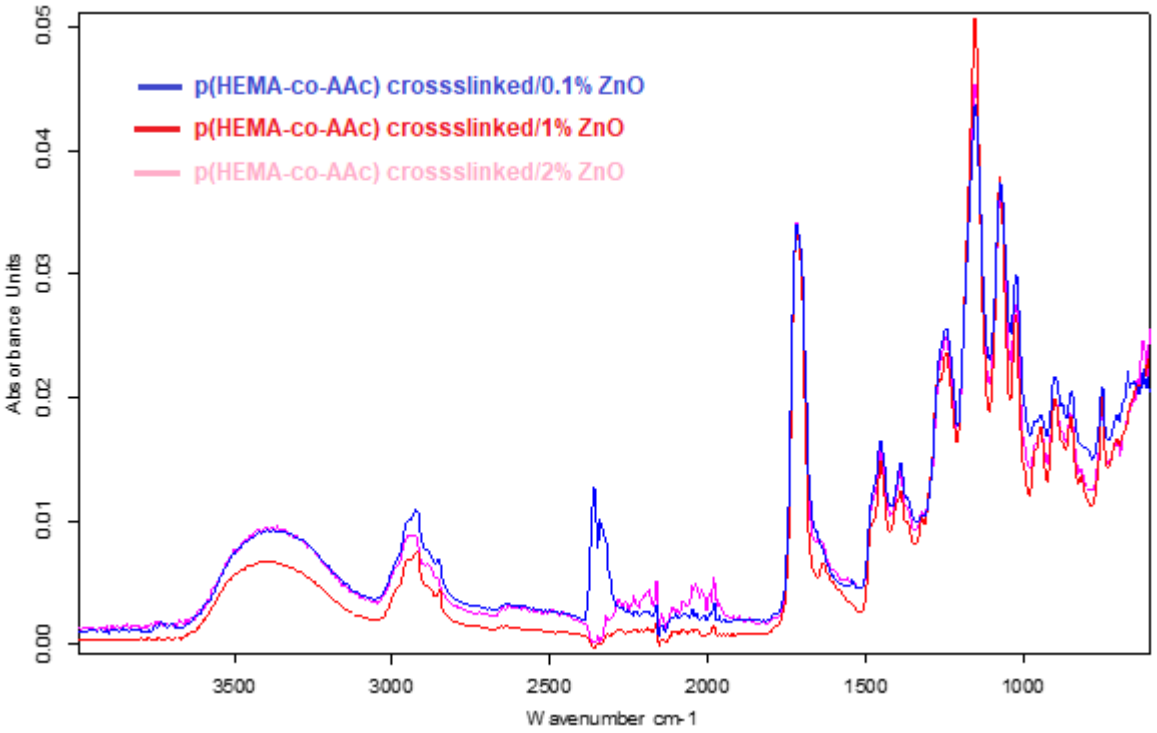


**Figure 2** Comparison of FT-IR spectra of poly(HEMA-co-AAc) crosslinked samples with different percentages of ZnO.

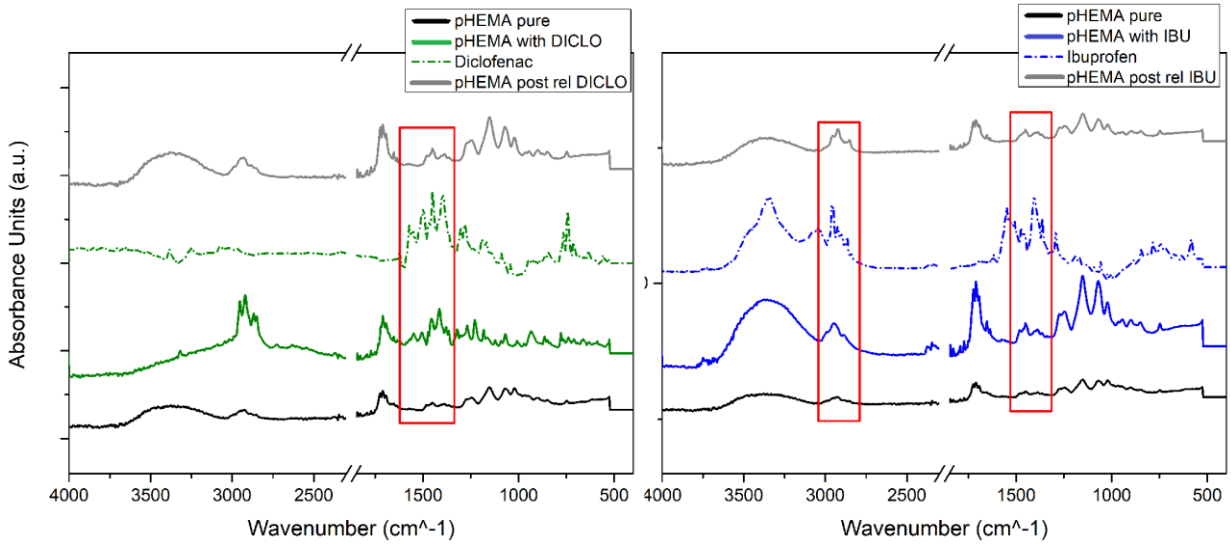


**Figure 3** IR analysis of pHEMA pure sample in case of (A) Diclofenac release and (B) Ibuprofen release.

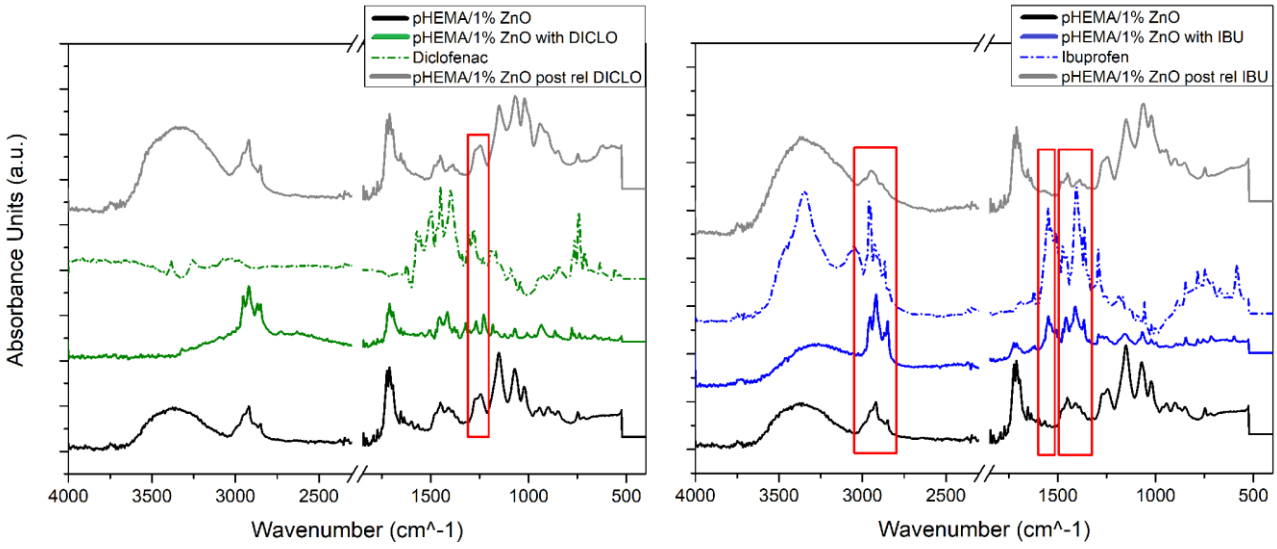


**Figure 4** IR analysis of p(HEMA)/1% sample in case of (A) Diclofenac release and (B) Ibuprofen release.

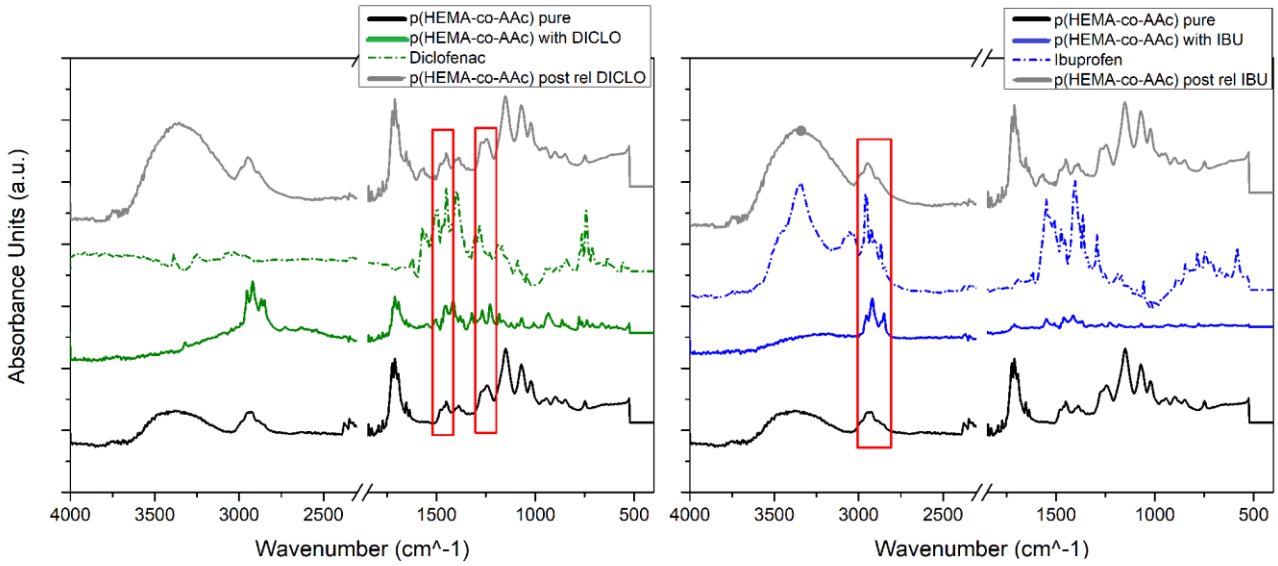


**Figure 5** IR analysis of p(HEMA-co-AAc) pure samples in case of (A) Diclofenac release and (B) Ibuprofen release.

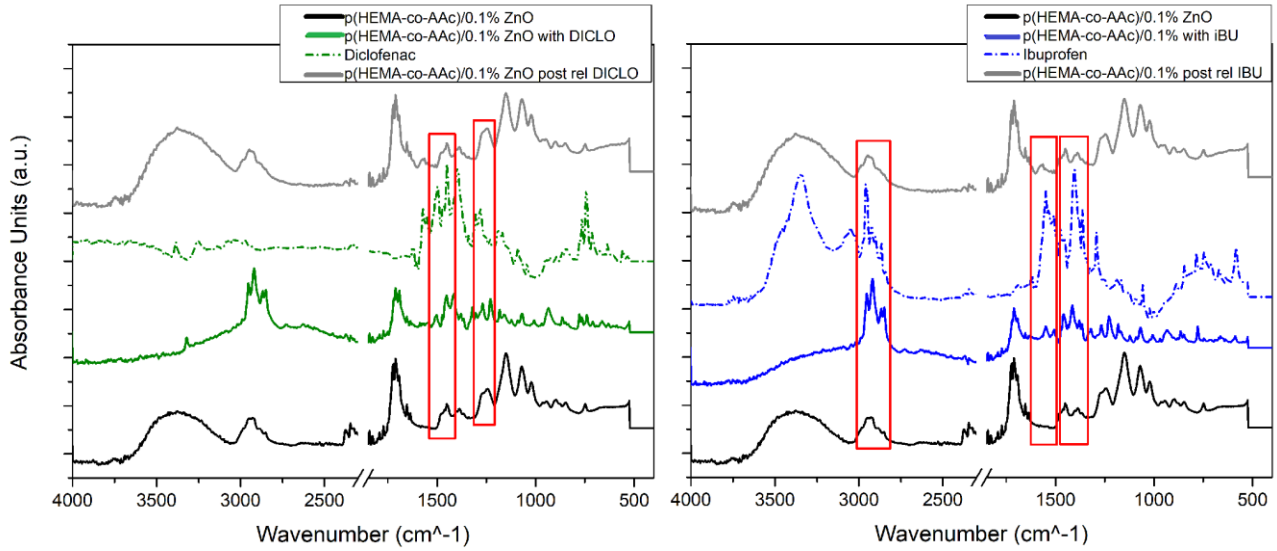


**Figure 6** IR analysis of p(HEMA-co-AAc)/0.1% samples in case of (A) Diclofenac release and (B) Ibuprofen release.

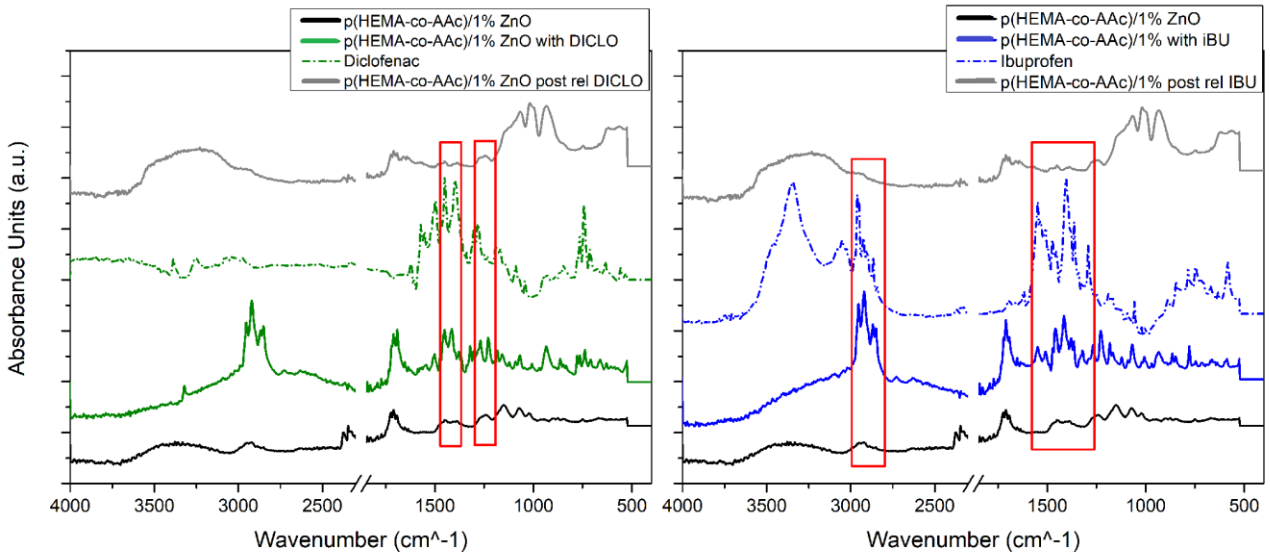


**Figure 7** IR analysis of p(HEMA-co-AAc)/1% samples in case of (A) Diclofenac release and (B) Ibuprofen release.

## Bibliography


A. Matei, I. C. (April 2008). Synthesis and characterization of ZnO – polymer nanocomposites. *International Journal of Material Forming*, Volume 1, Supplement 1, pp 767–770. DOI: 10.1007/s12289-008-0288-5.

Abdulrahman Al-Aown, I. K. (2010). Ureteral stents: new ideas, new designs. *Therapeutic Advances in Urology*.

Ahmed M. Nawar, N. A.-T. (Jul-Aug. 2014). Improving the optical and electrical properties of Zinc Oxide thin film by Cupric Oxide dopant. *IOSR Journal of Applied Physics (IOSR-JAP) , .Volume 6, Issue 4*, 2278-4861.Volume 6, Issue 4 Ver. II .

Alexandre Barros, A. R. (December 2017). Ureteral Stents Technology: Biodegradable and Drug-Eluting Perspective. DOI: 10.1016/B978-0-12-803581-8.10189-4.

B. Dumontel, M. C. (2017). Enhanced Biostability and Cellular Uptake of Zinc Oxide Nanocrystals Shielded with Phospholipid Bilayer. *JOURNAL OF MATERIALS CHEMISTRY B*, Vol.5, pp. 8799—8813, ISSN 2050-750X, doi: 10.1039/c7tb02229h.

Bazak R, H. M. (2014). Passive targeting of nanoparticles to cancer: A comprehensive review of the literature. *Molecular and Clinical Oncology*, 2(6):904–908. doi:10.3892/mco.2014.356.

Carmine Lops, A. A. (2019). Sonophotocatalytic degradation mechanisms of Rhodamine B dye via radicals generation by micro- and nano-particles of ZnO. *Applied Catalysis B: Environmental 243*, 629-640.

Cauda, V. C. (2012). *Polyurethane in Urological Practice.*

Deepak S. Ipe, G. C. (2016, August). Evaluation of the in vitro growth of urinary tract infection-causing gram-negative and gram-positive bacteria in a proposed synthetic human urine (SHU) medium. *Journal of Microbiological Methods*, p. 164–171, https://doi.org/10.1016/j.mimet.2016.06.013.

Deepalekshmi Ponnamma, J.-J. C. (May 2019). Synthesis, optimization and applications of ZnO/polymer nanocomposites. *Materials Science and Engineering: C*, Volume 98, Pages 1210-1240. DOI: 10.1016/j.msec.2019.01.081.

Dexue Liuab, D. Y. (2019, January-March). Mechanical properties, corrosion resistance and biocompatibilities of degradable Mg-RE alloys: A review. *Journal of Materials Research and Technology*, p. Pages 1538-1549, https://doi.org/10.1016/j.jmrt.2018.08.003.

Dijana Takić Miladinov, S. T. (August 2016). Synthesis, Swelling Properties and Evaluation of Genotoxicity of Hydrogels. *Materials Research*, DOI: 10.1590/1980-5373-MR-2016-0222.

F. Cauda, V. C. (2009). *Biomaterials and Tissue Engineering in Urology - Coated ureteral stents, Chapter 6.* J. Denstedt, A. Atala .

Fabio Manoni, G. G. (2016). Esame fisico, chimico e morfologico delle urine: proposta di linee guida per la fase analitica del Gruppo Intersocietario Analisi delle Urine (GIAU). *SIBioC DOCUMENTS* , vol. 40, n. 4 DOI: 10.19186/BC_2016.037.

Furio Cauda, V. C. (20 Mar 2008). Heparin Coating on Ureteral Double J Stents Prevents Encrustations: An in Vivo Case Study. *Journal of Endourology*, Volume: 22 Issue 3.

Geert-Jan Janssen, R. F. (s.d.). *Information on the FESEM (Field-emission Scanning Electron Microscope)* . Radboud University Nijmegen .

Greenstein G1, P. A. (1998 May). The role of local drug delivery in the management of periodontal diseases: a comprehensive review. *J Periodontol*, 69(5):507-20.

Hilary Brotherhood, D. L. (2014 Sep). Advances in ureteral stents. *Translational Andrology and Urology*, 3(3): 314–319. doi: 10.3978/j.issn.2223-4683.2014.06.06.

Ian Richard Cooper, M. P. (1 December 2016). The potential of photo-deposited silver coatings on Foley catheters to prevent urinary tract infections. *Materials Science and Engineering: C, Volume 69*(Materials Science and Engineering: C), Volume 69, Pages 414-420.

Information., N. C. (2019, Sept 22). *PubChem Database*. Tratto da Diclofenac: https://pubchem.ncbi.nlm.nih.gov/compound/Diclofenac

J. W. Rasmussen, E. M. (2010). Zinc oxide nanoparticles for selective destruction of tumor cells and potential for drug delivery applications. *Expert Opin. Drug Deliv.*, vol. 7, no. 9, pp 1063-77.

(1998). *JCPDS File.* International Centre for Diffraction Data.

Joey Lo, D. L. (2014). Ureteral Stents and Foley Catheters-Associated. *Antibiotics*, 3, 87-97; doi:10.3390.

K. M. Reddy, K. F. (April 2007 ). Selective toxicity of zinc oxide nanoparticles to prokaryotic and eukaryotic systems. *NIH Pubblic Acces*, 213902-1–213902-3. https://doi.org/10.1063/1.2742324 .

Karnabatidis, P. K. (October 2011). Evaluation of Zotarolimus-Eluting Metal Stent in Animal Ureters. *Volume 25*(Number 10).

Latifa B. Khan, H. M. (2017, Septembrer 01). Artificial Urine for Teaching Urinalysis Concepts and Diagnosis of Urinary Tract Infection in the Medical Microbiology Laboratory. *Journal of Microbiology & Biology Education*, p. 18(2):18.2.46. DOI:10.1128/jmbe.v18i2.1325.

Laurenti, C. (2018). Gentamicin-releasing mesoporous ZnO structures. *Materials*, 11, 314; doi:10.3390/ma11020314.

LiverTox. (2019, July 01). *NIH - National Institutes of Health*. Tratto da livertox.nlm.nih.gov: https://livertox.nlm.nih.gov/Ibuprofen.htm

Luo Yang, S. W. (2015 Oct). Ureteral stent technology: Drug-eluting stents and stent coatings. *Asian Journal of Urology*, 194–201.

Marco Laurenti, V. C. (2017 Nov). ZnO Nanostructures for Tissue Engineering Applications. *Nanomaterials, 7(11), 374*, vol. 7, no. 11, p. 374.

Material Interface inc. (2019). *X-Ray Diffraction (XRD)*. Tratto da Material Interface: https://www.materialinterface.com/analytical-services/microscopy-diffraction/x-ray-diffraction/

Matthias Beysens, T. O. (1 February 2018;). Ureteral stents in urolithiasis. *Asian Journal of Urology*, 5, 274e286.

Matthias T. Buhmann, 1. D.-W. (2019 Apr 13). Encrustations on ureteral stents from patients without urinary tract infection reveal distinct urotypes and a low bacterial load. *Microbiome*.

Mendez-Probst CE1, G. L. (2012 Sep). The use of triclosan eluting stents effectively reduces ureteral stent symptoms: a prospective randomized trial. *BJU Int.*, 110(5):749-54.

Messersmith, J. L. (2005). Protein Resistance of Titanium Oxide Surfaces Modified by Biologically Inspired mPEG−DOPA. *Langmuir*, 212640-646.

Minardi D1, C. O. (2012 Jul). Efficacy of tigecycline and rifampin alone and in combination against Enterococcus faecalis biofilm infection in a rat model of ureteral stent. *J Surg Res*, 176(1):1-6.

Monika Pietrzyńska, A. V. (2017, September). Stability of simulated body fluids such as blood plasma, artificial urine and artificial saliva. *Microchemical Journal*, p. 197–201. https://doi.org/10.1016/j.microc.2017.06.004.

Muthu Vignesh Vellayappan, A. B. (2015). Multifaceted prospects of nanocomposites for cardiovascular grafts and stents. *International Journal of Nanomedicine*, pp 2785–2803. doi: 10.2147/IJN.S80121.

n.d. (s.d.). *libero.it*. Tratto da Spettrofotometria: https://digilander.libero.it/righetti48/spettrofotometria.htm

Nadia Garino, P. S.-B.-R. (11th April 2019). Zinc oxide nanocrystals as a nanoantibiotic and osteoinductive agent. *The Royal Society of Chemistry*, DOI: 10.1039/C8RA10236H (Paper) RSC Adv., 2019, 9, 11312-11321.

Nadia Garino, T. L. (2019). A Microwave-Assisted Synthesis of Zinc Oxide Nanocrystals Finely Tuned for Biological Applications. *Nanomaterials*, 9(2), 212; https://doi.org/10.3390/nano9020212 .

Nanakoudis, A. (2018 , June 21). *ThermoFIsher Scientific*. Tratto da EDX analysis with a scanning electron microscope (SEM): how does it work?: https://blog.phenom-world.com/edx-analysis-scanning-electron-microscope-sem

NIC - Institute, N. C. (2019). *NCI Term Browser*. Tratto da www.cancer.gov: https://ncit.nci.nih.gov/ncitbrowser/ConceptReport.jsp?dictionary=NCI_Thesaurus&ns=NCI_Thesaurus&code=C561

Norbert Laube, *. L. (1 May 2007). Diamond-Like Carbon Coatings on Ureteral Stents—A New. *Journal of Urology*, Volume 177, Issue 5, Page: 1923-1927.

Panagiotis S. Kallidonis, I. S. (2014). Drug-eluting metallic stents in urology. *Indian J Urol.* , 30(1):8–12. doi:10.4103/0970-1591.124198.

Paula Judith Perez Espitia, N. d. (July 2012). Zinc Oxide Nanoparticles: Synthesis, Antimicrobial Activity and Food Packaging Applications. *Food and Bioprocess Technology*, pp 1447–1464, DOI: 10.1007/s11947-012-0797-6.

PerkinElmer, Inc. (2010). *Thermogravimetric Analysis (TGA).* Tratto da perkinelmer.com: https://www.perkinelmer.com/lab-solutions/resources/docs/FAQ_Beginners-Guide-to-Thermogravimetric-Analysis_009380C_01.pdf

PerkinElmer, Inc. (2013). *Differential Scanning Calorimetry (DSC).* Tratto da https://www.perkinelmer.com/CMSResources/Images/46-74542GDE_DSCBeginnersGuide.pdf

Ranita Roy, a. M. (2018). Strategies for combating bacterial biofilms: A focus on anti-biofilm agents and their mechanisms of action. *Virulence*, 9(1): 522–554.

Remondini. (December 20, 1996). *Fundamentals of UV-Visible Spectroscopy, chapter 1.*

RTI Laboratories. (2015). *Techniques - FTIR Analysis*. Tratto da Environmental, Chemical & Materials Testing: http://rtilab.com/techniques/ftir-analysis/

Ruixia Shi, P. Y. (2012). Growth of flower-like ZnO via surfactant-free hydrothermal synthesis on ITO substrate at low temperature. *CrystEngComm*, 5996-6003, DOI: 10.1039/C2CE25606A.

Tieppo Francio V, D. S. (2017 Jun). Oral Versus Topical Diclofenac Sodium in the Treatment of Osteoarthritis. *J Pain Palliat Care Pharmacother*, 31(2):113-120. DOI: 10.1080/15360288.2017.1301616.

TM, O. B. (2018, April 2nd). *Molecular analysis using UV/Visible spectroscopy*. Tratto da Molecular Biology: https://orbitbiotech.com/molecular-analysis-using-uv-visible-spectroscopy-spectroscopy-uv-absorption-reflection-spectra-electromagnetic-radiation/

Translations, D. &. (2019, July 29). *Definitions.net*. Tratto da calibration curve: https://www.definitions.net/definition/calibration+curve

V. Cauda, A. C. (2016). Ureteral double-J stents performances toward encrustation after long-term indwelling in a Dynamic In-Vitro Model. *JOURNAL OF BIOMEDICAL MATERIALS RESEARCH – PART B APPLIED BIOMATERIALS*, Vol. 105 (8) pp. 2244-2253, ISSN: 1552-4981, doi: 10.1002/jbm.b.33756.

Vaidhya, R. B. (2017). NOVEL DRUG DELIVERY SYSTEMS: AN OVERVIEW. *International Journal Of* .

Valentina Cauda, R. G. (January 2014). Nanostructured ZnO Materials: Synthesis, Properties and Applications. *Handbook of Nanomaterials Properties*, pp 137-177, DOI: 10.1007/978-3-642-31107-9_32.

Vijaya B. Kolachalama, P. S. (2013). Mechanisms of Tissue Uptake and Retention in Zotarolimus-Coated Balloon Therapy. *Circulation*, 127(20):2047–2055. doi:10.1161/CIRCULATIONAHA.113.002051.

XOS. (2019). *X-Ray Diffraction (XRD)*. Tratto da XOS: https://www.xos.com/XRD?_bt=266567961265&_bk=&_bm=b&_bn=g&_bg=52848751417&gclid=Cj0KCQjw7sDlBRC9ARIsAD-pDFo6OibOuEiE4CtUi_6aNPXfxhsp8gdqFa8kAzkJkI0ALSMqOU9GQx8aAuEREALw_wcB

Zelichenko G1, S. D. ( 2013 Mar). Prevention of initial biofilm formation on ureteral stents using a sustained releasing varnish containing chlorhexidine: in vitro study. *J Endourol*, 27(3):333-7.

## Ringraziamenti

Prima di tutto vorrei ringraziare i miei relatori, Valentina Cauda e Marco Laurenti, per la disponibilità completa e la gentilezza che hanno dimostrato durante tutto il lavoro di tesi. Inoltre ci tenevo a nominare anche Marta Grochowicz, professoressa che mi ha ospitata durante il periodo in Polonia: grazie per l'impegno e l'interesse che ha mostrato nell'accogliermi e aiutarmi durante la mia prima esperienza in un laboratorio. Grazie anche per il continuo entusiasmo che ha mostrato nel farmi credere nelle mie conoscenze.
Un grande ringraziamento va ovviamente ai miei genitori, mamma e papi, che semplicemente con il loro esempio, senza mai il bisogno di troppe parole mi hanno dato gli insegnamenti più grandi e belli che possa portare ora nel mio piccolo bagaglio di esperienza. Grazie per la libertà che mi avete lasciato sempre in ogni mia scelta: solo ora ne apprezzo a pieno la ricchezza. Grazie per il sostegno economico che mi ha permesso di fare ogni esperienza utile ma non scontata per la mia crescita; ma soprattutto grazie per il sostegno morale che mi avete sempre fornito silenziosamente da dietro le quinte, con consigli giusti e mai invadenti che nel momento giusto mi hanno sempre dato la spinta necessaria per affrontare le mie scelte.
Grazie a tutto il resto della mia famiglia: a Nonna, che purtroppo se ne è andata al momento finale di questo percorso, ti penso sempre e il tuo esempio e i nostri ricordi insieme li porto sempre con me.
Grazie a Francesca ed Elisabetta, per le chiacchierate su qualsiasi argomento che mi hanno sempre lasciato qualcosa su cui riflette e pensare. Grazie a mio zio Max, per il suo essere di poche parole, ma che con le sue carezze spontanee e inaspettate mi ha sempre scaldato il cuore. Grazie ai piccoli topini (Maria, Caterina e Marco): il vostro affetto innocente e puro è un grande dono.

Grazie alla Padu: ci conosciamo da anni ormai, e nonostante le nostre strade si siano separate un pò di tempo fa, è rimasto comunque un legame speciale. Grazie per tutte le volte in cui avevo bisogno e ci sei stata. Grazie per tutte le volte che ci sentiamo, perche anche se sono poche, sono speciali perche trasmettono tutta la volontà di voler coinvolgere l'altra nella propria vita. Grazie per il sostegno di sempre e grazie anche per la Padu "pazza e scatenata" che è sbocciata in questi ultimi anni.

Grazie agli amici storici di Lugo: nonostante la distanza, nonostante gli alti e bassi, comunque rimanete sempre un punto fisso di riferimento presente nella mia vita. Casa è casa anche perche ci siete voi.

Per ultimo, ma non per importanza, ci tenevo a ringraziare una persona che è entrata a far parte della mia vita solo in quest'ultimo anno, ma che fin da subito si è rivelato essere una bellissima scoperta e un regalo speciale. Grazie Gigio per il sostegno che mi hai sempre dato durante tutto il periodo di la stesura di questa tesi, e grazie anche per quello che mi dai quotidianamente quando mi perdo nelle mie insicurezze o negatività. Grazie per la persona buona, matura e generosa che sei. Grazie per il compagno presente, dolce, paziente, (disordinato) e premuroso che sei. Grazie perché entrambi stiamo percorrendo la nostra strada, ma tenedoci sempre per mano.
Grazie perche mi hai fatto scoprire quanto bene si possa stare avendo a fianco la persona giusta.

Grazie a tutti,
Elena Dragoni
Torino, 23/10/2019